On the Dynamics of Epileptic Spikes and Focus Localization in Temporal Lobe Epilepsy

by

Balu Krishnan

A Dissertation Presented in Partial Fulfillment
of the Requirements for the Degree
Doctor of Philosophy

Approved April 2012 by the
Graduate Supervisory Committee:

Leonidas Iasemidis, Chair
Kostantinos Tsakalis
Andreas Spanias
Jennie Si

ARIZONA STATE UNIVERSITY

May 2012

ABSTRACT

Interictal spikes, together with seizures, have been recognized as the two hallmarks of epilepsy, a brain disorder that 1% of the worlds population suffers from. Even though the presence of spikes in brains electromagnetic activity has diagnostic value, their dynamics are still elusive. It was an objective of this dissertation to formulate a mathematical framework within which the dynamics of interictal spikes could be thoroughly investigated. A new epileptic spike detection algorithm was developed by employing data adaptive morphological filters. The performance of the spike detection algorithm was favorably compared with others in the literature. A novel spike spatial synchronization measure was developed and tested on coupled spiking neuron models. Application of this measure to individual epileptic spikes in EEG from patients with temporal lobe epilepsy revealed long-term trends of increase in synchronization between pairs of brain sites before seizures and desynchronization after seizures, in the same patient as well as across patients, thus supporting the hypothesis that seizures may occur to break (reset) the abnormal spike synchronization in the brain network. Furthermore, based on these results, a separate spatial analysis of spike rates was conducted that shed light onto conflicting results in the literature about variability of spike rate before and after seizure. The ability to automatically classify seizures into clinical and subclinical was a result of the above findings. A novel method for epileptogenic focus localization from interictal periods based on spike occurrences was also devised, combining concepts from graph theory, like eigenvector centrality, and the developed spike synchronization measure, and tested very favorably against the utilized gold rule in clinical practice for focus localization from seizures onset. Finally, in another application of resetting of brain dynamics at seizures, it was shown that it is possible to differentiate with a high accuracy between patients with epileptic seizures (ES) and patients with psychogenic nonepileptic seizures (PNES). The above studies of

spike dynamics have elucidated many unknown aspects of ictogenesis and it is expected to significantly contribute to further understanding of the basic mechanisms that lead to seizures, the diagnosis and treatment of epilepsy.

ACKNOWLEDGEMENTS

My doctoral dissertation has been a culmination of learning experience both at the technical and emotional level. There are many people to whom I owe gratitude to make this document a reality and some of them needs special mention.

Foremost, I would like to thank Dr. Iasemidis for providing me timely guidance and mentoring during my life at Arizona State University. I am indebted to my committee members: Dr Tsakalis, Dr. Spanias and Dr. Si for the guidance and advice, exemplifying intellectual and professional standards I aspire for.

I am also extremely thankful to Dr. Papandreou, Dr. Rivera, Dr. Cochran for sharing their knowledge on signal processing and the motivation they provided during my student life at ASU. A special mention to the administrative staff of Electrical Engineering and Biomedical Engineering for their support.

My heartfelt thanks to my colleagues at Brain Dynamics Lab: Dr. Ioannis Vlachos, Aaron Faith, Dr. Shivkumar Sabesan, Jobi George, Vinay Venkataraman, Shashank Prasanna, Austin Roth, Eddie Tobin, Rashaad Sidique, Steven Mullane, Sterling Noelck, David Guffrey for their advice and support.

A big source of my motivation has been my school teachers. I would like to thank them all for never giving up on me and providing me guidance for life. One person who needs special mention is Late Mrs. Sos Alexander, who has been supportive, inspiring and mother-like guide to me.

I also thank my friends at ASU and home; especially Gatha, Maya, Raju, Sarath, Roshith, Hardik, Namrata, Rupa, Thalia, Vassia, Prasun, Anupriya, Aneesh, Rahul, Subash, Arvind, Nikhil, Raseem, Balamurali, Aiswaria, Sincy, Manu, Prasanth, Rijoy Shanas and all those who made sure that I had a life beyond my lab.

My parents and my siblings had always been there for me. I cannot thank them enough for the memories, love and support they provided me with.

I also thank my Late Grandfather and my uncle for being a source of inspiration for me taking up a technical career.

Lastly, I would like to thank a special person who came into my life four years earlier and who is my wife now. Bhadra I cannot thank you enough for what you have been for me. Thanks for being there to share my hardship and motivating me through my entire doctoral research career. Learning to love you is my next doctoral thesis.

To the smallest of perturbation that made this dissertation a reality

TABLE OF CONTENTS

Page

CHAPTER Page

LIST OF FIGURES

LIST OF TABLES

Chapter 1

INTRODUCTION

1.1 OVERVIEW

Epilepsy affects around 50 million people worldwide and is one of the most common neurological disorders after stroke. It is characterized by two hallmarks: epileptic seizures and epileptic spikes. Seizures occur due to the synchronous firing of a massive group of neurons, and their duration may extend from seconds to minutes. The seizure (ictal state) causes temporary disturbance of brain function (eg. motor, responsiveness, recall). Seizure onset and termination typically occur spontaneously, without any external intervention. The seemingly abrupt initiation and termination of epileptic seizures reflects intrinsic but poorly understood properties of the epileptic brain.

The other hallmark of epilepsy is the presence of interictal (between seizures) spikes. Interictal Spikes (IS) are also abnormal, synchronized neuronal discharges of group of neurons that can be observed in the electroencephalogram (EEG) of patients with epilepsy. Interictal spikes are high amplitude ($>$50 μV) fast electrographic activity followed by a slow wave (See Fig.1.1, 1.2), and last for only a couple of hundreds of milliseconds when recorded at the brain surface (e.g. via scalp electroencephalography - scalp EEG). Although spikes have been recognized as a diagnostic tool for epilepsy, the reason for their occurrence still remains elusive. Spiking may occur interictally, preictally (before seizures) and postictally (after seizures), and the neural networks generating seizures and spikes may be different from each other. It has been demonstrated in an animal model of epilepsy that every interictal spike is characterized by a pattern of cellular discharge, called paroxysmal depolarizing shift (PDS; See Fig.1.1D). PDS consists of a fast (200 to

500 Hz) sequence of action potentials, superimposed on a slow depolarizing potential [1]. Correlation of PDS and interictal spikes has been observed under multiple experimental conditions. Investigation into the cause and effects of interictal spikes may give possible clues to epileptogenesis and may also serve to provide new treatment avenues for epilepsy. From an engineering perspective, changes in interictal or peri-ictal (around seizures) spiking could be used to predict an impending seizure and explain the change in dynamics of the transition from interictal to ictal periods.

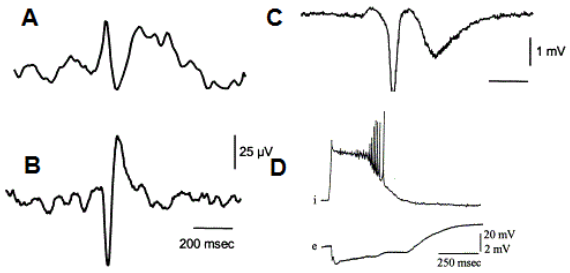

Figure 1.1: Interictal spikes recorded from (A) scalp EEG in human focal lesional epilepsy (B) human focal idiopathic epilepsy (C) extracellularly in an experimental in vitro model of focal epileptogenesis. (D) Paroxysmal Depolarizing Shifts (PDS) recorded from hippocampal neuron in status epilepticus induced by sustained electrical stimulation (Modified and reprinted from [1, 2], with permission from Elsevier Science)

1.1.1 Interictal spiking and interictal to ictal transition

A quantitative analysis of spiking in patients with temporal lobe epilepsy in the past has revealed that the epileptogenic focus (the region of the brain that triggers a seizure) generates spikes at maximum mean spiking rate, minimum variance in inter-spike intervals, and minimum coefficient of variation in spiking [3]. Treating interictal spikes as a point process, Sherwin [4] found that the distribution of inter-spike interval became far less Gaussian prior to a seizure. Spatiotemporal changes in preictal spike activity in human temporal lobe epilepsy [5] revealed that the degree of bilateral dependence in medial temporal lobe spike activity increased prior

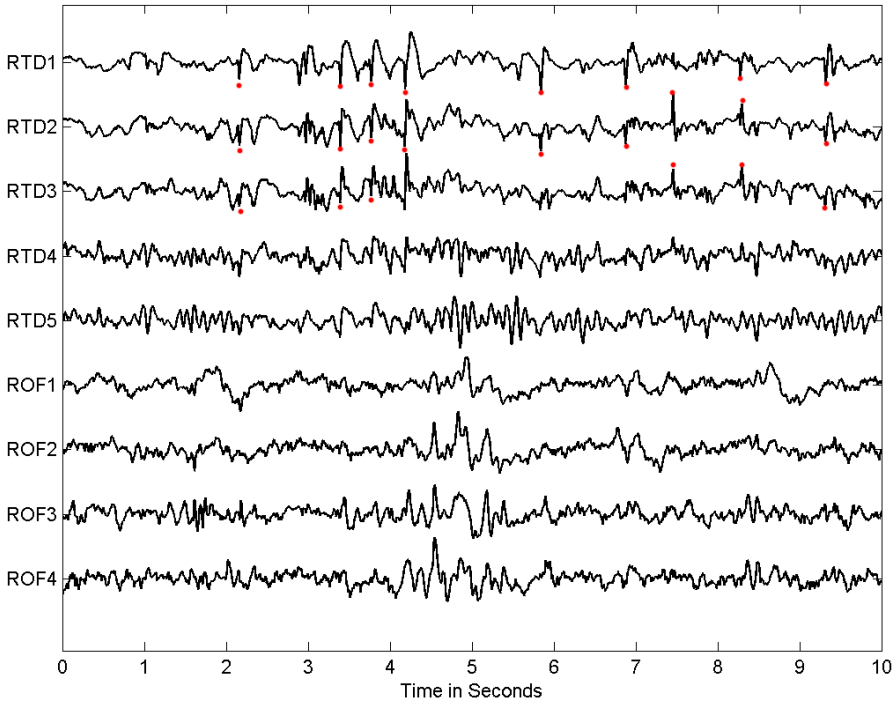

Figure 1.2: Epileptic spikes (red dots) observed in 10 seconds of interictal EEG data from a patient diagnosed with right temporal lobe epilepy. The epileptogenic focus for this patient is identified as RTD2, RTD3. (RTD-Right Temporal Depth and ROF-Right Orbito Frontal)

to onset of a temporal lobe seizure, thus indicating that spikes may herald the interictal to ictal transition. Engel et al. reported that a high spiking rate was associated with a low probability of occurrence of seizure [6]. A study conducted on amygdala kindled epileptic rats [7], correlated severity of behavioral seizures with spike frequency, and came up with the hypothesis that spikes may inhibit seizures. Contrary to this hypothesis, Gotman reported that, in amygdala kindled cats, interictal spiking appeared as a result of seizures, and probability of occurrence of a seizure is not affected by the spike rate [8]. Postictal increase in spike rate in human focal epilepsy was observed independently by Gotman [9, 10] and Katz et al. [11]. It

was also noted in that study, that seizures occurred when the spiking rate was high as well as when it was low, thus the hypothesis that spikes beget seizures, and the view of spikes as "mini-seizures" may then stand invalid. Studies on the effects of anti-epileptic drugs (AEDs) on spikes revealed that spiking was not affected by medication [9, 12] while seizures were, an additional evidence that the mechanism that generates spikes may differ from that of generating seizures. Recently, analysis of EEG using data mining techniques found reproducible sequences of activation pattern in interictal spike discharges [13]. Hidden Markov modelling of spike propagation was performed on interictal MEG data by Ossadtchi et al. [14]. The study however was conducted in only one patient and the primary aim was to localize the epileptogenic focus.

1.1.2 Do Interictal Spikes Drive Epileptogenesis?

Jensen et al. studied the mechanisms behind the generation of spontaneous seizures and spikes and suggested that seizures may occur due to non-synaptic (electrical-gap) interactions while spikes to synaptic (chemical) transmission [15]. The study points out that focal seizures arise independent of interictal spikes, as ictal events (seizures) were observed even after interictal spikes were abolished with synaptic transmission blockers. Moreover, it has been pointed out that the area that produces interictal spikes (called the irritative area) and the ictal-onset area may be different. Thus the neural networks responsible for the generation of spikes and seizures appear to be different. Results thus indicate that the relation between epileptic spikes and epileptic seizures is not straight-forward as one would expect. Interictal spikes are usually observed after a brain injury in human and experimental epilepsy, much earlier than the onset of the first spontaneous seizure. Thus the period between the appearance of the first spikes and the first seizure offers a window for investiga-

tion into ictogenesis. Spontaneous neural activity similar to interictal spikes has been observed in networks of self organization in the mammalian cortex and hippocampus [16, 17, 18]. It has also been hypothesized that, with the aid of interictal spikes, the injured axons of neurons may grow back into their original destination. Axonal sprouting was observed in the dentate gyrus of the hippocampus during epileptogenesis [19, 20]. The newly grown axon increases the positive feedback in the network [21]. The excessive positive feedback makes the network unstable, thus producing spontaneous seizures. Experimental evidence suggests that spikes may play a role in other forms of synaptic plasticity, such as long-term potentiation (LTP) of synaptic strength [22]. This evidence indicates that interictal spikes may play a role in guiding axons back into their network of origin and also help in maintaining/generating synaptic plasticity.

1.2 Research Objectives

The major objective of this dissertation is to enhance the understanding of the dynamics of interictal spikes through a spatiotemporal dynamical analysis of their occurences and in relation to epileptic seizure occurences. The majority of approaches in the literature deal with increase or reduction in spike rate and its correlation with seizure susceptibility and seizure severity. This has led to two contrasting views: researchers observed increase in spike count preictally versus postictally, and the reverse. Some of the few approaches which studied the spatio-temporal changes of interictal spikes prior to an epileptic seizure include [4, 5]. Our work has been inspired by Lange's research on spatio-temporal evolution of preictal spike activity in human temporal lobe epilepsy. Lange pointed out that bilateral dependencies of spikes increased prior to the onset of a seizure. He followed a qualitative approach in relating how spiking in one region of the brain is related to another.

Ten years later, Iasemidis et al. observed that the brain transits to a state of synchrony hours to minutes before an ictal onset and back to desynchronized state after seizure termination [23, 24, 25]. This means that different regions of the brain move or are driven into a pathological hypersynchronized state prior to an epileptic seizure. Spikes were not considered separately in that analysis of EEG. Assuming the brain as a network of coupled oscillators, they hypothesized that during the preictal period the oscillators synchronize with each other and tend to have similar epileptic activity. In that sense, spikes also will occur in synchrony as a seizure approaches. This might give valuable insight into the process of epileptogenesis and ictogenesis. The major objective of this research is to perform a systematic study on this role of spikes in ictogenesis. We try to answer whether pre-ictal synchronization of spikes is observed, and if so what is its relation with pre-ictal entrainment of the EEG observed by Iasemidis et al.

Another open question this research addresses is epileptogenic focus localization (identification of the region of brain that initiates the seizure) based on interictal spiking activity. Epileptogenic focus localization has been an active area of research in the past decades. In the 80s, physicians related epileptogenic focus to the region in the brain which had the highest spiking rate. However with the advancement of computers technology and quality of digital EEG recording units, it has been observed that contrary to the popular belief, the epileptogenic focus is not nevessarily the region with the highest spike rate. Clinically, current methods for localization of the focus include the identification of the location of seizure onset via EEG and imaging technologies. In this research, we investigated how interictal spikes are related to epileptogenic focus and whether it is possible to localize the epileptogenic focus from the interictal period.

1.3 THESIS ORGANIZATION

The rest of this thesis is organized as follows. In Chapter 2, we first discuss spike detection algorithms in the literature. We then introduce a novel spike detection algorithm based on morphological filtering techniques and compare its performance with an established spike detector from the literature. We then apply our spike detection algorithm on the EEG data from five patients with temporal lobe epilepsy and investigate long term trends in spike rate profiles at different brain regions.

In Chapter 3, we investigate the spatial synchronization of spikes, develop measures of spike synchronization and compare them with existing ones in the literature. We then apply the developed measures and evaluate their performance on coupled neuronal oscillator models that can generate spiking activity. We then apply the developed synchronization measures on interictal spikes detected from our five patients and investigate the long-term and short-term trends in spike synchronization profiles.

Chapter 4 describes the application of epileptic spike synchronization to localization of the epileptogenic focus. We utilize a measure of connectivity from graph theory and show its application to epileptic spike synchronization. We then apply the developed measure on spikes from models of coupled oscillators and epileptic spikes detected from the EEG of our five patients. A prospective epileptogenic focus localization algorithm is described in this section.

In Chapter 5, we investigate the relation of seizure severity with peri-ictal spike rate. We show that clinical seizures are preceded by high and spatially spread spike activity while subclinical seizures are not.

In Chapter 6, we discuss the resetting of brain dynamics at seizures in terms of spike synchronization and synchronization of brain dynamics. We quantify the dy-

namical changes in spike synchronization profiles at seizures using a novel measure for brain resetting. Comparison of brain resetting results from nonlinear dynamics and the novel spike-based brain resetting results are presented in this section. We herein also present the results of seizure resetting by analysis of scalp EEG from epileptic and nonepileptic pyschogenic patients. We provide empirical evidence that differential diagnosis is possible between those patients on the basis of resetting of brain dynamics.

In Chapter 7, we provides the conclusion and future directions of this line of research.

Chapter 2

INTERICTAL SPIKE DETECTION

2.1 INTRODUCTION

Algorithms for automatic detection of epileptic spikes is a valuable diagnostic tool for clinicians and researchers. Visual spike marking by an experienced EEGer is a time consuming process and prone to bias, whereas automatic spike detection is a difficult task because of the variation of spikes' characteristic morphology across elecrodes, both within a patient and across patients. A rule of thumb for spike detection among the clinical community is sharpness and distinguishability from the background EEG. Such a simplistic definition of epileptic spikes makes the development of a robust detection algorithm difficult. Over the years several spike detection algorithms have been proposed. Broadly, these algorithms can be classified into three types : mimetic-based, signal processing-based, and template-matching.

Gotman and Gloor [26] detected spikes by dividing the spike waveform into a set of half-waves by distinguishing segments between amplitude extrema. Using the distinguishability of the half-waves from the background, their sharpness and duration were used to produce appropriate detection criteria. Gueds et al. [27] used a similar set of attributes (sharpness of the peak, duration of the wave, and steepness at the edges) to also come up with a spike detection algorithm. Instead of using the absolute value of these attributes, they used relative attributes with respect to the background. A rule-based variation of Gotmans algorithm was proposed and tested on a single 320 sec EEG segment by Davey et. al [28].

Autoregressive (AR) modeling of EEG was used by Sankar et al. [29] to detect spikes. AR coefficients were computed for every 5 second segment of EEG, and the obtained coefficients were compared to a previously stored template of AR

coefficients for spike waveforms. The algorithm had a very low sensitivity and specificity. Wavelet analysis of epileptic spikes was perfomed by Senhadji, Park, Adeli [30, 31, 32]. Wavelet coefficients were computed from segments of EEG data and later used as features for neural network training. Parameterization of EEG spikes using the matching pursuit decomposition put forward by Mallat and Zhang [33], was performed by Durka et al [34]. These parameters were later used to detect spikes.

Neural Network-based interictal spike detection algorithm was performed by Hellmanm, Ko, Ozdamar [35, 36, 37]. Ozdamar and Ko proposed an algorithm which takes raw EEG fed to a neural network classifier for epileptic spike identification whereas Hellmann used morphological features of the wave as attributes to neural network classifier. Wilson et al. developed a Multiple Monotonic Neural Network (MMNN) for spike detection [38]. The neural network used was similar to the one proposed by Webber et al. [39], and assigned perception values to detected spikes. A high perception (1) is assigned to an unambiguous spike and low perception (0.1) is assigned to an ambiguous spike.

Morphological filter is an efficient tool to decompose raw EEG waveform into background activity and fast epileptic spike activity. Investigation into application of morphological filter to spike detection was performed by [40, 41, 42]. The primary difference in the three methods is the selection of the structure element. Xu et al. provided an efficient method to construct the structure element, however the algorithm requires considerable optimization time.

2.2 Morphological Filtering based Spike Detection

Morphological filters (MF) are a class of nonlinear filters used to separate characteristic morphologies in multi-dimensional signals. The theory behind math-

ematical morphology was developed by Matheron and Serra in 1964 and it has been widely applied to detect edges and to perform pattern recognition in images [43, 44, 45, 46].

Morphological filters rely on a structuring element of a predefined shape that probes the multi-dimensional signal. A wide variety of structuring elements can be defined based on the shape of the morphology to be extracted from the signal. However there is no defined theory on the selection of an appropriate structuring element. Commonly used structuring elements include squares, discs, parabolas etc.

2.2.1 Morphological Filter Operators

Morphological filtering includes four basic operations formulated using Minkowski addition and subtraction. Consider two sets X and Y in Euclidian space, then their Minskowski sum is defined as

$$X \oplus Y = \{x+y \mid x \in X, y \in Y\} \tag{2.1}$$

i.e. every element of X is added to every element of Y to produce the Minkowski sum. Then four basic morphological operators can be defined as

1. Erosion

$$(x \ominus y^s)(t) = min\{x(\tau) - y(-(t-\tau))\}, \ \ \tau \in D \tag{2.2}$$

2. Dilation

$$(x \oplus y^s)(t) = max\{x(\tau) + y(-(t-\tau))\}, \ \ \tau \in D \tag{2.3}$$

3. Opening

$$(x \circ y)(t) = [(x \ominus y^s) \oplus y](t) \tag{2.4}$$

4. Closing

$$(x \bullet y)(t) = [(x \oplus y^s) \ominus y](t) \tag{2.5}$$

where $x(t)$ is the raw data and $y(t)$ is the structuring element and $y^s(t) = y(-t)$, D is the set of real numbers. The notation $\oplus$, $\ominus$, $\circ$, $\bullet$ indicates Minkowski addition, Minkowski subtraction, Opening and Closing operations respectively.

The effect of each of the four operations on a signal is shown in Fig. 2.1. Erosion of $x(t)$ using $y(t)$ will attenuate the peaks, whereas dilation enlarge the valleys. The opening operation is erosion followed by dilation thus it smooths the signal from below, i.e. it will cut down the peaks of the signal. The closing operation is basically dilation followed by erosion and has the effect of smoothing the signal from above by filling up its valleys. Thus, in principle, a combination of opening and closing can be used to detect spikes in signal. From 2.1(a) and 2.1(b) we can observe that the epileptic spikes occur with both positive and negative peaks. Thus, to detect these spikes we follow the approach detailed in [42]. We obtain $OC(t) = x(t) \circ y_1(t) \bullet y_2(t)$ (Opening of $x(t)$ using $y_1(t)$ and closing using $y_2(t)$) and $CO(t) = x(t) \bullet y_1(t) \circ y_2(t)$ (Closing of $x(t)$ using $y_1(t)$ and opening using $y_2(t)$). Thus the, combination of closing and opening will eliminate any spikes in the data (see Fig. 2.2). Now we define $\hat{x}(t)$,

$$\hat{x}(t) = x(t) - \frac{OC(t) + CO(t)}{2} \tag{2.6}$$

From Fig. 2.2's low panels we can observe that $\hat{x}(t)$ contains just the spike component devoid of any background activities.

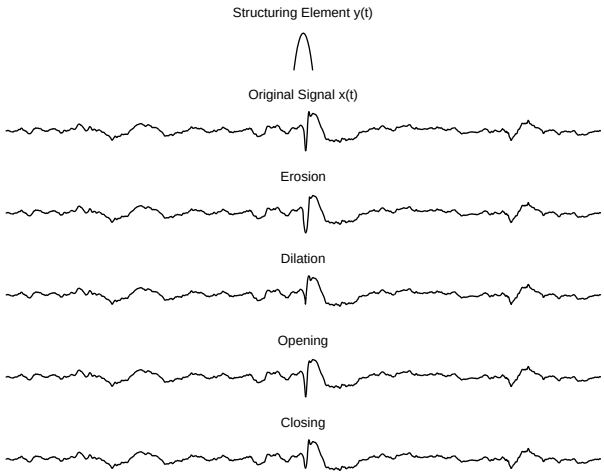

(a)

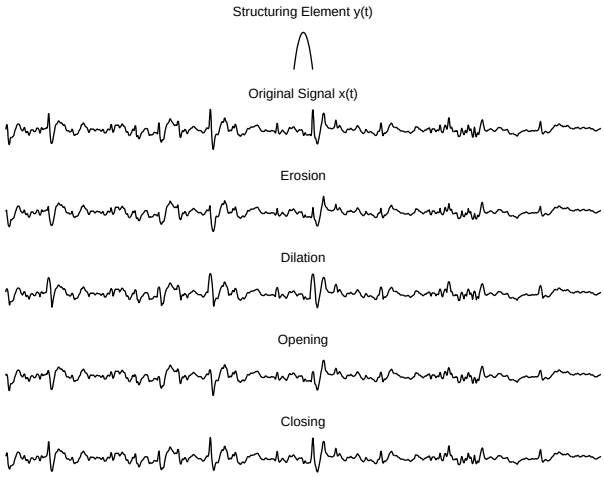

(b)

Figure 2.1: Illustration of the results of the four basic operations of a morphological filter (a) on a negative spike (b) on a positive spike

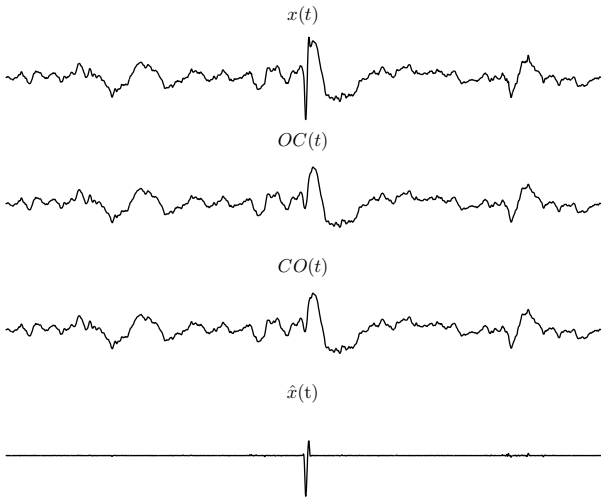

(a)

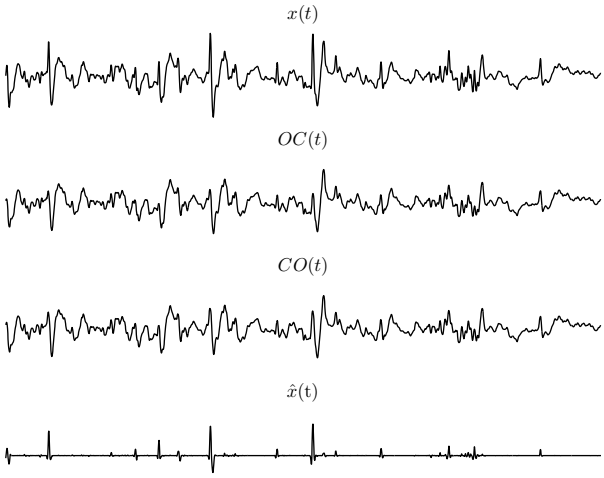

(b)

Figure 2.2: Extraction of epileptic spikes by morphological filtering from background EEG. (a) Filtering of a negative spike. (b) Filtering of positive spikes.

2.2.2 *Selection of structural elements*

Selecting an appropriate structural element improves the efficiency and accuracy of the spike detector. Due to the lack of theoretical framework, the task of selecting a structural element becomes a non-trivial problem. Commonly used structural elements include parabolic, triangular and line shaped elements (see Fig. 2.3). The dynamical properties of EEG change over time, so the design of structuring element should take into account these changes, i.e the structuring element should be adaptive. Xu et.al proposed parabolic structuring elements whose width and height are optimized to extract the peaks in the signal while at the same time supressing the background activity [42]. We use a modified version of Xu's algorithm for designing the optimal structuring element.

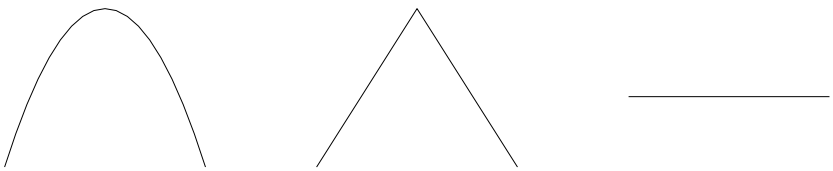

(a) (b) (c)

Figure 2.3: Structural element commonly used in morphological filtering. (a) Parabolic (b) Triangular (c) Line.

2.2.3 *Design of structural element*

We first define the n^{th}-order difference of $x(t)$ as follows

$$d^n(t) = |x(t+n) - x(t)| \tag{2.7}$$

Then $D(n)$, the 75% quantile of $d^n(t)$, is estimated for all values of n. $D(n)$ is then an approximates the significant values of $d^n(t)$. We then estimate the structur-

ing elements $y(t)$ as

$$y(M-n) = y(M+n) = -a_{opt}D(n), \;\; n \in [1, M-1] \tag{2.8}$$

where $M = (N_{opt}+1)/2$, $y(M) = 0$. N_{opt} and a_{opt} are the optimal width and optimal amplitude of the structuring element respectively (see Section 2.2.4). The structuring element y(t) thus carries information about the average local variation of the signal under consideration. For a signal with slow dynamics the structuring element will be approximately flat, and for a signal with fast transient activities the structuring element will be sharp (see Fig. 2.4).

2.2.4 Optimization of structuring element

The length and amplitude of the structuring element play an important role in optimal detection of epileptic spikes. We use the K-criterion detailed in [42] for optimal selection of amplitude and width of the structuring element. For a signal $x(t)$ we estimate two structuring elements $y_1(t)$ and $y_2(t)$. The shape of the structuring element is estimated based on section 2.2.2. The width and amplitude of the structuring elements are selected as follows

1. Intialize amplitude a_1 and width n_1 of $y_1(t)$. Intialize amplitude a_2 and width n_2 of $y_2(t)$. We choose a_1. Value ranges for a_1, a_2, n_1, n_2 are provided below
2. Estimate $\hat{x}(t)$ using Eq. 2.6.
3. Estimate N_{pz} of $\hat{x}(t)$ as

$$N_{pz} = \sum_{t=1}^{N-1} \Theta(\hat{x}(t) * \hat{x}(t+1)) \tag{2.9}$$

where

$$\begin{aligned} \Theta(x) &= 1 \;\; x \leq 0 \\ &= 0 \;\; x > 0 \end{aligned} \tag{2.10}$$

and N is the length of the signal $\hat{x}(t)$

4. Estimate $R_{pz} = N_{pz}/N$

5. Estimate $I_f = \tilde{x}/\bar{x}$, where $\tilde{x} = max(|\hat{x}(t)|)$ and $\bar{x} = \frac{1}{N}\sum_{t=1}^{N}|\hat{x}(t)|$

6. Estimate $K = I_f/R_{pz}$

7. Repeat steps 1-6 for different values of a_1, a_2, n_1, n_2

8. Select the maximum value of K and the corresponding set of a_1, a_2, n_1, n_2

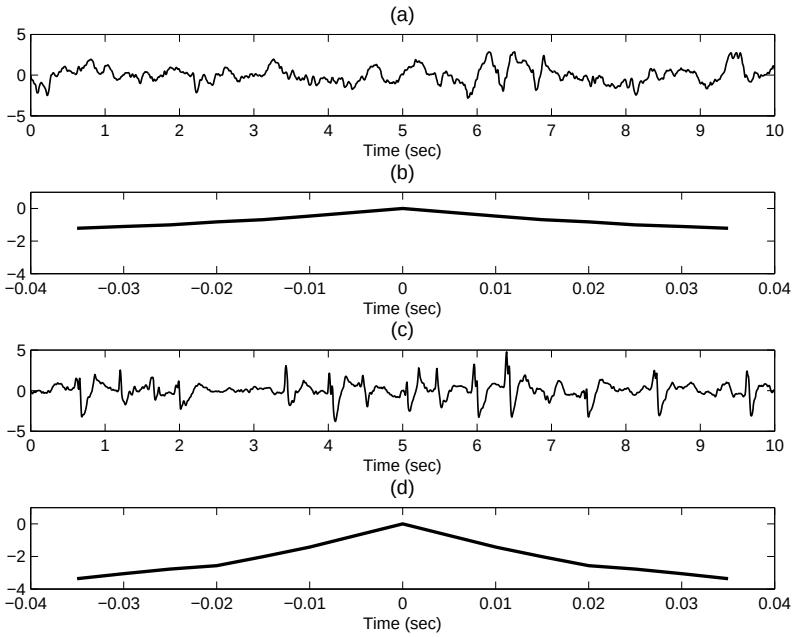

Figure 2.4: Shape change of structural element $g(t)$ with changes in dynamical properties of signal. (a) EEG segment with slow dynamics (b) Structural element for EEG segment in (a). (c) EEG segment with epileptic transients like spikes. (d) Structural element for EEG segment in (c).

I_f is the pulse index of $\hat{x}$ and is sensitive to the transient component of the signal. R_{pz} is the zero-crossing rate of $\hat{x}$ and reflects the degree to which background

activity is to be compressed. A large value of K thus means that spike components are better extracted and background activities are better compressed. To remove effects of EEG scaling and other factors from affecting detector performance, we normalize (using standard deviation) and filter the data between 0.1Hz and 30Hz using a 4^{th} order Butterworth filter. Values of a_1, a_2 range between 0.1 to 2 (upto 2 standard deviation), and n_1, n_2 can range from 5 to 21 samples which corresponds to 25 msec to 100 msec for a data sampled at 200 Hz (typical spike duration is around 50-80 msec).

2.2.5 Detector Performance

Performance of the detector is dependent on how accurately it can detect spikes and also how efficiently it can restrain background activities. We compare the performance of four morphological filters

- Adaptive Morphological Filter (AMF) (see section 2.2.3)
- Modified Morphological Filter (MMF) [42]
- Morphological Filter with Parabolic Structure Element (MFP)
- Morphological Filter with Triangular Structure Element (MFT)

We used marked epileptic EEG spikes and artifacts from a public database [47]. The data set consisted of a total of 53 spikes in thirty 8 second epochs. Ten minute of artifacts consisting of spike like events was also analyzed to test the specificity of our algorithm. Fig. 2.5 shows the performance of the four spike detectors on the data set. We can see from the plot that AMF and MFT has superior performance compared to MMF and MFP. Even though the performance of MFT is slightly better than AMF we selected AMF over MFT, since AMF adapts itself to changes

in EEG dynamics within a recording site and also adapts to variability in EEG across electrodes and patients.

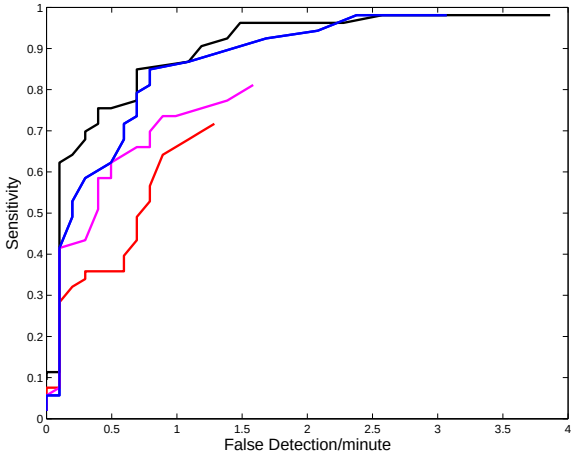

Figure 2.5: Performance characteristics of the four spike detector. The blue curve denotes the detection characteristics curve for AMF, the red curve denotes the detection characteristics for MMF. The magenta line denotes the detection characteristics for MFP and the black line denotes the detection characteristics curve for MFT.

To compare the efficiency of the detector in restraining background activity, we select 50 EEG segments of duration 10 sec each, containing no epileptiform discharges or activities. We estimated $\hat{x}(t)$ for every EEG segment using each of the four morphological filters. Since the EEG segment contains no epileptiform discharges we assume that morphological filter should extract the background completely and $\hat{x}(t)$ is the misfit. We therefore estimate the Signal to Noise Ratio (SNR) for each segment for the four filters as:

$$SNR = 10\log_{10}\left(\frac{P_x}{P_{\hat{x}}}\right) \tag{2.11}$$

where P_x and $P_{\hat{x}}$ are the powers of the signals $x(t)$ and $\hat{x}(t)$ respectively.

The mean SNR for the four filters are shown in Table 2.1. From this Table it can be observed that the Adaptive morphological filter performs better in restraining background activity than the traditional and improved morphological filters.

Table 2.1: Performance of Morphological Filters in restraining background EEG

Type of Filter	Mean SNR (dB)
Adaptive MF	22.84
Xu's Improved MF	17.79
MF with parabolic Structure Element	16.86
MF with triangular Structure Element	16.30

2.2.6 Comparison with Persyst Spike Detector

We now compare the performance of the our spike detector with the commercially available software for epileptic spike detection called Persyst. Two hours of continuous intracranial EEG recordings of a single electrode from a single patient was used for this purpose. Spikes were detected for this electrodes using DAMF and Persyst. The sensitivity of Persyst spike detector was automatically set by the software itself. The spikes picked up both the algorithms, the spikes missed by DAMF but detected by Persyst and the spikes missed by Persyst but picked up by DAMF is shown in Fig. 2.6. We can observe that spike detector based on DAMF is more robust when compared to Persyst.

2.3 DESCRIPTION OF EEG DATA:

EEG data from a total of five patients who underwent presurgical evaluation and long-term intracranial EEG recordings were chosen for dynamical analysis. Informed consent for participation in this study was obtained from all patients. The recordings included 4-29 seizures (with clinical manifestation and sub-clinical seizures) over a period of 5 to 13 days per patient (see Table 2.2).

2.3.1 Electrode Placement:

The five patients used in this study had the following electrode placement (also see Fig. 2.7)

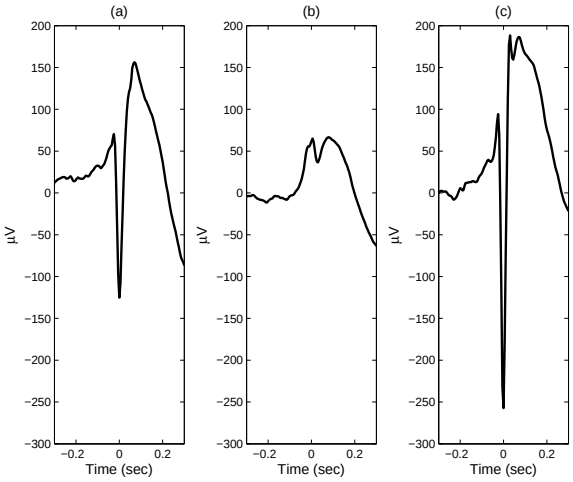

Figure 2.6: Comparison of DAMF with commercially available spike detector on two hour EEG recorded from a single channel of a patient with temporal lobe epilepsy. Average of spikes detected by (a) both DAMF and Persyst (b) Persyst but missed by DAMF (c) DAMF but missed by Persyst. The perception level (threshold) for the Persyst algorithm was fixed at 0.7. A higher or lower threshold did not change the results. Approximately 50% of spikes detected by DAMF were detected by Persyst. DAMF missed 65% of spikes detected by Persyst, the average of this missed detection corresponds to the second panel in (b).

- A stereotactic placement of bilateral depth electodes in the hippocampi (RTD1 anterior to RTD6 posterior in the right hippocampus, with RTD1 adjacent to right amygdala; LTD1 anterior to LTD6 posterior in the left hippocampus with LTD1 adjacent to the left amygdala).

- Two subdural stip electrodes over the orbitofrontal lobes (LOF1 to LOF4 in the left and ROF1 to ROF4 in the right lobe, with LOF1, ROF1 being most mesial and LOF4 and ROF4 most lateral).

- Two subdural strip electrodes were placed bilaterally over the temporal lobes (LST1 to LST4 in the left and RST1 to RST4 in the right, with LST1, RST1 being more mesial and LST4 and RST4 being more lateral).

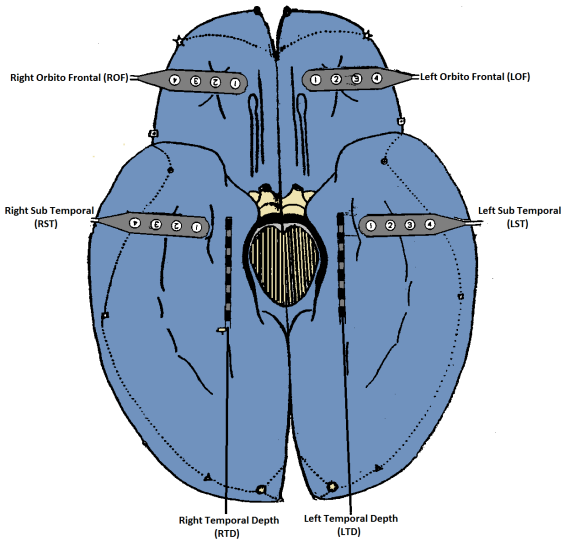

Figure 2.7: Schematic diagram of the horizontal section of the brain showing the depth and subdural electrode placement.

2.3.2 EEG Recording:

The EEG was recorded using a Nicolet BMSI 4000 EEG machine. The EEG signals were recorded using an average common reference with analog band-pass filter settings of 0.1 Hz -70 Hz. The data were sampled at 200 Hz with a 10 bit quantization and recorded on VHS tapes continuously over days via 3 time-interleaved VCRs. The data from tapes were subsequently decoded and transferred to computer media for storage.

2.4 Application on EEG Data

Epileptic spikes were detected per electrode for the entire duration of recording for each of the five patients using the improved morphological filter with adaptive structuring element. Spike detection was expedited with the help of High Perfomance Computing Cluster available at ASU. Two hundred and fifty six computer cores were used at a time to speed up the calculations. The algorithm is computa-

Table 2.2: Patient and EEG Data Characteristics

Patient ID	Number of Electrodes	Duration (Hours)	Number of Seizures	Focus (Clinical Assessment)
1	28	200.2	30	Right temporal lobe (RTD)
2	28	143.4	19	Right temporal lobe (RTD)
3	28	149.6	23	Left temporal lobe (LTD)
4	28	322.8	17	Right temporal lobe (RTD)
5	28	268.6	7	Right temporal lobe (RTD)

tionally efficient and is faster than real time (less than 0.5 sec for 10 sec of EEG from 28 channels). However, the volume of data to be analyzed was approximately 2 weeks per patient, which necessiated the use of high computation power.

2.4.1 Long-term trends in spike rate

To investigate the long-term evolution in spike rate per brain site, we estimated the number of spikes in every 10.24 second of EEG segment at each of the brain sites for the entire duration of recording. Figs. 2.8, 2.9, 2.10 show the spike rate profiles of six brain sites (one from each region) in a single patients with temporal lobe epilepsy. Each brain site has its own distinct spike rate profile. For the left sub-temporal and left temporal depth regions, we can observe an immediate increase in spike frequency following a seizure, whereas for the left and right orbito frontal there is an increase in spike frequeny prior to a seizure. The behavior of spike activity in the right orbitofrontal is an interesting phenomenon. We can observe long-term increase in spike frequency till the first clinical seizure for this electrode. Also, across seizures and patients (See Fig. 2.11), there is an increase in the number of spikes in the orbito frontal cortex preictally. Previous studies in mesial temporal

lobe epilepsy have shown functional connectivity and propagation of ictal activity between hippocampi and orbitofrontal cortex in humans [48, 49, 50]. These results suggest that the orbitofrontal cortex can be involved in the interhemispheric propagation of mesial temporal lobe seizures. The spike rate profile of left orbitofrontal cortex (LOF; See Fig. 2.10(a)) is similar to the one of right orbitofrontal (ROF). Based on this observation we can hypothesise, a possible propagation pathway between the abnormal hippocampus and the orbitofrontal region which becomes increasingly active during ictogenesis. Seizure itself then get initiated as a defensive mechanism of the brain to break this functional connectivity. We investigate these phenomena in the next chapter where we measure functional connectivity in terms of spike synchronization.

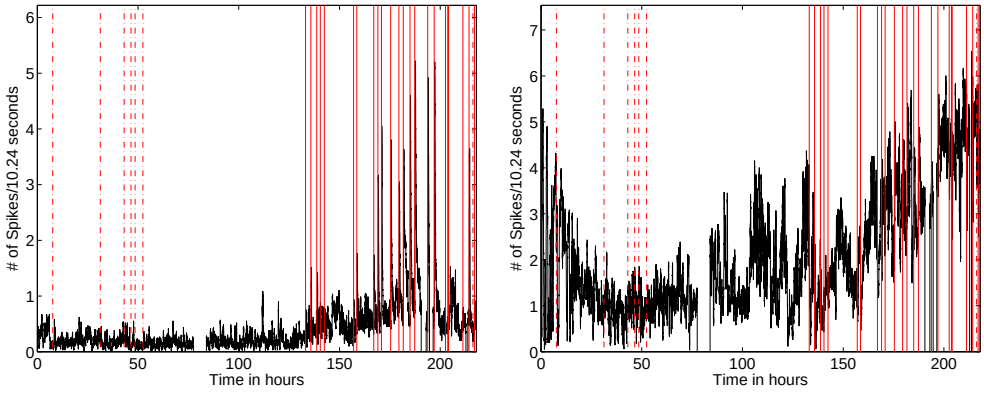

(a) (b)

Figure 2.8: Spike rate profile for two brain sites located in the left and right hippocampal regions in Patient 1. (a) Left Temporal Depth (LTD) . (b) Right Temporal Depth (RTD). Vertical solid red lines denote clinical seizures and dashed red lines denote subclinical seizures.

From Fig. 2.8(b) and 2.9(b) we notice that RST has a higher spike rate than RTD, which is the clinically identified focus (first area that shows seizure onset). Fig. 2.12 shows the mean rate of spikes (number of spikes/30.72 sec) for the first interictal segment of Patient 1. It can be observed that RTD1, RST2, RST3 and

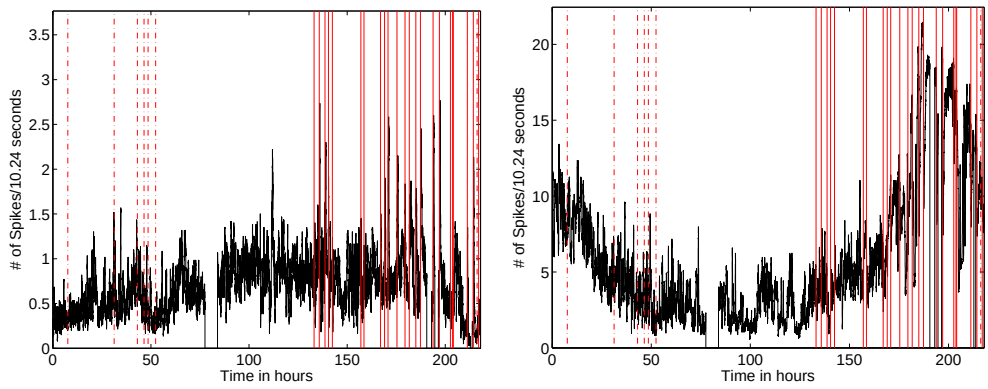

(a) (b)

Figure 2.9: Spike rate profile for two brain sites located in the left and right subtemporal regions in Patient 1. (a) Left Sub Temporal (LST) . (b) Right Sub Temporal Depth (RST). Vertical lines are as in Fig. 2.8

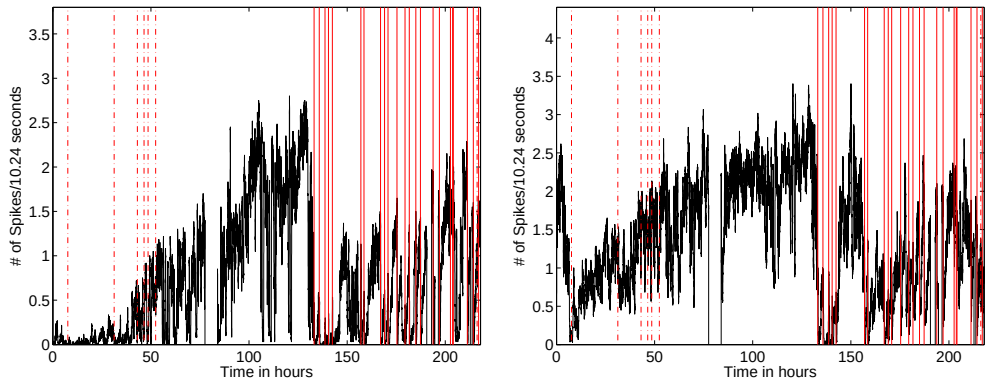

(a) (b)

Figure 2.10: Spike rate profile for two brain sites located in the left and right orbitofrontal regions in Patient 1. (a) Left Orbitofrontal (LOF) . (b) Right Orbitofrontal (ROF). Vertical lines are as in Fig. 2.8.

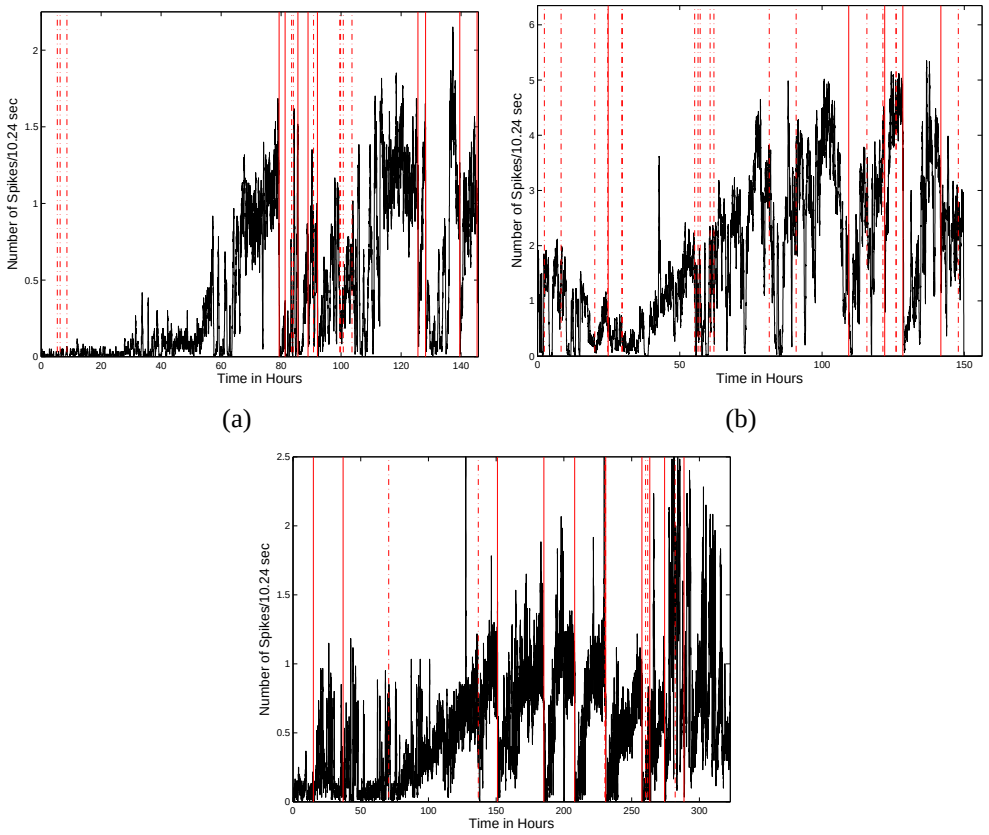

Figure 2.11: Spike rate profile for the right orbitofrontal (ROF) region of three patients. Spike rate for the ROF region monontonically increases prior to epileptic seizure. This might indicate existence of functional connectivity or pathways between the epileptogenic hippocampus and the ROF in the preictal period. Seizure breaks this functional connectivity and a more normal functionality is restored. Vertical red lines denote clinical seizures and dashed red line denotes subclinical seizures.

RST4 have the highest spike rate. RTD2 and RTD4 which are the clinically determined focus have very low spike rate (comparable to ROF3 and LOF4). Thus spike rate may not provide us with accurate information about the location of the focus. This is in agreement with the findings by Jensen et. al [15].

The spike frequency profiles at the epileptogenic focus for four patients with temporal lobe epilepsy are shown in Fig. 2.13. We can see that there is no consistent behavior over time and across patients, specific to the focal region. Seizures tend to occur at high as well during low rates of spike activity. In Patient 1, we can see a progressive increase in spike rate with increasing seizure activity, however similar observations cannot be made across patients. In patient 4, we observe circardian oscillations in spike rate (according to the patient report, the majority of this patient's seizure occured during sleep). Relationship between epileptogenic focus, interictal spikes and depth of sleep has been investigated in [51, 52, 53]. However since the sleep stages were not marked for our patient we were not able confirm the results of this study.

2.5 CONCLUSIONS

In this chapter, we developed a novel method for detection of epileptic spikes using an improved morphological filtering technique. In particular morphological filter was constructed using a data adaptive structuring element, which changes its width and amplitude depending on the data under consideration. The performance of the detector in identifying epileptic spikes from background EEG was tested and compared with similar algorithms available in the literature on known data from publically available database. We further tested the robustness of the detector in compressing background EEG activity by applying the algorithm on segments of EEG containing no epileptiform activity and estimating the signal to noise ratio.

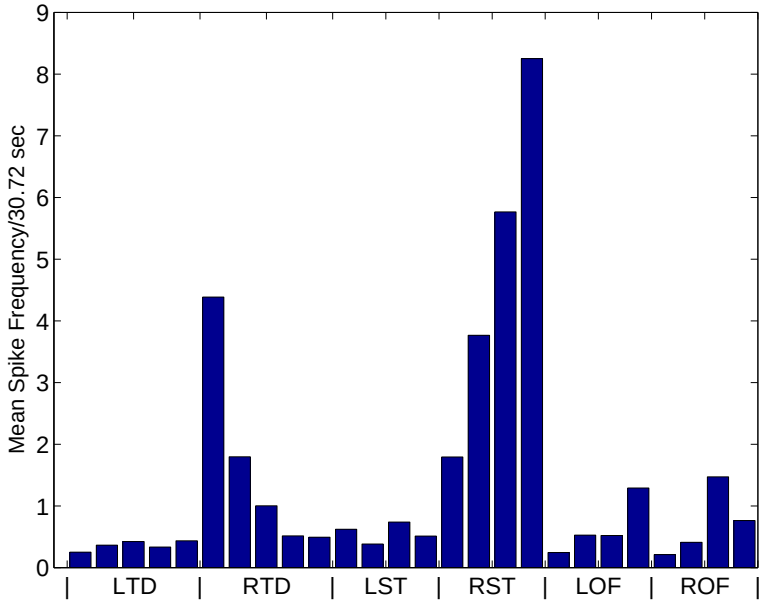

Figure 2.12: Mean spike rate(# of spikes per 30.72 sec) at different brain sites for the interictal segment of Patient 1. RTD (Right Temporal Depth), which is the clinically identified focus, has lower mean spike frequency when compared to RST (Right Subtemporal). This indicates that localization of epileptogenic focus is not possible using spike counting techniques.

Based on analysis an ROC (Reciever Operating Characteristics), the detector was constructed and an optimal threshold for detection was identified. Application of the detector to EEG recordings from five patients with temporal lobe epilepsy was then performed. We observed that a high spike rate was not correlated with the location of the epileptogenic focus. In particular we observed, that the epileptogenic focus might have similar spike rate as that of a normal brain sites. Spike rate at the epileptogenic focus also did not show consistent trends across patients. An interesting observation was the behavior of Orbito-Frontal brain region across all patients. Progressively increasing spike rate was observed in these areas in the preictal period of most of the seizures and was followed by supression of spike rate in the postictal period.

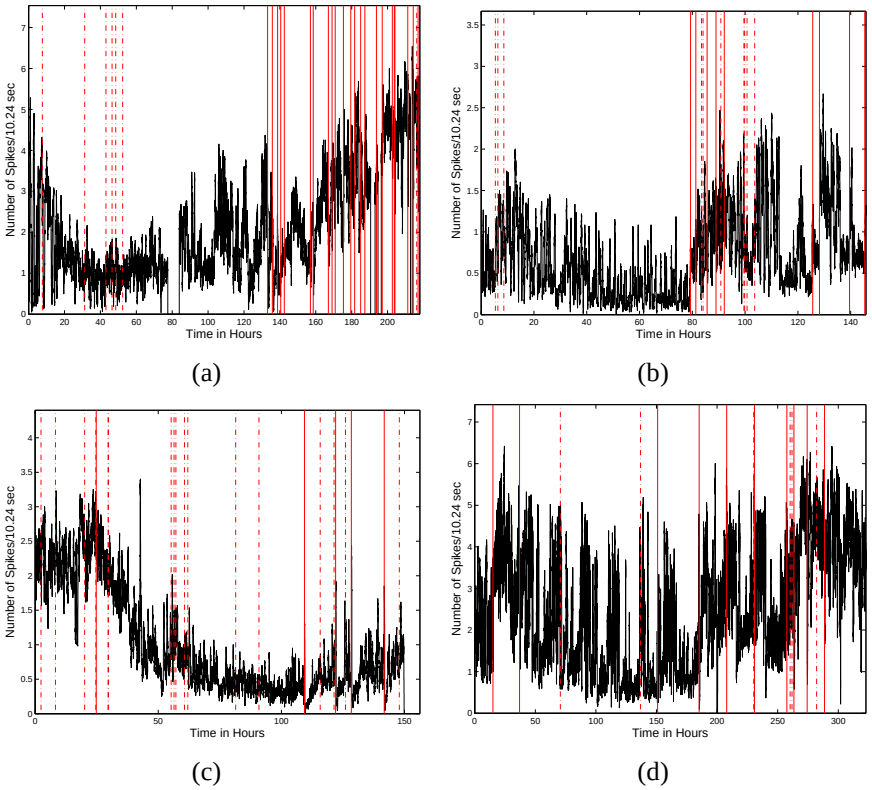

Figure 2.13: Spike frequency profile for the clinically accessed focus of four patients with temporal lobe epilepsy. Spike frequency was estimated by counting the number of spikes in every 10.24 seconds. Spike frequency for (a)Patient 1 (b)Patient 2 (c)Patient 3 (d)Patient 4 are shown. Vertical red lines denotes clinical seizures and vertical dashed red lines denotes subclinical seizures

The results in this chapter suggest complex relationship between spike rate, seizures and the epileptogenic focus. The rest of the dissertation is committed to deciphering this complex relationship. Taking insight from the results in this chapter, we set to test whether preictal spikes have more power, i.e. a tendency to spread across brain sites or equivalently act as communicating agents. In the postictal period, the ability of spikes to spread to multiple brain region may reduce due to a resulting disconnection from the occurence of the seizure (the resetting of brain dynamics)[54, 55]. We will be investigating this hypothesis in the next chapter, where we study the synchronization of epileptic spikes and its relation to seizures.

Chapter 3

SPIKE SYNCHRONIZATION

3.1 INTRODUCTION

Extracting information about neural codes in spike trains has been a key challenge in understanding the dynamics of the epileptic brain. To this effect, many methods of measuring spike train synchrony have been proposed. Most of the approaches discuss spike trains as point processes rather than continuous time processes. Considering the all-or-none nature of neural codes, a point process-based approach seems a viable method for decoding the information residing within spike trains.

In [56], Victor et al. proposed a family of metrics that are sensitive to different features of temporal coding such as absolute timing of individual pulses, duration of interspike interval, and pattern recurrence. A method to identify similarity between spike trains was also proposed by Victor [57]. The central idea of that proposed metric includes the evaluation of the cost required to transform one spike train to another through a series of elementary steps.

Cross-correlation between spike trains as a measure of synchrony was proposed by Schreiber et al [58] . The method consists of filtering the observed spike train with a Gaussian filter and estimating the cross-correlation between the filtered spike trains which have now become a continuous time series. Quiroga et al. proposed event synchronization as a measure to evaluate synchronization patterns in point processes [59]. The measure is conceptually very simple and essentially counts the number of event pairs that occurred close in time. Kreuz et al. put forward a family of measures to estimate synchrony between spike trains [60, 61, 62]. The measures termed as ISI-distance, Multivariate ISI-distance and Spike-distance evaluate the degree of synchrony between bivariate point processes and multivariate point

processes based on interspike interval and spike coincidence. The ISI-distance is sensitive to firing rate of spikes and measures the similarity of interspike interval between two point processes. Multivariate ISI distance is an extension of ISI-distance to multiple spike train. Spike-Distance was proposed to essentially overcome the disadvantages of ISI-distance. Spike-Distance is sensitive to both firing rate of neurons and to the fraction of coincident spikes. Spike distance is essentially parameter free, time scale adaptive and time resolved.

In this chapter, we discuss different spike synchronization measures and their application to spiking neuron models and EEG recordings of patients with temporal lobe epilepsy. In particular, we discuss the measure of Spike-Distance developed by Kreuz et al. [62] to estimate the synchronization between spike trains of different brain sites. We first explain the theory behind spike distance and test it on coupled neuronal models. We discover its limilations and propose a novel and improved measure of spike synchronization based on event synchronization [59]. We then apply the new measure of event synchronization and spike distance on epileptic EEG data and observe the long-term and short-term trends in spike synchronization that lead to seizures.

3.2 Spike Distance

Spike-Distance is a measure of spike synchrony and is sensitive to spike timings and fraction of coincident spikes. The advantage of spike distance lies in the fact that it is parameter-free and time-scale adaptive. The measure is computationally very simple and relies on the differences between spike times of two spike trains under consideration and the interspike interval.

Consider two point process x and y containing M_x and M_y spikes respectively. Let t_i^x and t_j^y denote the time of occurence of spikes in process x and y respectively.

We define t_x and t_y the time series vector containing spike times of x and y as

$$t_x = \{t_1^x, t_2^x \ldots t_{M_x}^x\} \tag{3.1}$$

$$t_y = \{t_1^y, t_2^y \ldots t_{M_y}^y\} \tag{3.2}$$

Now we define $t_P(t)$, the time instant of the previous spike as

$$t_P^k(t) = max(t_i^k | t_i^k \leq t), \quad k \in (x,y) \quad and \quad t_1^k \leq t \leq t_M^k \tag{3.3}$$

Similarly we define $t_F(t)$, the time instant of the following spike as

$$t_F^k(t) = min(t_i^k | t_i^k > t), \quad k \in (x,y) \quad and \quad t_1^k \leq t \leq t_M^k \tag{3.4}$$

The interspike interval can be defined as

$$x_{ISI}^k(t) = t_F^k(t) - t_P^k(t) \tag{3.5}$$

We estimate the instantaneous difference between the previous and following spike times of x and y as

$$\Delta t_P(t) = t_P^x(t) - t_P^y(t) \tag{3.6}$$

and

$$\Delta t_F(t) = t_F^x(t) - t_F^y(t) \tag{3.7}$$

The locally weighted average of $\Delta t_P(t)$ and $\Delta t_F(t)$ is estimated as

$$< \Delta t_j(t) >_{j=P,F} = \frac{\sum\limits_{j=P,F} |\Delta t_j(t)| f(x_j^k(t))}{\sum\limits_{j=P,F} f(x_j^k(t))} \quad where \;\; k \in (x,y) \tag{3.8}$$

To define a weighting function, we estimate $d_P^k(t)$ and $d_F^k(t)$ as

$$d_P^k(t) = t - t_P^k(t) \tag{3.9}$$

and

$$d_F^k(t) = t_F^k(t) - t \tag{3.10}$$

The values $d_P^k(t)$ and $d_F^k(t)$ are the distance to the previous and following spike.

The weighting function $f(x_P^k(t))$ and $f(x_F^k(t))$ are then defined as inverse of the average value of $d_P^k(t)$ and $d_F^k(t)$ over $k = (x,y)$. We denote this average over the two spike trains $k = (x,y)$, as $\langle d_P(t)\rangle_k$ and $\langle d_F(t)\rangle_k$. Replacing $f(x_P^k(t))$ and $f(x_F^k(t))$ in Eq. 3.8 we get

$$\begin{aligned}\langle \Delta t_j(t)\rangle_{j=P,F} &= \frac{|\Delta t_P(t)|\frac{1}{\langle d_P(t)\rangle_k} + |\Delta t_F(t)|\frac{1}{\langle d_F(t)\rangle_k}}{\frac{1}{<d_P(t)>_k} + \frac{1}{<d_F(t)>_k}} \\ &= \frac{|\Delta t_P(t)|\langle d_F(t)\rangle_k + |\Delta t_F(t)|\langle d_P(t)\rangle_k}{\langle d_P(t)\rangle_k + \langle d_F(t)\rangle_k}\end{aligned} \tag{3.11}$$

The denominator of Eq. 3.11 is the mean inter spike interval (ISI) of spike train x and y, which we denote $\langle x_{ISI}(t)\rangle_k$. Thus Eq. 3.11 can be written as

$$\langle \Delta t_j(t)\rangle_{j=P,F} = \frac{|\Delta t_P(t)|\langle d_F(t)\rangle_k + |\Delta t_F(t)|\langle d_P(t)\rangle_k}{\langle x_{ISI}(t)\rangle_k} \tag{3.12}$$

To make the measure of spike distance time-scale invariant (i.e insensitive to compression and stretching), we divide $\langle \Delta t_j(t)\rangle$ by $\langle x_{ISI}(t)\rangle_k$. We thus get the instantaneous spike distance, $S(t)$ as

$$S(t) = \frac{|\Delta t_P(t)|\langle d_F(t)\rangle_k + |\Delta t_F(t)|\langle d_P(t)\rangle_k}{\langle x_{ISI}(t)\rangle_k^2} \tag{3.13}$$

The bivariate spike distance is then estimated as

$$D_s = \frac{1}{T}\int_{t=0}^{T} S(t)dt \tag{3.14}$$

The value of D_s is bounded between $[0,1]$ with a value of zero occuring only for two perfectly identical spike trains.

3.3 EPILEPTIC SPIKE SYNCHRONIZATION

A fundamental problem with bivariate spike distance is that it leads to erroneous values of synchronization if the spikes trains are well separated in time. For example, if spike train t_x occurs in the time interval $[t_A^x \ t_B^x]$ and spike train t_y occurs in the time interval $[t_A^y \ t_B^y]$, where $t_A^y >> t_B^x$, we obtain D_s close to 0. This is due to the localized nature of estimation of spike distance. We further investigate this in the subsequent section. To overcome this we propose an improved version of event synchronization [59] which is parameter-free and also takes into consideration the local dynamics of the spike trains.

Consider two spike trains x and y, as defined in Section 3.2 with their spike times given in Eq. 3.2. We define $e^i(x|y)$ for spike i in process x as

$$e^i(x|y) = 0.5 \exp\Big(- \frac{d_i^{min}}{(t_{i+1}^x - t_i^x)} \Big) \quad i = [1, 2 \ldots . M_x] \tag{3.15}$$

where $d_i^{min} = min(t_j^y - t_i^x)$ for $j \in (1, 2 \ldots M_y)$ such that $d_i^{min} \geq 0$. Similarly we estimate $e^i(y|x)$ for spike i in process y as

$$e^i(y|x) = 0.5 \exp\Big(- \frac{d_i^{min}}{(t_{i+1}^y - t_i^y)} \Big) \quad i = [1, 2 \ldots . M_y] \tag{3.16}$$

Now we estimate the symmetrical and asymmetrical combinations of $e(x|y)$ and $e(y|x)$ as

$$Q = \frac{\sum_{i=1}^{M_x - 1} e^i(x|y) + \sum_{i=1}^{M_y - 1} e^i(y|x)}{\sqrt{(M_x - 1)(M_y - 1)}} \tag{3.17}$$

$$I_{x \to y} = N_n \frac{\sum_{i=1}^{M_x - 1} e^i(x|y) - \sum_{i=1}^{M_y - 1} e^i(y|x)}{\sqrt{(M_x - 1)(M_y - 1)}} \tag{3.18}$$

where $N_n = \frac{2}{1 - e^{-1}}$ is the normalization factor so that the value of $I_{x->y}$ is bounded between $[-1 \ 1]$. $I_{x \to y}$ tends to 1 when process x drives process y and -1 when

process y drives process x. Q takes values between $[0\ \ 1]$, 0 when spike trains are desynchronzied and 1 when there is perfect coincidence of spikes.

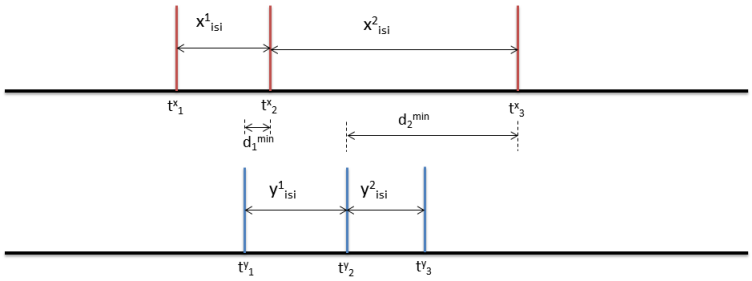

Figure 3.1: Pictorial representation of estimation of the measure Epileptic Spike Synchronization

Quiroga's definition of event synchronization laid a constrain parameter τ for the time difference between spikes in two channels. However due to the dynamical variation of EEG, a global definition of τ is not intuitive. We compensate it by using an exponential decay function of interspike interval of the point process under consideration. The modified measure of event synchronization incorporates the firing rate of the process into the calculation, making it robust to dynamical changes.

3.4 Application to Spiking Neuron Models

In 1984, Hindmarsh and Rose introduced the Hindmarsh-Rose (HR) coupled neuronal model for burst action potential generation [63]. Compared to the Hodgkin-Huxley model [64] for action potential, the HR model is less complex and has better convergence properties. We analyze the performance of Spike Distance (SD) and Modified Event Synchronization (MES) in estimating synchronization and direction of coupling between coupled nonlinear HR models.

The HR model can be described as follows

$$\begin{aligned} \dot{x}_i &= y_i - ax_i^3 + bx_i^2 - z_i + I_{0_i} + \frac{\alpha}{K} \sum_{j=1, j\neq i}^{N} (x_j - x_i) \\ \dot{y}_i &= c - dx_i^2 - y_i \\ \dot{z}_i &= r[s(x_i - x_0) - z_i] \end{aligned} \tag{3.19}$$

where x,y, and z represent membrane potential, fast current and slow current respectively with $a = 1.0$, $b = 3.0$, $c = 1.0$, $d = 5.0$, $r = 0.006$, $s = 4.0$ and $x_0 = 1.6$; K is the number of connections per neuron. The amplitude of external current applied to neuron i is controlled by the parameter I_{0_i}. The value of $I_{0_i} \in [2.5\ 3.4]$ is generated randomly, such that the oscillators have nonidentical properties. The membrane potential for input current $I_0 = 3.3$ is shown in Fig. 3.2. Parameter α determines the strength of coupling between the oscillators.

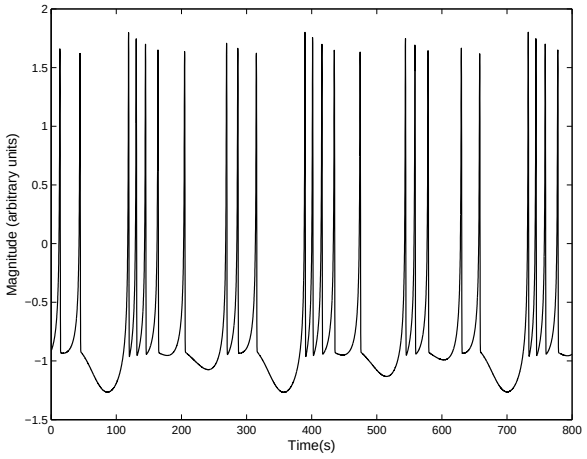

Figure 3.2: Membrane potential generated using HR model

3.4.1 Uni-directionally Coupled Oscillators

Two coupled Hindmarsh Rose oscillator models were constructed with oscillator X driving Y (See Fig. 3.3A). The coupling strength (α_{12}) is varied from 0 (No

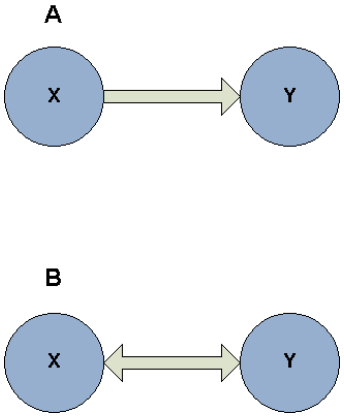

Figure 3.3: Coupled oscillator network (A) Uni-directionally coupled Hindmarsh Rose (HR) oscillators (B) Bi-directionally coupled HR oscillators

coupling) to 2.5 (High Coupling), whereas α_{21}, the strength of coupling from Y to X is kept at 0. The data is generated from Eq. 3.20 using a 4^{th} order Runge-Kutta integration method with integration step of 0.1. Per value of α_{12}, 5000 points from the time series of oscillators X and Y are generated and the first cordinate x_1, x_2 are used. The process is repeated 1000 times for different values of I_0. The D_S, Q and $I_{X\to Y}$ are estimated for each realization. The variation of D_S, Q and $I_{X\to Y}$ with increasing coupling strength is shown in Fig. 3.4

From Fig. 3.4 we observe that D_S saturates to 0 for α_{12} close to 1.5, whereas Q monotonically increases till perfect coincidence of spike trains is achieved. The directional information transfer metric $I_{X\to Y}$ increases monotonically till $\alpha_{12} = 0.85$ and then monotonically decreases and saturates at $\alpha_{12} = 1.5$. The decrease in $I_{X\to Y}$ can be attributed to the increase in synchronization between the oscillators.

3.4.2 Bi-directionally Coupled Oscillators

Two bi-directionally coupled HR oscillators are constructed as in Fig. 3.3B. The coupling strength ($\alpha_{12} = \alpha_{21}$) is varied from 0 to 2.5 in steps of 0.025. Similar to

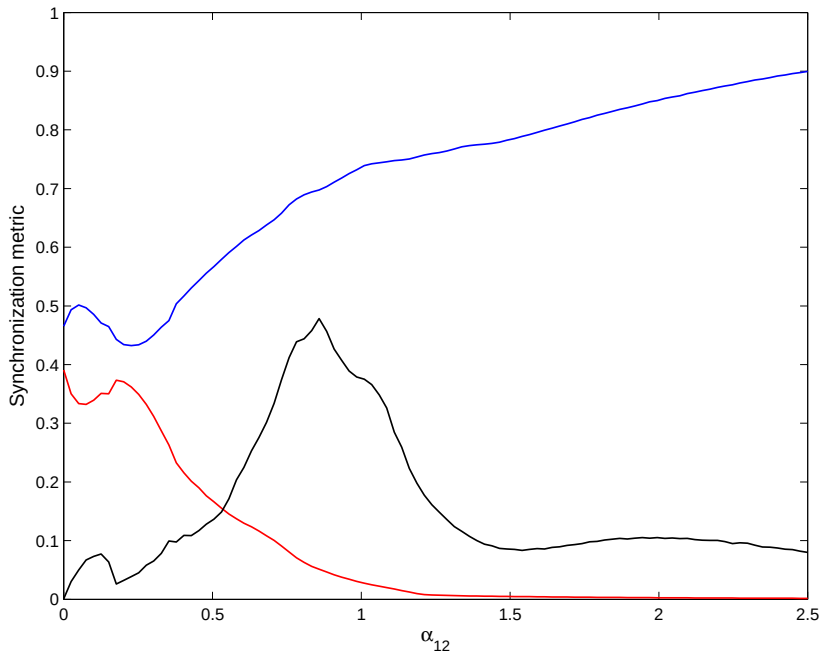

Figure 3.4: Dynamical synchronization between coupled nonlinear HR spiking neurons as a function of uni-directional coupling coefficient α_{12} for the oscillator model in 3.3A. The red line depicts the results from synchronization metric D_S. The values of D_S approach 0 (perfect coincidence of spikes) with increasing coupling strength. The blue line depicts the modified event synchronization measure Q and the black line depicts the directional information transfer metric $I_{X\to Y}$

.

the uni-directionally coupled oscillators, we generate 5000 points from time series of oscillator X and Y for every α are generated and the first cordinate x_1, x_2 are used. The process is repeated 1000 times for different values of I_0. The D_S, Q and $I_{X\to Y}$ are estimated for each realization. The variation of D_S, Q and $I_{X\to Y}$ with increasing coupling strength is shown in Fig. 3.5

3.4.3 Spike Distance (SD) vs. Epileptic Spike Synchronization (ESS):

The analysis of both measures SD and ESS on coupled oscillators revealed that ESS is more sensitive to subtle changes in synchronization compared to SD (see

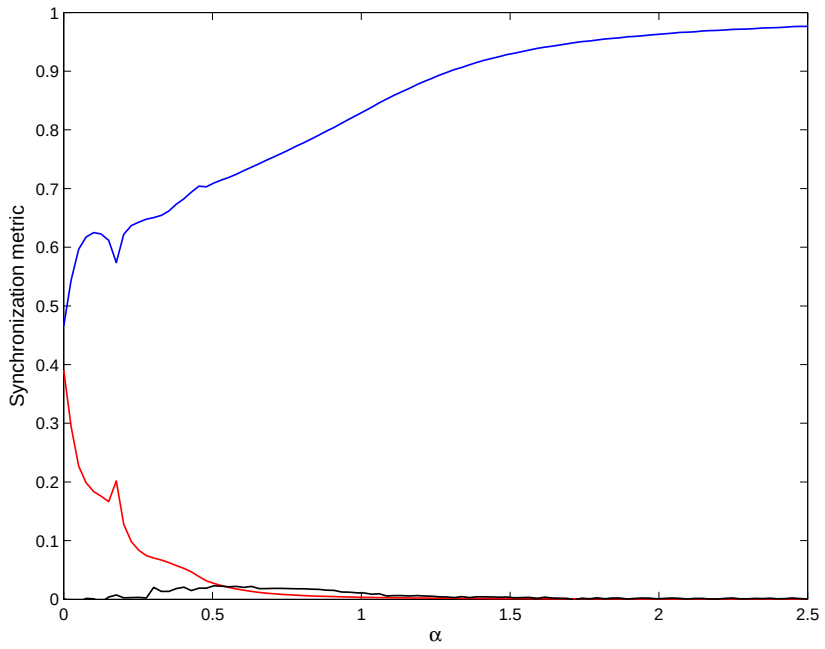

Figure 3.5: Dynamical synchronization between coupled nonlinear spiking neuron models as a function of bi-directional coupling coefficient α for the oscillator model in Fig. 3.3B. The red line depicts the synchronization metric D_S. Observe that the values of D_S approaches 0 (perfect coincidence of spikes) with increasing coupling strength. The blue line depicts the modified event synchronization measure Q and the black line depicts the directional information transfer metric $I_{X\to Y}$ (note that it has very small values for all coupling coefficient values).

Fig. 3.4 and 3.5). ESS also allows us to determine directional interactions between spike trains using the metric $I_{x\to y}$. It should be observed that both SD and ESS are time-scale invariant metrics, i.e. they are not affected by stretching or contracting the spike train series. We now provide an extreme scenario of SD, where the synchronization metric D_S estimates ambiguous values for synchrony. To show this, we consider two spike trains X and Y where spike times were generated by a Gaussian random process (see Fig. 3.6(a)). We estimate the SD and ESS measures for these spike trains and obtain $D_S = 0.062$ and $Q = 0.39$. Now we shift the spike train

Y by 5000 time points to obtain a new spike train series (see Fig. 3.6(b)). We re-estimate the synchrony metrics and obtain $D_S = 0.20$ and $Q = 0$. Observe that the spike trains X and Y are totally offset in time, however D_S gives non-zero values for synchrony between the spike trains, while Q converges to zero as expected. Even the value of D_S for the case where the spikes in X and Y occur within the same time scale is quite low ($D_S = 0.062$), indicating synchronization, however both spike trains are uncoupled (since they are generated at random using independent seeds).

We further investigate this by providing an variable offset to the spike train Y (with respect to its initial spike times) and re-estimating the values of D_S and Q at every offset value. The resulting D_S and Q as a function of time offset are shown in Fig. 3.7.

It can be observed from the figure that with increasing offset the estimate of D_S tends to increase initially (indicating decreasing synchronization). This is mainly due to the effect of increasing values of Δt_P and Δt_F with increasing offset in the estimation of $S(t)$. However with increasing offset, $\langle x_{ISI} \rangle_k$ tends to increase, countering the increase in Δt_P and Δt_F and thus decreasing the value of $S(t)$. It appears that ESS performs better in quantifying synchronization between spike trains when compared to SD.

3.5 Application to Interictal Spikes

Epileptic spikes were detected per electrode for the entire duration of recording using improved morphological filter with adaptive structuring element as described in Chapter 2. The proposed measures of synchrony (D_S and Q) and direction ($I_{x \to y}$) were estimated from successive EEG segments of 30.72 seconds duration (6144 points per segment at 200 Hz sampling rate) and overlapped by 10.24 seconds (2048 points) per pair of electrodes for the days of EEG recording per patient. The de-

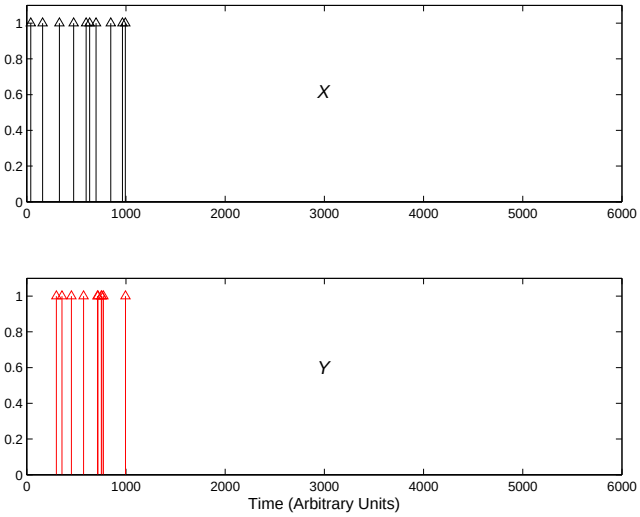

(a)

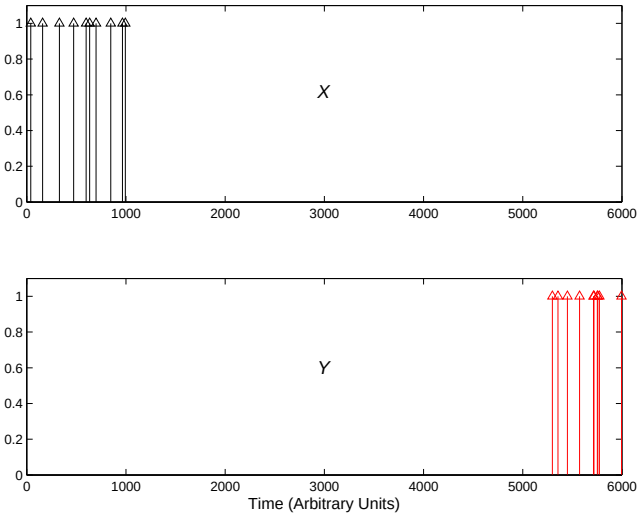

(b)

Figure 3.6: Comparison of SD and ESS. (a) Spike trains X and Y occur within the same time frame ($D_S = 0.062, Q = 0.39$) (b) Spike train Y is offset in time with respect to spike train X ($D_S = 0.20, Q = 0$).

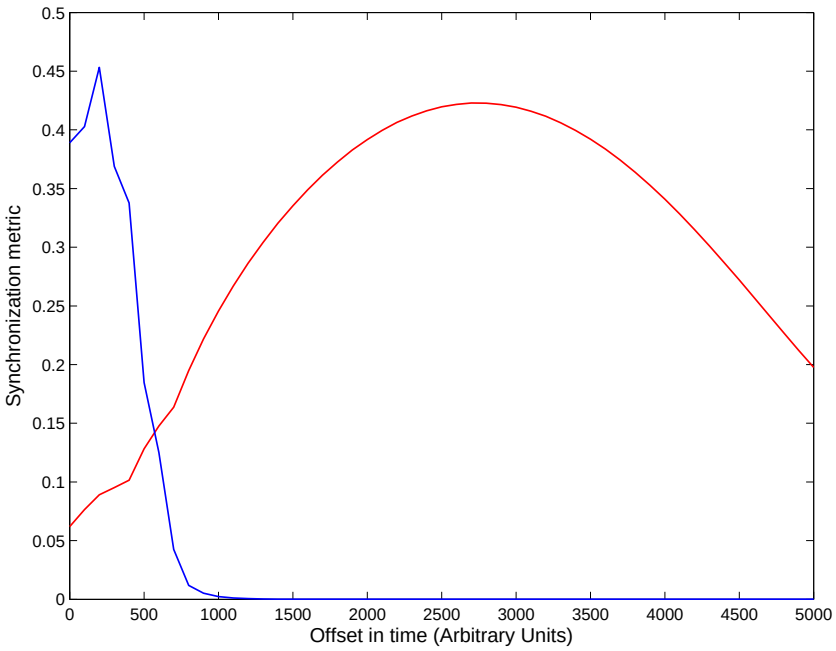

Figure 3.7: Effect of spike train offset in the estimation of synchronization metrics D_S and Q. The red curve depicts an increasing D_S value (decreasing synchronization) upto an offset of around 2800 followed by decreasing D_S value (increasing synchronization). The blue curve depicts a decreasing Q value (decreasing synchronization) with increasing offset as expected.

tection of spikes and estimation of measures of synchrony was performed using the High Performance Computing facility at Arizona State University.

3.5.1 Optimal Window Size:

Selection of the optimal window size for estimation of measures of synchrony from EEG data is of outmost importance. A low number of spikes per window will lead to improper estimation of synchrony measures, while using a large window size may lead to non-stationarity issues. To obtain an optimal window size, we estimate the spike rate metric as described in [65]. For a window of size T sec, containing n spikes, the rate metric r_T is given as n/T (the number of spikes per second).

We estimate r_T for $T \in [10.24, 20.48, 30.72, 40.96, 51.20, 61.44]$ sec in a pool of electrodes from recorded EEG data. We then estimate the spatio-temporal average difference $D_{r,k}^{T_i}$ for electrode k as follows

$$D_{r,k}^{T_i} = \frac{1}{N} \sum_{j=1, j\neq i}^{6} \sum_{t=1}^{N} (r_{T_i}^k(t) - r_{T_j}^k(t))^2 \tag{3.20}$$

where $r_{T_i}^k(t)$ is the spiking rate metric at time t for electrode k for a window length of T_i. The plot of $D_{r,k}^{T_i}$ for k $\in$ [LTD2, RTD1, LST1, RST2, LOF4, ROF4] is shown in Fig. 3.8. It can be observed that $D_{r,k}^{T_i}$ converges to a minimum for $T_i = 30.72$.

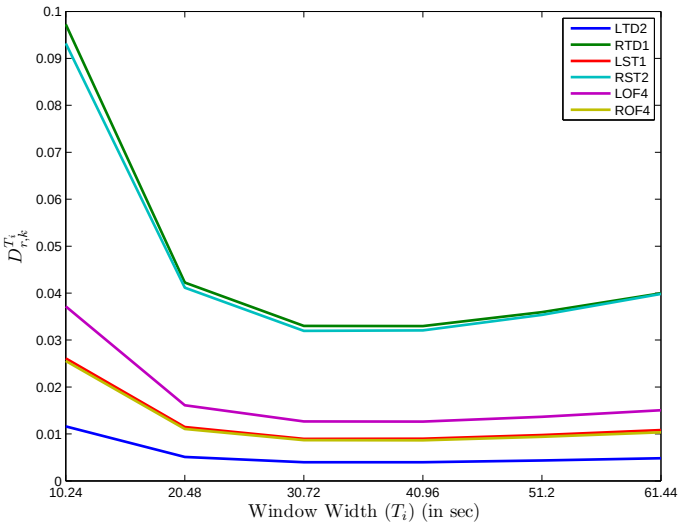

Figure 3.8: Selection of optimal window size. Values of $D_{r,k}^{T_i}$ are plotted for different values of T_i.

Thus we use a window size of 30.72 for our ensuing analysis.

3.5.2 Long-term evolution of synchronization

Ictogenesis, the transistion of an epileptic brain from interictal to ictal states is a significant area of research for understanding the dynamical behavior of the epileptic brain. Previous work in our lab and elsewhere has shown that the transition from an interictal state to ictal state is not abrupt [24, 23, 25, 66, 67, 68].

Within the framework of spike synchronization presented in the previous sections, we investigate whether there is any quantitative evidence supporting the long-term evolution of the brain towards the first clinically manifested seizure in our data. To this effect we did not consider subclinical seizures (seizures with no clinical manifestation) in the analysis and followed only the trends in synchronization from the start of an EEG recording till the first clinical seizure.

To extract the long-term trends from the synchronization profiles we use a Hodrick-Prescott (HP) filter [69]. HP filter is used to separate cyclical from trend components in the raw data, and has found application in the study of macroeconomics. The filter can be formulated as follows. Consider a time series $y_t = c_t + T_t$, where c_t is the cyclical component and T_t is the trend component. We then minimize the quantity':

$$\sum_{t=1}^{T}(y_t - T_t)^2 + \lambda \sum_{t=2}^{T-1}[(T_{t+1} - T_t) - (T_t - T_{t-1})]^2 \tag{3.21}$$

where λ is a positive constant that penalizes the trend component. The first term in Eq. 3.21 determines the goodness of fit and the second term is the second derivative of the trend component and quantifies the smoothness of the trend component. As $\lambda \to \infty$, the solution approaches the least squares fit and as $\lambda \to 0$, the trend component $T_t \to y_t$. For our data, the performance of HP filter did not outperform that of a simple low-pass moving average filter. However, moving average filter suffered from edge artifacts and hence we opted for HP filter.

Fig. 3.9 shows the long-term increase in spike synchronization in a subset of pairs of electrodes in Patient 1. Similar behavior can be observed in subset of pairs of electrodes in Patient 2 (see Fig. 3.10). This indicates that the brain transits from a normal state to a state of abnormal synchronization during the interictal time period. The incidence of seizure to break this abnormal synchronization was previously

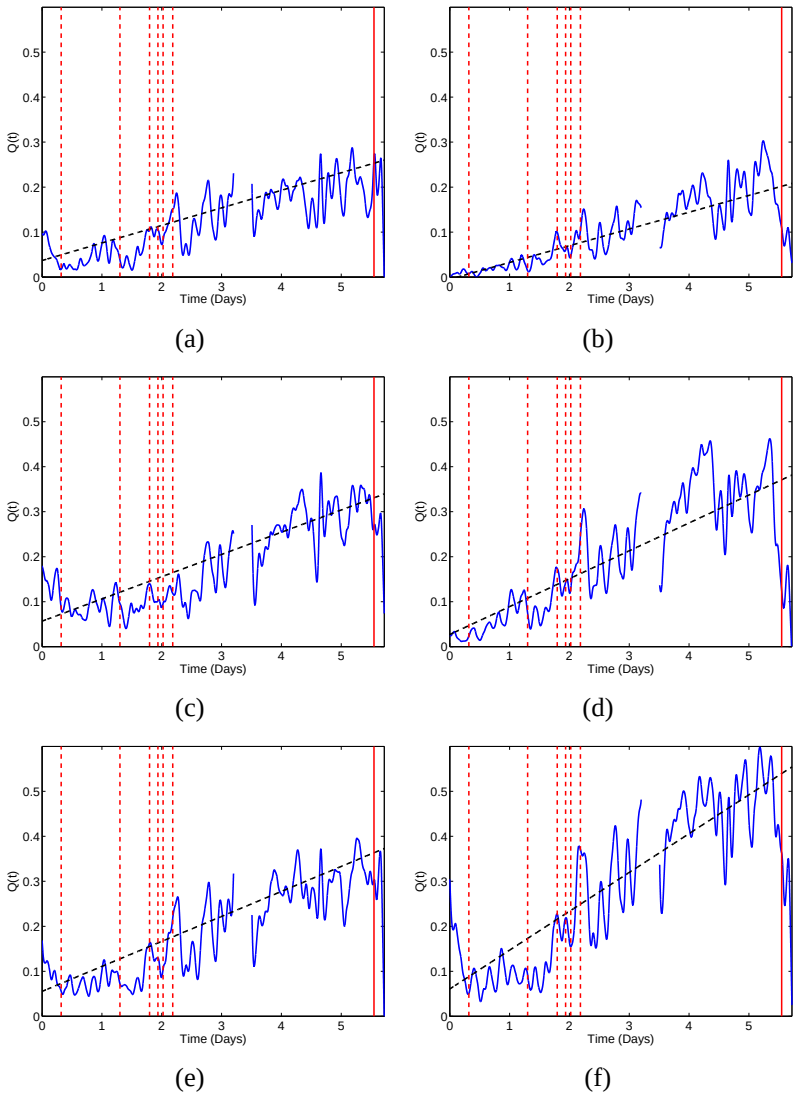

Figure 3.9: Long-term trends in spike synchronization ($Q(t)$) profile for six pairs of electrode till the incidence of first clinical seizure in Patient 1. (a) LTD4-RTD4 (b) LOF1-ROF1 (c) LTD3-LTD4 (d) ROF3-ROF4 (e) RTD3-RTD4 (f) RTD8-RTD10. The red dashed line denotes subclinical seizures. The red solid lines denotes the first clinical seizure. The black dashed line is the line of best fit for the smoothed synchronization profile. Notice the gap in plotted $Q(t)$ profile of approzimately 6 hours between the 3^{rd} and 4^{th} day, due to the presence of artifacts in the recorded EEG data.

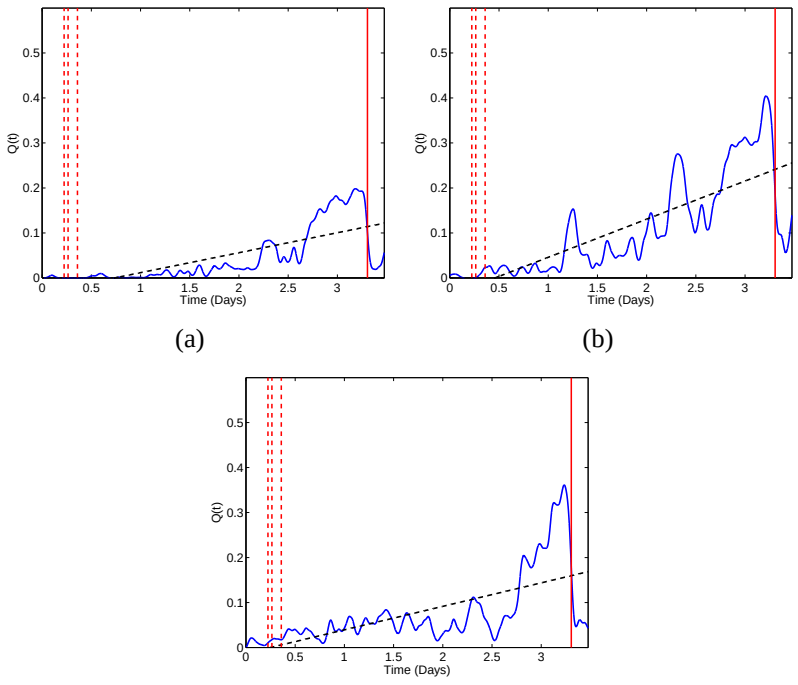

Figure 3.10: Long-term trends in spike synchronization ($Q(t)$) profile for six pairs of electrodes till the incidence of first clinical seizure in Patient 2. (a) LOF2-ROF3 (b) LTD2-LST3 (c) RST2-RST3. The vertical red and black dashed lines are as in Fig. 3.9.

hypothesized by Iasemidis et. al. [23, 25]. However not all pairs of electrode exhibit such an abnormal and progressive increase in synchronization. For example, in Fig. 3.11 we can observe that there are pairs of electrode where the synchronization level remains approximately constant. This indicates that selection of appropriate pairs is important in observing long-term trends in EEG. These results can be interpreted in two ways

- As a seizure approaches, the spikes generated at one brain site propagate to another site. This means that different parts of the brain start to synchronize with each other thus enabling faster transmission of information among them.

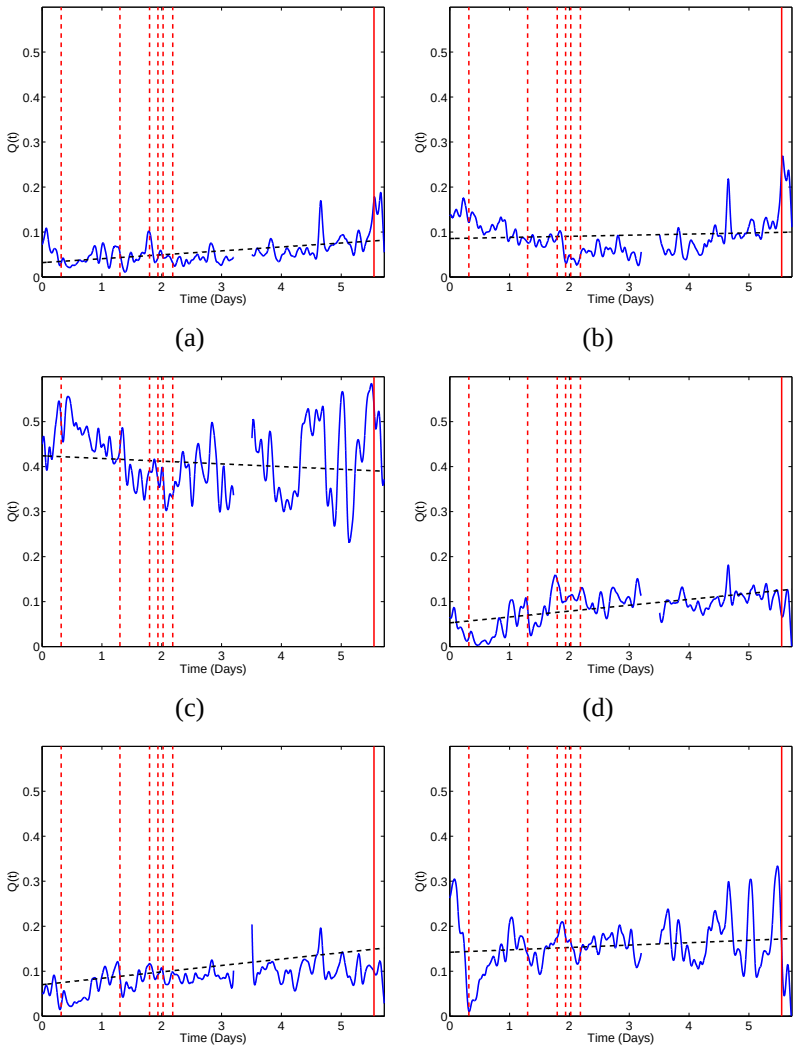

Figure 3.11: Long-term trends in spike synchronization profiles ($Q(t)$) for six pairs of electrodes till the incidence of first clinical seizure in Patient 1. (a) LTD1-LTD4 (b) LTD2-LST1 (c) RTD1-RST2 (d) RTD1-LOF4 (e) RTD2-LOF4 (f) RST3-ROF3. The vertical red and black dashed lines are as in Fig 3.9.

- The dynamics of the underlying governing the brain sites synchronize which leads to generation of spikes at the times of synchronization.

An important question that remains unanswered is the causal relationship between spikes and synchronization, i.e. whether spikes causes synchronization or vice versa. At present, we lack any quantitative evidence supporting either case.

3.5.3 Interictal to Ictal Transition:

Previous studies from epileptic seizure prediction have revealed the existence of a preictal period where the dynamics of different brain sites become entrained or synchronized. The existence of a pre-ictal period provides us with a time window where prediction of epileptic seizure and intervention to prevent seizure precipitation becomes possible. However, physiological substrate of the observed entrainment of dynamics was never established. In this section we further investigate whether pre-ictal synchronization could be a physiological substrate for the epileptic spikes can be observed and its relation with the preictal entrainment observed by Iasemidis et.al in [23, 70, 71, 24, 25].

Fig. 3.12 shows the plots of synchronization profiles for three pairs of electrodes from the left hemisphere (LTD1-LOF2), right hemisphere (RTD2-ROF3) and contralateral hemispheres (RTD6-LOF2)as well as in the spatially averaged $Q(t)$ profile. We see that progressive increase in synchronization can be observed hours to minutes prior to the onset of epileptic seizures denoted by red lines. Postictally desynchronization of epileptic spikes occurs for over hours.

To compare across seizures and patients, for each brain site i in every patient we estimated the spatially averaged synchronization value (ESS^i_T) at time t as

$$ESS^i_T(t) = \sum_{j=1, j\neq i}^{N_e} ESS_{i,j}(t) \tag{3.22}$$

where $ESS_{i,j}(t)$ is the epileptic spike synchronization value at time t between brain sites i and j.

Fig. 3.13 shows the average ESS_T across seizures of four patients for two hours of preictal and two hours of postictal centered at the seizure. The presence of high preictal synchronization and postictal desynchronization across patients supports our original hypothesis. We then tested whether such transistions from abnormal synchronization to desynchronization are present during the interictal period. For each patient, we randomly selected N_{SZ} time points in the interictal, where N_{SZ} is the number of seizures the patient had in the duration of his/her EEG recording. We then estimated the average ESS_T at these randomly selected time points from the interictal periods (see Fig. 3.14). We observed that such a dynamical transition from synchronization to desynchronization occurs mostly at seizures when compared to interictal. We statistically validate this observation using our measure of resetting in Chapter 6.

Fig. 3.15 compares the dynamical measure of synchronization (T-index) between lyapunov developed by Iasemidis et al. with $Q(t)$ at a seizure. The pairs were selected based on the criteria defined in [72] and their average T-index and $Q(t)$ profiles were estimated. Similar changes in dynamical synchronization can be observed in both the $Q(t)$ profile and T-index profile near seizures. Comparing the long-term trends of synchronization in individual pairs using either measure, we observe that there are pairs of sites where we can observe similar trends in both profiles (see Fig. 3.16(a) and (b)) and pairs with opposite trends (see Fig. 3.16(c)).

3.5.4 Dynamical changes at sub-clinical seizures

Sub-clinical seizures are epileptic seizures with electrographic but without clinical manifestations (correlates). Typically, the seizure manifests itself electrographi-

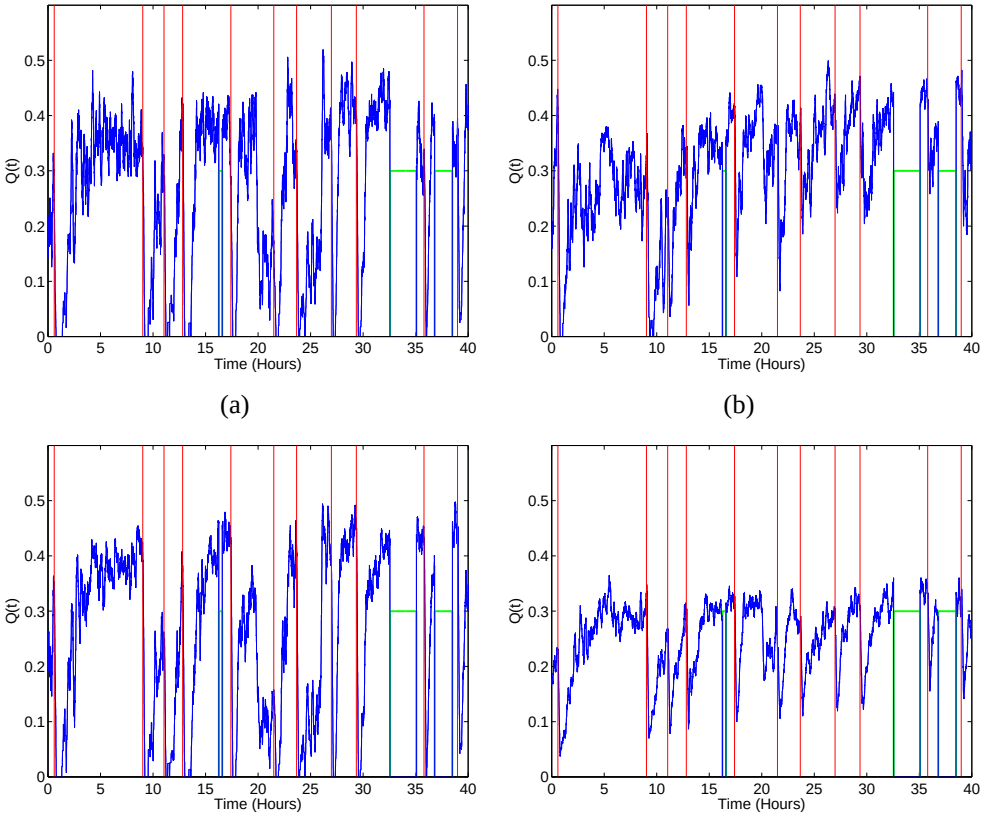

Figure 3.12: Dynamical changes in synchronization profile ($Q(t)$) during seizures for 40 hours of continuous EEG recording of Patient 1 for (a) LTD1-LOF2. (b) RTD1-ROF3. (c) Electrode pair RTD6-LOF2. (d) Spatial average of $Q(t)$ across all pairs of sites. Red solid lines denote clinical seizures. The green horizontal bars indicate gap in the recording.

cally around the focus. We can view sub-clinical seizures as electrographic seizures with spatially limited resetting power, i.e. we might be able to observe resetting during these types of seizure in a few localized regions of the brain. Thus a metric based on many pair counts may not be ideal for quantifying the dynamical changes occuring at sub-clinical seizures.

Fig. 3.17 shows the dynamical changes in synchronization at sub-clinical seizures from two patients. We can observe that there is sharp drop in synchronization at a

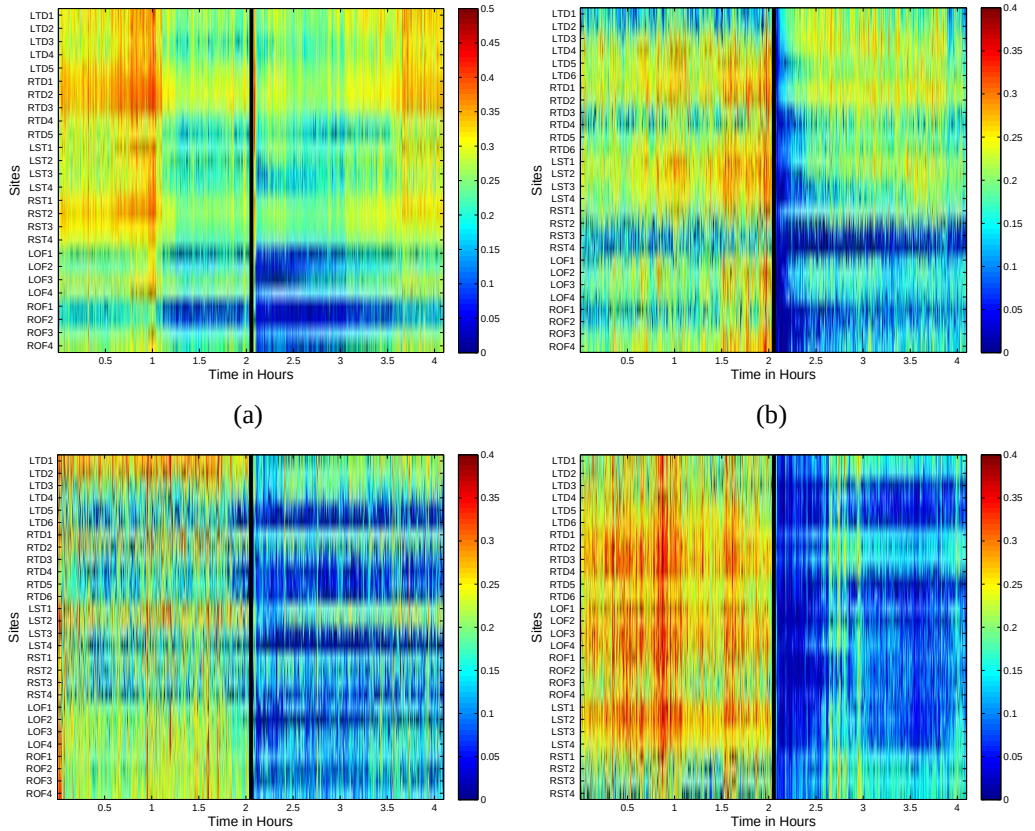

Figure 3.13: Dynamical changes in spike synchronization profiles around seizures in 4 hours of continuous EEG recording from four patients. (a) Patient 1. (b) Patient 2. (c) Patient 3. (d) Patient 4. The black vertical line denotes the seizure occurence. We can observe increased preictal synchronization and posticta desynchronization. This supports our hypothesis that seizures occur to reset the abnormal synchronization that may exist between brain regions

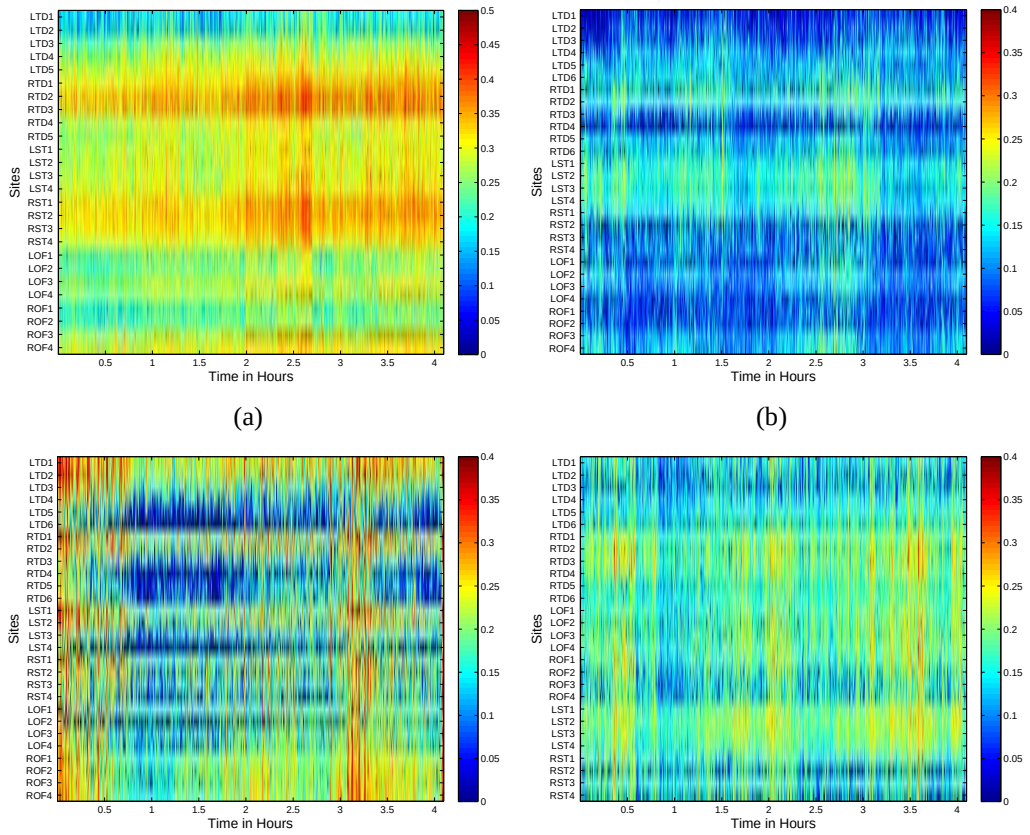

Figure 3.14: Dynamical changes in spike synchronization profile at random time points in the interictal period (4 hours of continuous EEG recording) from four patients. (a) Patient 1. (b) Patient 2. (c) Patient 3. (d) Patient 4.

sub-clinical seizure. However the spatial extent of this change in dynamics is limited.

3.6 Conclusion

In this chapter, we investigated the spatial synchronization of interictal spikes in EEG from patients with focal epilepsy. To measure the degree of synchronization between the spike trains of different channels, we used a modified version of event synchronization. We called this Epileptic Spike Synchronization (ESS) proposed by Quiroga et al. We also investigated a novel measure of spike synchrony, called

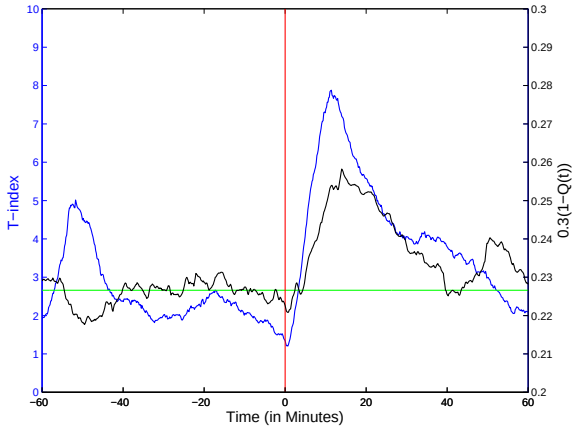

Figure 3.15: Comparison between the measure of synchronization of nonlinear dynamics (T-index) and Spike Synchronization ($Q(t)$) around a seizure. The blue curve denotes the T-index of preictally entrained pairs (selected based on the criteria defined in [72]). The green horizontal line indicates the statistical threshold of synchronization for Tindex. The black curve denotes the average spike synchronization profile for the same pairs. The vertical red line denotes the seizure. Notice that both profiles have been scaled down for representation purposes.

Spike Distance (SD), proposed by Kreuz et al. We evaluated the performance of ESS and SD on uni-directionally and bi-directionally coupled spiking neuron models. Analysis revealed that ESS performed better than SD in measuring synchrony between spike trains.

Subsequent application of measures of spike synchrony on epileptic spikes in the EEG data from five patients revealed monotonically increasing long-term synchronization between spike trains of different brain sites long before the first clinical seizure. The drop in synchrony at the onset of the first clinical seizure validates our hypothesis that seizures occur to break high entrainment or synchrony in the pathological brain network. We also observed progressive increase in synchronization in the preictal period and desynchronization in the postictal period of subsequent seizures.

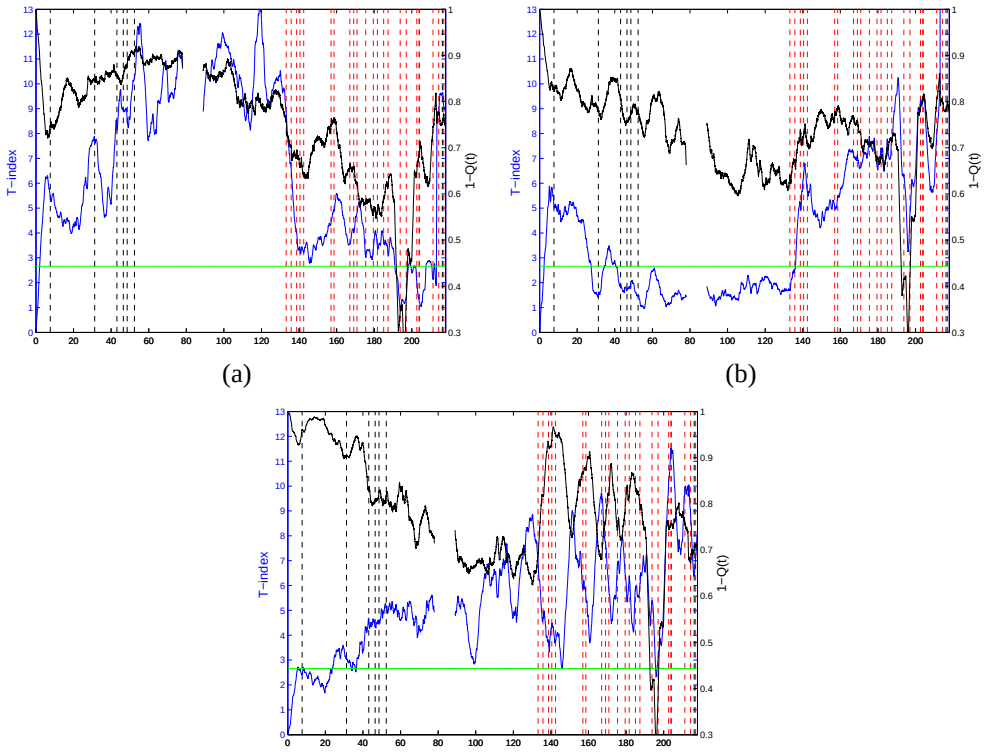

Figure 3.16: Comparison between the measure of synchronization of nonlinear dynamics (T-index) and Spike Synchronization ($1 - Q(t)$) for the electrode pairs (a) LTD2-LTD3 (b) LTD3-RTD2 (c) LST4-LOF2. The blue curve denotes the T-index. The green horizontal line indicates the statistical threshold of synchronization for T-index. The black curve denotes the average spike synchronization profile for the same site selected in the (average) T-index. The vertical red dashed line denotes the clinical seizures. The vertical dashed black lines denote subclinical seizures.

The presence of preictal synchronization hours to minutes prior to the onset of the ictal state implies the predictive value for seizure occurrence interictal spikes may have. Based on these results a possible role of epileptic spikes n ictogenesis in unveiled. A simple computational model for generation of interictal spikes has been proposed and discussed by Demont et al. [73]. The model simulated interictal spike-like activity of different amplitude, duration and morphology when the excitatory current (AMPA and NMDA) and inhibitatory (GABA) current to the

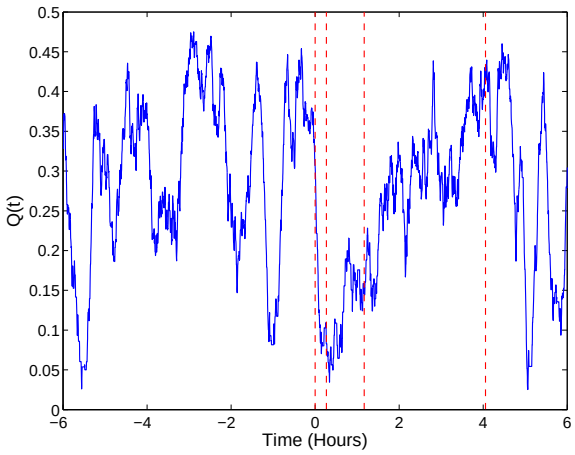

(a)

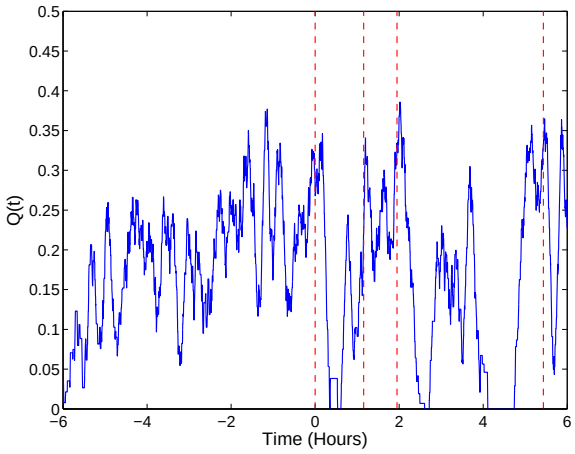

(b)

Figure 3.17: Different trends of spike synchronization at subclinical seizures. (a) $Q(t)$ profile for the pair RTD1-ROF3 from Patient 2 (b) $Q(t)$ profile for the pair LOF3-ROF4 from Patient 3. The vertical red dashed lines denote subclinical seizures.

modeled neuronal network is tuned appropriately. With increased excitatory current the amplitude of the spikes increased whereas the negative wave following the spikes became more pronounced with decreased GABA conductance. With further increase in excitatory current to the model and reduced inhibitatory current, the model started generating ictal like activity. Such an increased excitation can be caused by increase in positive feedback within the epileptogenic focus as proposed by [74, 75, 76, 77, 78]. We propose that long prior to complex partial seizures the excitation spreads and brain sites get recruited. When ictal activity finally begins, it propagates to the recruited brain sites leading to secondary generalization. However, we found no substantial spread of interictal spike synchronization prior to a subclinical seizures, and this might be why they remain tend to be localized to a few brain regions mostly around the focus. This gives us a good general concept on how interictal spikes and different types seizures may be related. However a formal conclusion could be drawn only after investigating these phenomena using more complex models of ictogenesis and engaging a larger patient population.

Upto this point we investigated the dynamics of spiking activity in the interictal, preictal and postictal periods. The role of epileptogenic focus in interictal spike activity and ictogenesis needs to be further investigated. In the next chapter we address exactly this question. In particular we investigate if we can localize the epileptogenic focus by complementing our spatio-temporal analysis of interictal spikes with insights from graph theory and social networking.

Chapter 4

EPILEPTOGENIC FOCUS LOCALIZATION

4.1 INTRODUCTION

An epileptogenic focus is defined as the particular area(s) in the brain that first exhibits the electrographical onset of a seizure. Typically epileptogenic focus is identified by physicians through visual inspection of ictal EEG and images of brain produced by modalities like PET, MRI, SPECT. However visual marking of seizure onset is a time-consuming process and neccessiate the recording of seizures, which means that the patient has to be admitted to the hospital and withdraw from his/her antiepileptic medication.

Identification of the epileptogenic focus is the primary objective in presurgical evaluation of patients who are deemed candidates for ablative removal of focus. Once the focus is accurately identified, resection of focal tissue is performed to reduce seizure frequency or abolish seizures completely. A high success rate (around 70%) has been reported in these cases. However it should be noted that not all epilepsy patients are candidates for surgery and hence control of epilepsy in all patients is not possible using resective surgery.

Automatic identification of the epileptogenic focus has been widely discussed in the literature. Techniques from information theory [79], nonlinear techniques [80, 81] and dipole modelling [82, 83] have been applied in the past by researchers towards localization of epileptogenic focus from EEG.

In this research we applied concepts from sociology and graph theory in combination with spike synchronization to identify the epilepogenic foci from EEG. In particular we utilized a graph theory concept named centrality, which is a measure the relative importance of a vertex within the graph. Our underlying hypothesis

here is that the epileptic focus is the most important node within a network and it might have either the most or the strongest connection within the whole or subset of the network.

4.2 EIGENVECTOR CENTRALITY

Eigenvector Centrality is a measure that quantify the relative importance of a node in a network and was proposed by Bonacich [84, 85]. The central idea of eigenvector centrality is to weigh more the connections to important nodes than those to insignificant nodes. Thus, a node having a number of significant connections is given more weight compared to a node with large number of insignificant connections. Consider a graph with N nodes and strength of connection between nodes i and j denoted by $w_{i,j}$. The popularity score P_i of node i is defined as the weighted linear combination of popularity of all nodes connected to node i, that is

$$\lambda P_i = w_{i,1}P_1 + w_{i,2}P_2 \ldots + w_{i,N}P_N \tag{4.1}$$

where λ is an arbitrary constant. We assume that the weight $w_{i,j}$ is zero (no connection) or positive (connection). The system of Eq. 4.1 for different values of $i \in (1,N)$ can be written in matrix form as $\lambda P = WP$ or $(W - \lambda I)P = 0$, which is the familiar characteristic equation of finding the eigenvalues and eigenvectors of W, where λ are the eigen values and P are the eigenvectors. Since it is required that λ and all the eigenvectors are positive, we tage the maximum eigenvalue and the corresponding eigenvector as our desired centrality measure. Thus, the popularity or centrality score (P_i) of node i is the i^{th} component of the dominant eigenvector.

Applying the concept of centrality to our EEG data, we first define a time varying adjacency matrix $W(t)$, whose element $(w_{i,j} = w_{j,i})$ at time t is the synchronization value $Q_{i,j}(t)$. A high value of $w_{i,j}$ means stronger connection between sites (i, j). The matrix $W(t)$ has always a maximum positive eigenvalue [84]. We

obtain the largest eigenvalue, λ_{max} and the eigenvector V that corresponds to the λ_{max} at every time instance t. We now define the central node ($SN(t)$) at time t as the node having the highest popularity score, i.e.

$$SN(t) = i : P_i = \max(P_1, P_2, \ldots, P_N) \tag{4.2}$$

The time-averaged significant node score, $TASN_i$ for node i is then defined as

$$TASN_i = \frac{1}{T} \sum_{t=1}^{T} \Theta(SN(t) = i) \tag{4.3}$$

where T is an arbitrary time duration of observation and $\Theta(n) = 1$, if n is true and $\Theta(n) = 0$, if n is false. $TASN_i$ is the probability that node i is the most popular or central node in the network. We hypothesize that the epileptogenic focus is the most central node of the epileptic network and should have the highest value of $TASN$.

4.3 Application to Spiking Neuron Model:

In this section, we construct a network of directionally coupled spiking Hindmarsh-Rose neurons. The model is constructed such that it simulates the observed spiking network in epileptic patients. A total of 3 subnetworks with HR neurons were constructed (see Fig. 4.1). The first subnetwork (SB1) consists of Oscillators 1-6. Oscillator 2 is coupled with Oscillator 1, 4, 5 and 6 at coupling strength ε. We add Oscillator 3 which is coupled with Oscillator 1 at a coupling strength of $\varepsilon + 0.4$. In the second subnetwork (SB2), Oscillator 7 is coupled with Oscillators 8, 9, 10, and 11 at coupling strength of ε. In the third subnetwork (SB3), Oscillator 12 (hig spike rate) is coupled with Oscillator 13 with coupling strength of $\varepsilon + 0.5$. For any two oscillators i and j in a subnetwork, the coupling strength is varied from 0 (no coupling) to 2.5 (high coupling). The data are generated from Eq. 3.20 using an integration step of 0.1 and the 4^{th} order Runge-Kutta integration method. Per value

of ε, 5000 points from x time series of the different oscillator are generated. The process is repeated 1000 times for different values of I_0 for all the oscillators in the network. Synchronization metric (Q) and significant node score (SN) are estimated for each realization and stored. The TASN for each node is then estimated and is shown in Fig. 4.2.

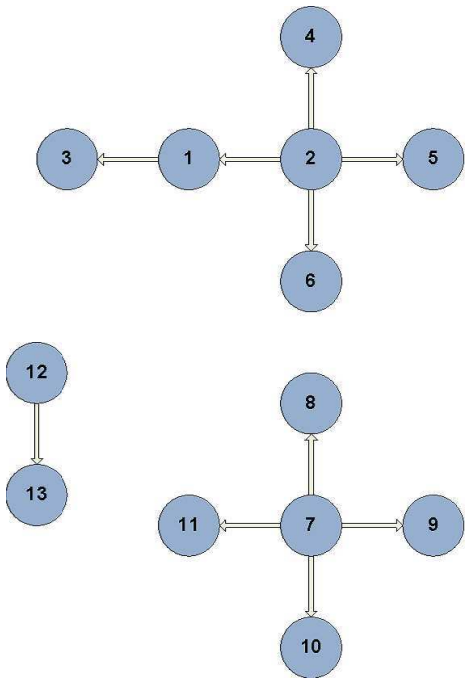

Figure 4.1: Network of Coupled Spiking Neurons. Oscillator 2 is uni-directionally coupled (coupling strength = ε) with Oscillators 1, 4, 5, and 6. Oscillators 1 and 3 have a strong uni-directional coupling (coupling strength = $\varepsilon + 0.4$). Oscillator 7 is uni-directionally coupled (coupling strength = ε) with Oscillators 8, 9, 10 and 11. Oscillator 12 has a very high spiking rate and it is strongly coupled (coupling strength = $\varepsilon + 0.5$) with Oscillator 13.

From Fig. 4.2 we can observe that for low values of coupling ($\varepsilon < 0.22$), Oscillator 12 with the highest spike rate appears to be the most significant node of the network. With increasing coupling strength ($\varepsilon > 0.22$), we can see a progressive increase in TASN score of Oscillator 2 and it becomes the most prominent node. However as ε increases above 0.5, we can see an increase in TASN score of Oscilla-

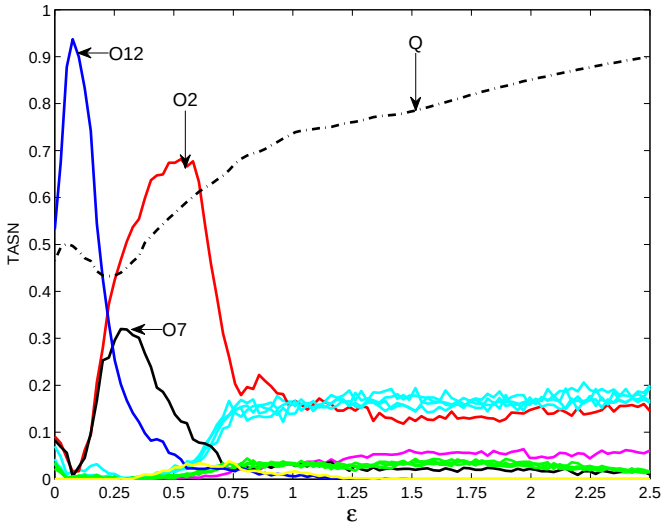

Figure 4.2: TASN score for oscillator network provided in Fig. 4.1 as a function of coupling strength (ε). The TASN score for the oscillators 2, 7 and 12 are denoted by red, black and blue solid lines respectively. The cyan solid line denotes the TASN score for the oscillator 1, 4, 5, 6. The green solid line denotes the TASN score for the oscillator 8, 9, 10, 11. The magenta and yellow solid line denotes the TASN score for Oscillator 3 and 13 respectively. The dashed black line is the synchronization metric Q between Oscillator 2 and 4 as a function of epsilon.

tors 1, 4, 5 and 6. This increase is due to the fact that with increasing coupling, the behavior of the coupled oscillator tend to be similar, thus our ability to distinguish the central node diminishes. As ε increases above 1, it becomes almost impossible to distinguish the central node of the network. These results imply that it might not be possible to identify a central node of a highly synchronized network. Associating this with epileptic EEG, in the peri-ictal (and especially in the preictal) periods we might not be able to localize the epileptogenic foci accurately. However, during the interictal period localization of foci should be possible. In the next section, we show that epileptogenic focus localization is possible, using TASN in our patients with intracranial EEG and temporal lobe epilepsy.

4.4 Application to Epileptic EEG Data:

We now combine the concept of centrality with the spike synchronization profiles estimated from the EEG recordings as described in Chapter 2 and 3 for epileptogenic focus localization. For each patient, we divide the data into two segments. Segment 1 (Interictal) is the period of time from the start of the recording till the first clinically observed seizure. Segment 2 is the period of time from the first clinically observed seizure to end of recording and including many clinical and subclinical seizures per patient. Notice that in Segment 1, subclinical seizures may have occurred. The segmentation of data is performed to see whether there is a difference in TASN profiles during the interictal versus more peri-ictal periods. We further divide the Segment 1 and 2 into non-overlapping segments of two hours duration and estimate the TASN at every subsegment.

Figs. 4.3 and 4.4 shows the mean *TASN* profile for the interictal segment and "peri-ictal" segment respectively for four patients with temporal lobe epilepsy. It is noteworthy that we could localize the focus accurately from TASN profiles from the interictal periods in four patients. Focus localization could not be achieved from analysis of the "peri-ictal" periods. These results can be explained by the fact that during the "peri-ictal" phase the brain is highly synchronized and, as we have shown before, identification of epileptogenic focus from a highly coupled network is difficult using the measure of centrality. This does not mean that it may not be possible to localize the focus using "peri-ictal" data by another method. It just refers to the fact that the concept of centrality lays a constraint when the system is highly coupled.

The significance of these results lies in the fact that it is not the absolute number of spikes (spike rate) that matters when it comes to localization of epileptogenic

focus. This is also clear from Fig. 2.12, where we plotted the spike rate for Patient 1. From that Figure we can observe that the right sub-temporal grid (RST) spikes most frequently without RST being the focus for Patient 1. The spikes in RST remain local to the region and do not propagate, which we infer from Fig. (a). Spikes in RTD, which is the epileptogenic focus for this patient, have more tendency to spread and couple with other regions. So, RTD is a more central node than RST.

This focus localization algorithm did not work well for Patient 5. We investigated the inconsistency in results for this patient by observing the synchronization profile and raw EEG over time. Analysis revealed amplitude saturation of EEG recorded from the focus during spikes and the spike detector failed to capture this. This led to the bad estimation of the synchronization profiles that then directly affected the focus localization algorithm. We suggest a clipping restoration algorithm at the front end of the spike detector or increase the range of recording of EEG to solve such problems in the future.

For Patient 3, we identified a left hippocampus (LTD) focus. The patient report did not conclusively suggest a focus. Majority of the clinical seizures for this patient originated from the left hippocampus (6 clinical seizures from the left, and one from the right) whereas majority of the subclinical seizures from the right hippocampus (12 subclinical from right hippocampus and 2 from left hippocampus). Interictal spikes also occured bilaterally, and slightly more frequently from LTD. We investigated this further by rank ordering the popularity scores. We define R_i, the rank of node i at time t, as

$$R_i(t) = \frac{1}{N_e}(N_e - \sum_{j=1, j\neq i}^{N_e} \Theta(P_i > P_j).\Theta(P_i \neq 0)) \tag{4.4}$$

where N_e is the number of electrodes and P_i is the popularity score for node i and $\Theta(n)$ is the Heaviside step function and is equal to 1 when n is true, and 0 otherwise.

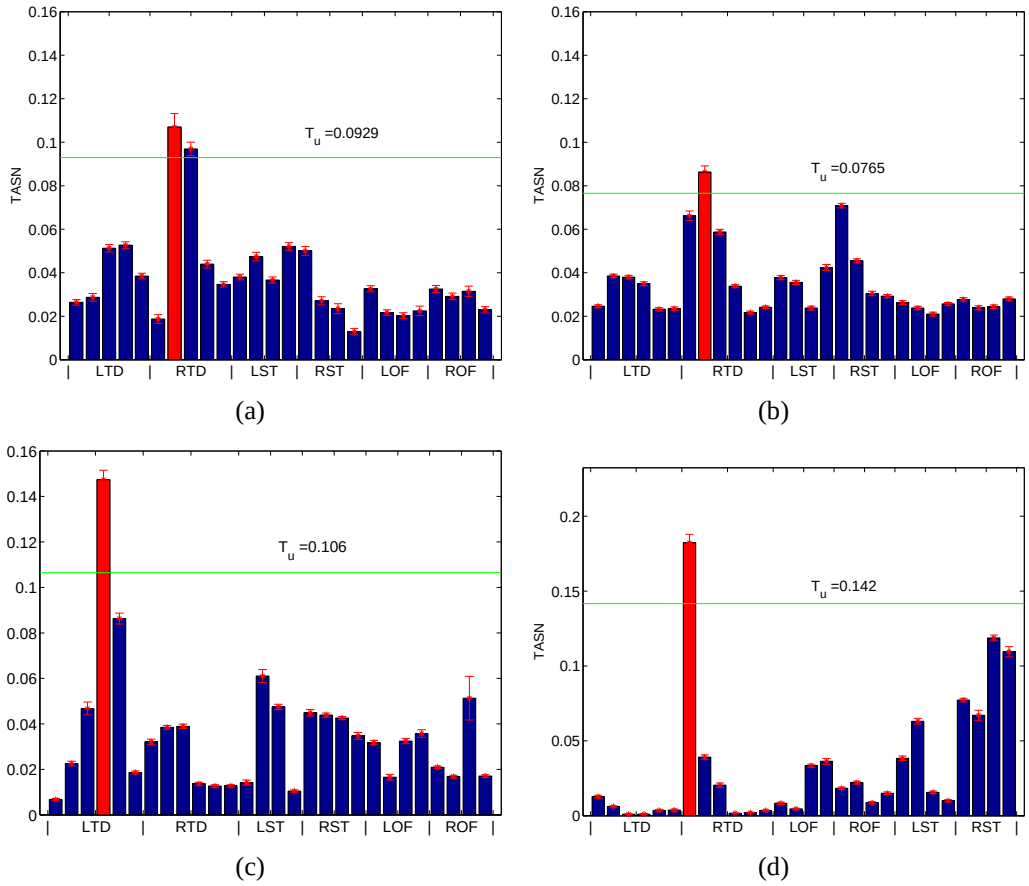

Figure 4.3: TASN profile for four patients estimated from the Interictal Segment. (a) Patient 1, (b) Patient 2, (c) Patient 3 (d) Patient 4. T_u is the arbitrary threshold used for the purpose of detecting the outliers ($T_u = \mu_{TASN} + 2.5\sigma_{TASN}$).

We then define the time averaged rank for node i as

$$TAR_i = \frac{1}{T}\sum_{t=1}^{T} R_i \tag{4.5}$$

The *TAR* profile for the four patients during the interictal segment is shown in Fig. 4.5. From this figure, for Patient 3 there are high TAR values for LTD2 and RTD1, indicating foci in both hemispheres. The clinical assesment suggested the same behavior for this patient as we described above.

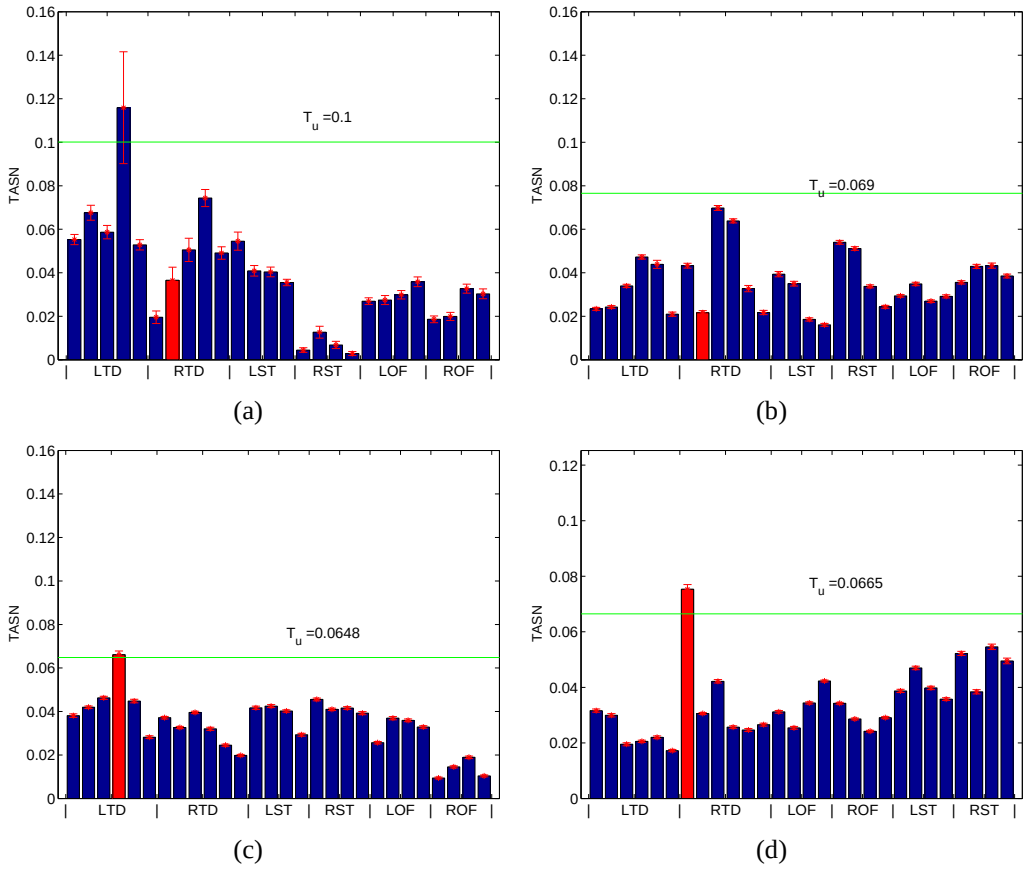

Figure 4.4: TASN profile for four patients estimated from the "peri-ictal" Segment. (a) Patient 1, (b) Patient 2, (c) Patient 3 (d) Patient 4. T_u is the threshold used for the purpose of detecting the outliers ($T_u = \mu_{TASN} + 2.5\sigma_{TASN}$). Red color denotes the focal sites per patient (clinically determined)

4.5 Automatic Detection of Epileptogenic Focus from Interictal EEG:

In this section we discuss a possible algorithm that can be used online to automatically detect the epileptogenic focus from interictal EEG data. To this effect we subdivide Segment 1 into two hour epochs and estimate the TASN score for each brain site. We perform Grubbs' Outlier detection test [86] on the TASN score to determine possible outliers. The fraction of such EEG epochs that exhibited an outliers for the interictal and "peri-ictal" period is shown in Figs. 4.6 and 4.7 respec-

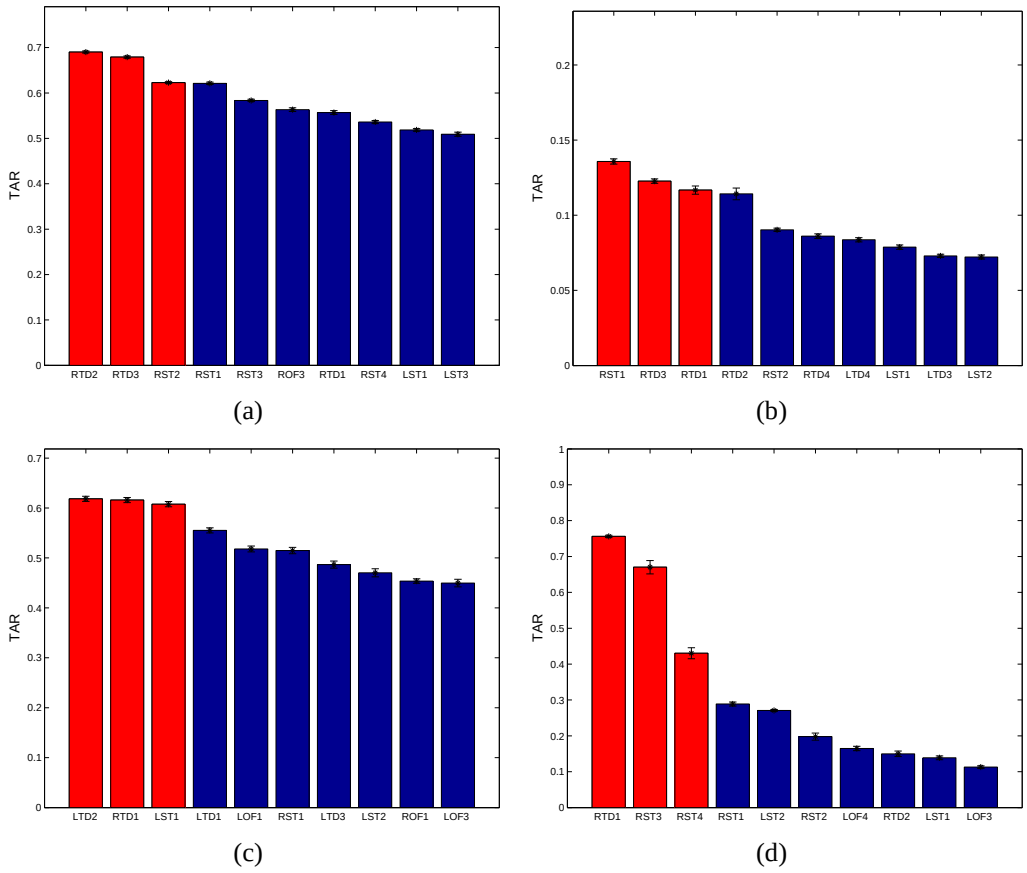

Figure 4.5: TAR profile for four patients estimated from the interictal segment. TAR profile for 10 brain sites (sorted in descending order) of (a) Patient 1, (b) Patient 2, (c) Patient 3, (d) Patient 4 are shown. The red bar represents the three brain sites with the hightest TAR values. For Patients 1,2, and 4, all such sites reside in the right hemisphere (correct focus laterization). We can observe that for Patient 3, the highest three TAR values are for LTD2, RTD1, and LST1, indicating central nodes from both left and right hemispheres.

tively. It can be seen that, on average, 50% of the time we could correctly identify the epileptogenic focus from the interictal EEG. However, localization algorithm performance from Segment 2 remained problematic.

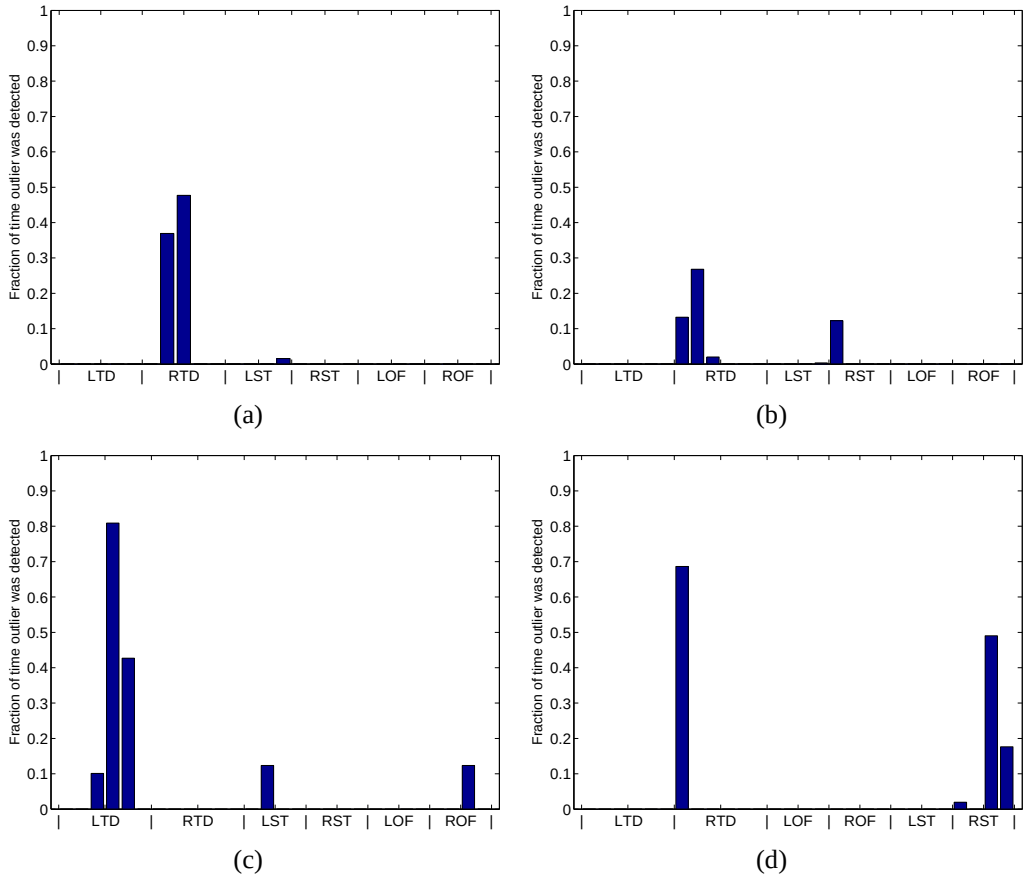

Figure 4.6: Epileptogenic focus localization from interictal EEG data using TASN and Grubbs' outlier detection (see text). (a) Patient ,1 (b) Patient 2, (c) Patient 3, (d) Patient 4.

We then ran the focus localization program in an online manner for a duration of time till an outlier for focus localization is detected. The detected outlier was compared with the clinically determined focus to estimate whether the localized site is a true or a false focus candidate . Table 4.1 shows the focus localization results of such an online focus localization attempt, as well as the average localization time

it took for each of the four patients. From the Table we can see that the average localization time to accurately determine the focus was around 2 hours from the beginning of the recording (Interictal 1) with an average accuracy rate of 90%. The average length of stay in hospital to localize the focus n these patients was about 7 days per patient. Thus, our proposed algorithm could determine the focus, without seizure precipitation, in a fraction of time with 90% confidence,which is a significant leap in the current technology of focus localization.

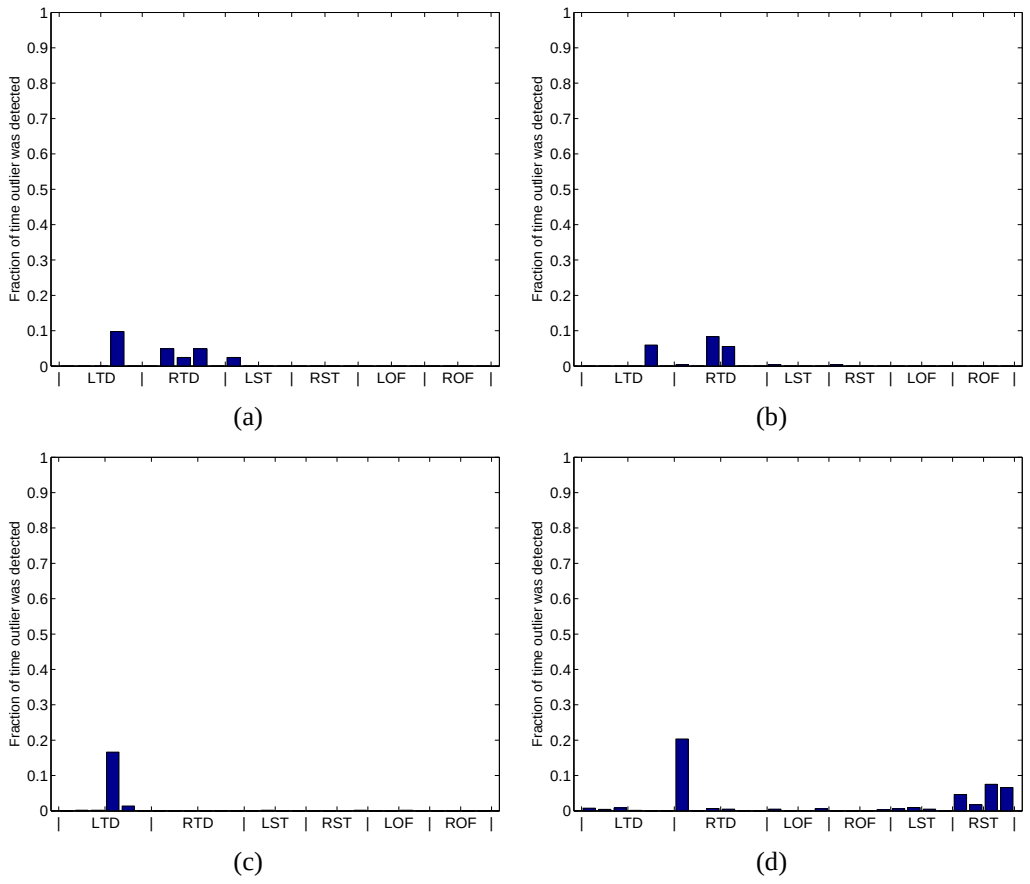

Figure 4.7: Epileptogenic focus localization from periictal EEG data using TASN and Grubbs' outlier detection (see text). (a) Patient 1, (b) Patient 2, (c) Patient 3, (d) Patient 4

Table 4.1: Epileptogenic Focus Localization by TASN versus clinical assessment

Patient ID	Focus Localized		Localization Time	True Detection Rate
	Clinical Assessment	Using TASN		
1	RTD2, RTD3	RTD2, RTD3	1.5±5.6 hrs	1
2	RTD1, RTD2	RTD1, RTD2	1.3±4.2 hrs	0.85
3	-	LTD4, LTD5	0.6±0.6 hrs	1
4	RTD1	RTD1	0.82±0.84 hrs	1
5	RTD1	-	-	0

4.6 CONCLUSION

In this chapter we focused on epileptogenic focus localization using the interictal spike synchronization across brain sites and a measure of centrality called eigenvector centrality. We first tested the developed measures on network models of spiking neurons with various degrees of coupling. We observed that for low degrees of coupling we were able to identify the focus precisely. However with increased coupling and the network became strongly synchronized, our ability to localize the focus with the proposed methodologies is reduced.

Focus localization was performed on fve patients with temporal lobe epilepsy and we were able to accurately localize the focus in four patients. In the one patient where our algorithm failed in identifying the focus, we observed that the EEG data from the focus was saturating at spikes and hence we were not able to detect spikes accurately using our spike-detection measures. We proposed an improvement in the preprocessing of EEG data to counter this problem in the future.

The results revealed that the epileptogenic focus is the most central node of the epileptogenic network and forms strong and significant connections with other brain sites. Our analysis suggested that centricity of the focus is more prominent during the interictal period than “peri-ictal” period. This is in agreeement with

our results from the models we employed, where we observed an inverse relationship between coupling and our ability to localize the focus. (Previous work from Iasemidis et al. suggested existence of excessive synchronization in the brain network in the preictal period [25, 87]. Preictal periods here are parts of the "peri-ictal" periods.). In one of the four patients, the clinical assesment suggested bifocal activities. We modified our measure by rank ordering the centricity values so that we take in consideration more than one brain site and observed that, for this particular patient, rank values were high for sites in both hemispheres, suggesting bilateral foci. For the other patients all high rank values concentrated to the ipsi-lateral hemisphere (hemisphere where the actual focus resided).

We finally discussed the implementation of our algorithm as an online focus localization algorithm. Using Grubbs' outlier detection method on our final centrality measures and and was able to localize the focus on average at 40 percent of the time when the patient was in interictal period. Further analysis revealed that online epileptogenic focus localization is possible using as least as two hour of interictal EEG. So, in addition to the benefits of having a pretty accurate focus localization assistive tool this would reduce significantly the duration of hospital stay for an epileptic patient, and hence cut down the related medical expenses and other overhead costs.

Chapter 5

SEIZURE CLASSIFICATION

5.1 INTRODUCTION

The nature of spiking in the preictal and postictal periods, has been a point of contention in the epilepsy community. Increased rate of epileptic spikes has been observed in the preictal as well as in the postictal, thus raising doubts whether epileptic spikes are actually precursors to a seizure or the aftershocks resulting from the occurence of a seizure. Attempts have been made to relate spike frequency to medication, drowsiness, seizure susceptibility, severity etc [3, 26, 51, 53, 88]. In this chapter we try to study seizure severity and preictal spiking, and find out if they correlate.

5.2 SEIZURE SEVERITY AND PREICTAL SPIKING

We compared the spike rate in the preictal period and postictal periods of 90 seizures across five patients with temporal lobe epilepsy. At every seizure onset time t_{sz}, we define a 20 minute preictal window $W_1(t) = [t_{sz} - 20min, \ldots t_{sz}]$ and 20 minute postictal window, $W_2(t) = [t_{sz} + D_{sz} \ldots t_{sz} + 25min]$, where D_{sz} is the maximum duration of seizures in our data (D_{sz} of 5 minutes in our analysis). Spike rates S_{PRE} and S_{POST} were estimated every 10.24 seconds in the 20 minute preictal window $W_1(t)$, and 20 minute postictal window $W_2(t)$ respectively. Mann-Whitney U Test was performed to compare the distributions of S_{PRE} and S_{POST}, and test the null hypothesis (H_0) that $S_{PRE} = S_{POST}$ against the alternative hypothesis (H_1) that $S_{PRE} \neq S_{POST}$. In case the null hypothesis is rejected we check whether $S_{PRE} > S_{POST}$ using the Z-test (since U-test is not directional). Fig. 5.1 shows the results of this analysis for four our of the five patients. For visualization purposes the results are color-

coded with red indicating that preictal spike rate is larger than the postictal spike frequency ($S_{PRE} > S_{POST}$), green that preictal and postictal spiking are statistically the same ($S_{PRE} = S_{POST}$), and blue that preictal spike rate is smaller than postictal ($S_{PRE} < S_{POST}$).

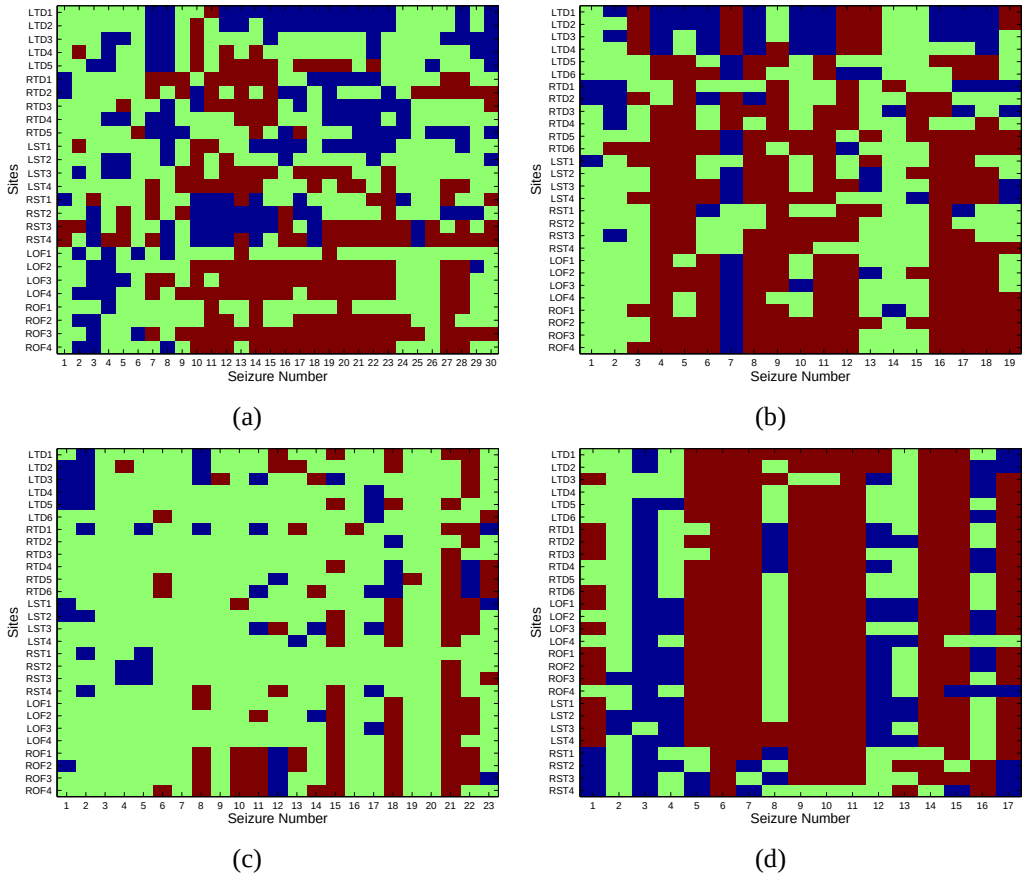

Figure 5.1: Comparison of spike rate per electrode site in the preictal and postictal segments across seizures in four patients with temporal lobe epilepsy. (a) Thirty seizures in Patient 1, (b) 19 seizures in Patient 2, (c) 23 seizures in Patient 3 and (d) 17 seizures in Patient 4 were compared using Mann Whitney U test (See Text). Horizontal axis denotes seizure number and vertical axis denote brain site for which the preictal and postictal spiking rates are compared. Red boxes indicate that $S_{PRE} > S_{POST}$, green boxes indicate $S_{PRE} = S_{POST}$ and blue boxes indicate $S_{PRE} < S_{POST}$

From Fig. 5.1, we observe that there are a class of seizures where we observe an increased spike rate in the preictal period compared to the postictal periods across

a number of brain sites; for example, seizures 4, 5, 8, 9, 11 ,15 in Patient 2 and seizures 5, 6, 7, 9, 10 ,11, 14, 15 in Patient 4. Based on this observation, we tried to address whether a classification of seizure severity based on preictal spike rate is possible.

We classified the seizures into the two several classes: clinical complex partial seizures (CPS) and subclinical seizures (SCS). The classification of seizures was performed by an expert physician by observing the behavioral and clinical symptoms of the patient during the event as well as electrographic signature of each seizure.

Our underlying hypothesis is that, a complex partial seizure is preceded by increased spike rate followed by postictal supression of spiking, and that a subclinical seizure, which is a less severe seizure, may not be accompanied by such increased spike frequency preictally and or reversal (resetting) of spike rates.

5.2.1 Classification using number of sites spiking preictally - Method 1

We first checked whether a seizure classification based on S_{PRE} and S_{POS} is possible by counting the number of sites that show significant preictal spike frequency when compared to the postictal one per seizure. We then constructed a feature space, by defining two parameters for every seizure. We define $F_{PR}(k)$ at seizure k, the fraction of brain sites where we observe larger spike rate in the preictal than the postictal:

$$F_{PR}(k) = \frac{1}{N_e} \sum_{i=1}^{N_e} \Theta(S_{PRE} > S_{POST}) \tag{5.1}$$

where N_e is the number of brain sites and $\Theta(n) = 1$, if n is true and $\Theta(n) = 0$, if n is false. The statistical test for checking $S_{PRE} > S_{POST}$ is outlined in section 5.1. Similarly we define $F_{PO}(k)$ at seizure k as, the fraction of brain sites where we

observe larger spike rate in the postictal than the preictal:

$$F_{PO}(k) = \frac{1}{N_e} \sum_{i=1}^{N_e} \Theta(S_{PRE} < S_{POST}) \tag{5.2}$$

F_{PR} and F_{PO} are the feature space for the classification algorithm, which we then implement using K-means with cluster size of two. Fig. 5.2 depicts the classification of seizures based on the preictal and postictal spike rate. We can observe that most of the complex partial seizures fall in the cluster with high values of F_{PR} (red cloud) whereas the subclinical seizures tend to have low values of F_{PR} (blue cloud). This means that during a subclinical seizure less sites tend to spike in the preictal period and this may be a reason for subclinical seizures to be less severe than compared to a complex partial seizures. We define our classification accuracy as

$$ACC = \frac{N_c}{N_{SZ}} \tag{5.3}$$

where N_c is the number of correct classification and N_{SZ} is the number of seizures. Using this method we were able to classify 88% of the seizures accurately into clinical and subclinical seizures. Interestingly, as per each patient's clinical report, some of the missclassifications were not severe seizures, like 'Auras', 'Simple Partial', 'Brief Complex partial seizures' or Subclinical seizures followed immediately (within 3 minutes) by a complex partial seizure. From Fig. 5.2, we can also see that the separation between the two classes of seizures mainly depends on the number of sites showing increased preictal spike rate and is independent of the number of sites showing increased postictal spike rate. This supports our hypothesis (see Chapter 3) that synchronized preictal spiking across sites and might have predictive value for seizures.

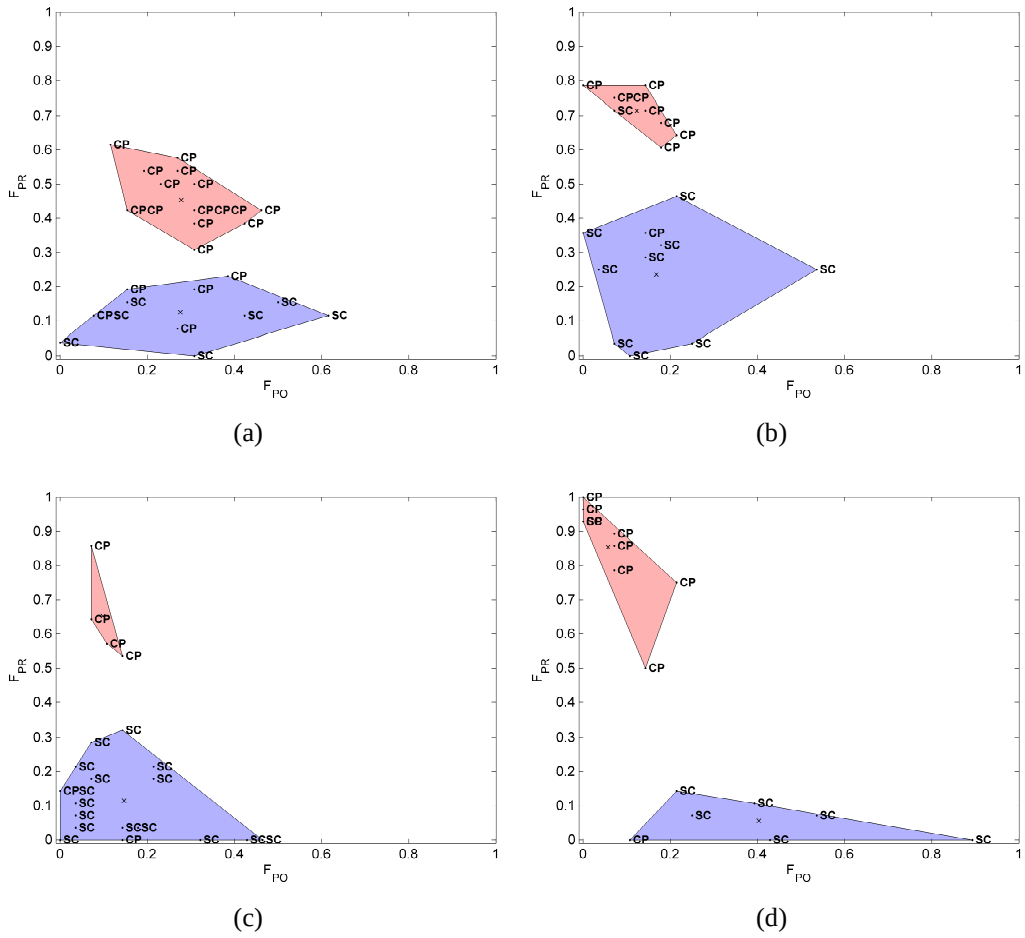

Figure 5.2: Classification of seizure's severity. The feature space for the classification is defined by F_{PR} and F_{PO} that is the number of sites per seizure that show $S_{PR} > S_PO$ and $S_{PR} < S_PO$ (see Eq. 5.2.1 and 5.2.1). Classification of each seizure was performed using K-means clustering on all the seizures from four patients with temporal lobe epilepsy (a) Patient 1, (b) Patient 2, (c) Patient 3, (d) Patient 4. The clouds denote the two classes the seizures were classified into. We not that most of the SC seizures were classified in the blue cloud and most of the CP seizures in the red cloud. Cloud point 'SC' mean Subclinical Seizure and cloud point 'CP' mean Clinical Partial Seizure

5.2.2 Classification using preictal/postictal spike rate - Method 2

We extended the analysis further by checking whether the preictal/postictal spike rate alone can be related to seizure severity. To test this, we repeat the analysis for each brain site by estimating the mean preictal spike rate (SF_{PR}) and postictal spike rate (SF_{PO}). The feature space is now defined by the mean spike rate themseleves over the preictal and postictal, rather than F_{PR} and F_{PO}. This allows us to address the question whether the intensity of preictal spiking and postictal spiking intensity relate to the severity of a seizure. We then classify every seizure based on SF_{PR} and SF_{PO} and obtain the classification accuracy as described in Eq. 5.3; i.e. we perform classification of seizures using SF_{PR} and SF_{PO} of each brain sites and estimate the classification accuracy thereby obtaining a distribution of classification accuracies for a single patient. The distribution of classification accuracy is shown in Fig. 5.3, with the red arrow indicating the classification accuracy using Method 1. We can observe that across patients, Method 1 performs better in classifying seizures than Method 2.

From Fig. 5.2, we observe that a complex partial clinical seizure is typically preceded by an increased spike rate across a set of sites and is followed by supression of this activity in the postictal. However, from Fig. 5.4 we are not able to make any such meaningful conclusion. For Patient 1, the subclinical seizures had larger spike frequency in the preictal/postictal period when compared to clinical seizures. In Patient 2, most clinical seizures had increased spike rate in the preictal and supression in the postictal, whereas the subclinical seizures had lower preictal spike rate compared to clinical seizures. Results from Patients 3 and 4 were similar to Patient 1. These results indicates that single channel studies of spike frequency changes may be insufficient to elucidate the relationship between spikes and seizures.

We further estimate, for each method the rand index and adjusted rand index [89, 90] which is a measure of similarity between two data clusters. Table 5.1 is the summary of classification of seizures using the two methods described before.

Table 5.1: Seizure Classification Results

Patient ID	Seizure Type		Method 1			Method 2			
	CPS	SCS	ACC	RI	ARI	Brain Site	ACC	RI	ARI
1	23	7	0.83	0.71	0.42	LOF4	0.90	0.81	0.57
2	9	10	0.89	0.80	0.60	ROF3	0.89	0.80	0.60
3	6	17	0.91	0.83	0.64	RST2	0.69	0.56	0.06
4	10	7	0.88	0.78	0.55	LOF1	0.82	0.69	0.39
5	6	1	0.85	0.41	0.71	LST1	1	1	1

5.3 Conclusion

In this chapter, we focused on understanding the relationship between "peri-ictal" spiking and seizure severity. The motivation for this study was previous work on the predictive value of preictal spiking for seizures [26, 88]. We investigated this question both via changes in peri-ictal spike rates, as well as just single-channel temporal changes in spike rates.

We first defined a feature space for classification of seizure severity based on the fraction of sites having increased preictal spiking compared to postictal and vice versa. We classified the space using K-means and obtained an overall classification accruacy of 88% across patients and consistent results within a patient. We found that severity of a seizure is directly related to the fraction of sites having higher preictal spike rate when compared to postictal spike rate (criterion); i.e. before a severe seizure spikes tend to appear across more brain sites. This supports our hypothesis in Chapter 3 that synchronized firing of spikes occurs prior to an epileptic seizure.

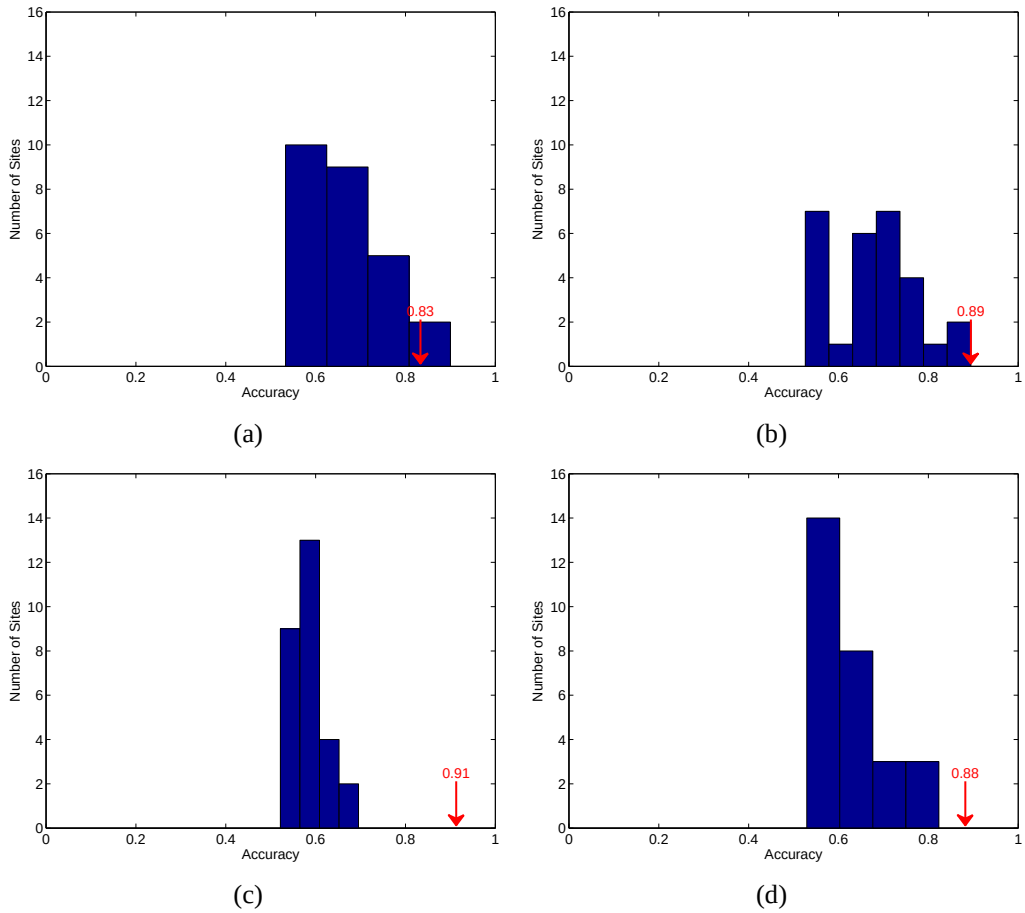

Figure 5.3: Accuracy of seizure classification. The distribution of accuracy of classification via Method 2 for (a) Patient 1 (b) Patient 2 (c) Patient 3 (d) Patient 4 is shown. The red arrow indicate the classification accuracy using F_{PO} and F_{PR} (Method 1 - see text)

We then tested whether preictal/postictal spike rate alone can provide information about seizure severity. Following similar steps as in the previous method we obtained a maximum classification accuracy of around 84%. However the two identified classes of seizures via this classification method were not consistent with any common preictal/postictal spike rate criteria across patients.

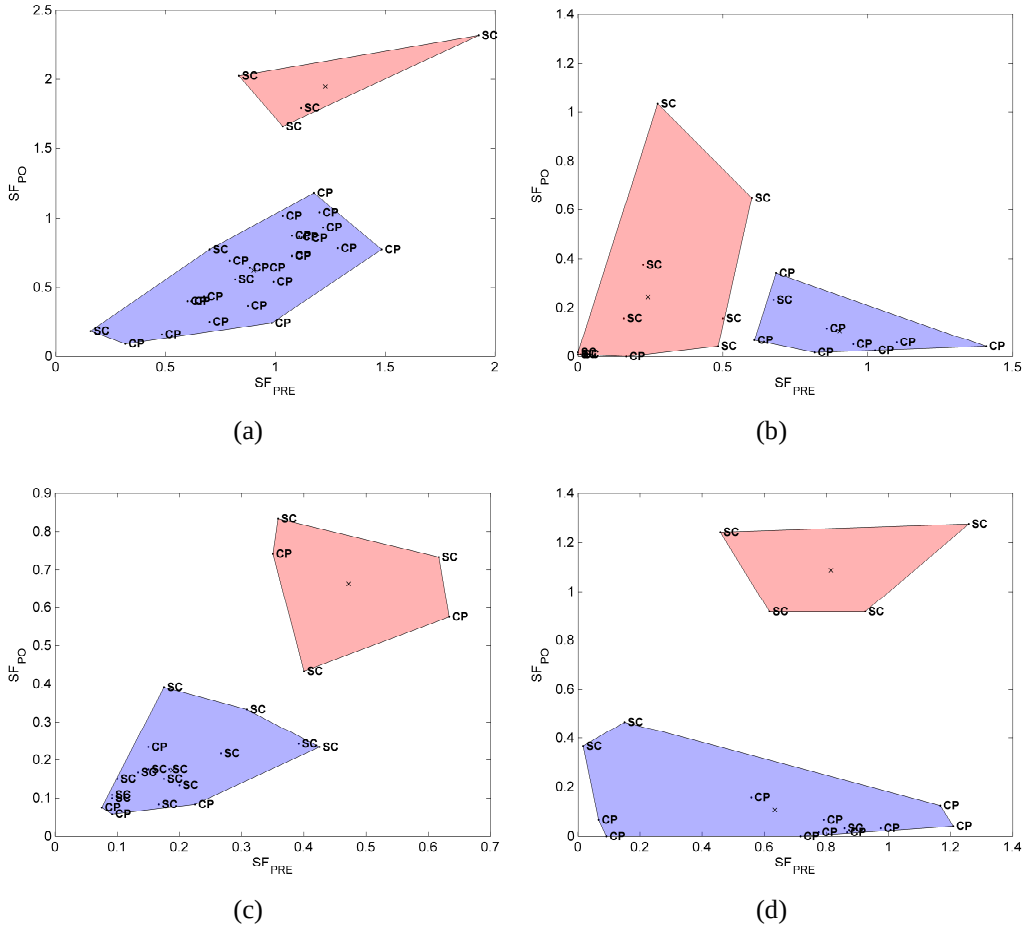

Figure 5.4: Classification of seizures severity using preictal/postictal spike frequency. The feature space for the classification is defined by SF_{PR} and SF_{PO} (See Text). Classification was performed using k-means clustering algorithm. (a) Patient 1, (b) Patient 2, (c) Patient 3, (d) Patient 4. The brain site used to estimate the preictal and postictal spike rate of each seizure in this figure was the one with the maximum classification accuracy in Fig. 5.3. The red and blue clouds denote the the two classes. Cloud point 'SC' mean subclinical seizures and cloud point 'CP' mean clinical partial Seizures

Chapter 6

RESETTING OF SYNCHRONIZATION AT SEIZURES

6.1 INTRODUCTION

We have shown in the past [91] that epileptic seizures are not abrupt transitions into and out of an abnormal ictal state, but instead they follow a dynamical transition that evolves over minutes to hours. During this pre-ictal dynamical transition, multiple regions of the brain progressively approach a similar dynamical state. In Chapter 3, we showed that there is a dynamical transition of critical sites from a synchronized (entrained) state during the preictal to a desynchronized (disentrained) state during the postictal. Epileptic seizures (ES) typically reset the pre-ictal dynamical entrainment and lead to the disentrainment of dynamics of the focus from the rest of the brain. (When epileptic seizures do not reset the established pathology in brains dynamics, cluster of seizures and/or status epilepticus may result [87]). We have called this reversal of dynamics "brain resetting at epileptic seizures" and we have observed it in focal as well as generalized seizures, within and across patients [54, 55]. Previous studies using nonlinear measures of STL_{max} and T-index demonstrated that dynamical resetting is quite specific to epileptic seizures; that is, dynamical resetting occurs with significantly higher probability at epileptic seizures compared with randomly selected time points in interictal periods (Significance level $\alpha = 0.05$). Furthermore, the observed dynamical resetting in patients with epilepsy is significantly sensitive ($p<0.01$) and specific ($p<0.05$) to seizures [55]. Other groups have independently observed similarly reversal trends using more classical methods of signal processing [92, 93]. This observation may reflect a passive mechanism e.g., high electrical activity during a seizure depletes critical neurotransmitters and thus deactivates critical neuroreceptors in the entrained neu-

ronal network. An alternative explanation is an active mechanism, that is, seizure activity releases neuropeptides that may subsequently contribute to the temporary repair of the pathological feedback network that allowed the preictal dynamical entrainment to occur. Such an explanation is analogous to mechanisms attributed to seizures associated with electroconvulsive therapy (ECT) [94, 95].

6.2 Chaos and Resetting at seizures

In this section, we investigate the possibility of differential diagnosis of patients with epileptic seizures (ES) and patients with psychogenics non-epileptic seizures (PNES) by an advanced analysis of dynamics of their (EEG). The underlying principle was resetting at epileptic seizures and absence of resetting at PNES.

6.2.1 Psychogenic Non-Epileptic seizures

In a recent critical review, Bodde et al. [96] presented a working definition of PNES as an observable abrupt paroxysmal change in behavior or consciousness, that resembles an epileptic seizure, but that is not accompanied by the electrophysiological changes of epileptic seizure or clinical evidence for epilepsy. Despite being discussed in the scientific literature for over a century, the etiology and mechanisms of PNES are not well understood. Although there is no consensus on the psychogenic features that lead to PNES, it is believed that a combination of psychogenic mechanisms and trigger mechanisms are at play [96, 97]. A traumatic experience in the past is found in 90% of PNES patients [98, 99, 100, 101]. Combined with the lack of understanding of the physiological mechanisms of PNES is a lack of understanding of the clinical manifestations of PNES. The presentation of PNES can also be indistinguishable from epileptic seizures [102].

Neurologists diagnose PNES based on seizure semiology, psychiatric history, seizure provocation techniques, postictal prolactin assay, and psychological testing

[102, 103, 104]. The gold standard for diagnosing PNES is currently video-EEG monitoring (VEM) [103, 105, 106], but it has its limitations [107, 108]. While VEM can misdiagnose PNES for epilepsy, epileptic seizures can also be misdiagnosed as PNES [96, 109]. Although the prevalence of PNES (2 to 33 per 100,000 [103, 110]) is much less than epilepsy (4-6 per 1,000 [103, 111], 25% to 30% of the patients referred to epilepsy centers for long-term EEG monitoring for spell characterization are eventually diagnosed with PNES [96, 112, 113]. The situation is complicated by the finding that 5% to 40% of PNES patients also have epileptic seizures [96, 114, 115]. Due to the high number of PNES patients in epilepsy centers and epilepsy monitoring units (EMUs), the ability to differentiate reliably and quickly between epileptic and non-epileptic events is critical for proper treatment of PNES patients and for reduction of the associated economic burden. There are at least three major concerns with the misdiagnosis of PNES as epilepsy. First, prognosis for PNES is worse if wrong diagnosis is perpetuated as the appropriate treatment is not prescribed. Second, if PNES is misdiagnosed for ES, and antiepileptic drugs (AEDs) are taken, unnecessary side effects may result. Third, the financial cost may be substantial [37]. The considerable social stigma attached to epilepsy can lead to patient hostility when the diagnosis is changed from epilepsy to PNES, especially in those patients who have been misdiagnosed for a long period of time [96, 116]. It is estimated that up to 75% of PNES patients, who do not have concomitant epilepsy, are initially treated with antiepileptic drugs (AEDs) [99, 105, 117] and can suffer from debilitating side effects. Estimates of the annual cost of misdiagnosing PNES ranged from 0.5 to 4 billion in the 1990's [118]. Another attempt at such an estimation concluded that the cost of misdiagnosing and treating PNES is similar to the cost of treating intractable epilepsy, which in 1995 was approximately $231,432 per patient [96]. Sadly, these three broad categories of concern are so significant be-

cause of the general principle that once a patient has been diagnosed with epileptic seizures it is perpetuated and requires an unusual intervention before the initial diagnosis is overturned [118, 119, 120]. For many reasons (e.g., infrequent episodes, not witnessed by medical personnel, or superficially resembling epileptic seizures), there can be a delay in the diagnosis of PNES, estimated to be between 7 and 10 years [105, 120, 121]. Delays in diagnosis have been prognostically associated with poorer likelihood of remission of PNES [120, 121, 122].

6.2.2 Measures of Chaos

The brain is inherently a nonlinear and nonstationary system. Among the important measures of the dynamics of a nonlinear system are the Lyapunov exponents that measure the average information flow (bits/sec) the system produces along local eigendirections through its movement in its state space [23, 70, 71]. Positive Lyapunov exponents denote generation of information while negative exponents denote destruction of information. A chaotic nonlinear system possesses at least one positive Lyapunov exponent, and it is because of this feature that its behavior looks random, even though as a system it is deterministic. Methods for calculating these measures of dynamics from experimental data have been published [123, 124]. Iasemidis et al. have shown that for a non-stationary system with transients like epileptic spikes, using the short-term maximum Lyapunov exponent (STL_{max}) is a more accurate characterization of the average information flow than the one using the regular maximum Lyapunov exponent (L_{max}) [23, 71]. STL_{max} is estimated from sequential EEG segments of 10.24 sec in duration per recording site over the entire EEG recording to create a set of STL_{max} profiles over time. The STL_{max} profiles computed over space and time characterize a spatiotemporal chaotic signature of the epileptic brain.

6.2.3 *Dynamical Entrainment*

Analyzing scalp, subdural, and depth EEG from patients with either temporal or frontal lobe epilepsy, we have shown that the STL_{max} profiles at brain sites systematically converge to similar values tens of minutes before a seizure. We have called these brain sites critical sites and their convergence entrainment or synchronization of the dynamics. In summary, the epileptic brain appears to be progressively entrained by the focal sites, leading to loss of relative independence of normal brain sites in processing of information long before a seizure develops (See Fig. 6.1(a), (b), (c) left panels) A statistical measure of entrainment between two brain sites i and j, with respect to a measure of their dynamics (e.g., $STLmax$), has been developed in the past [55, 125, 126]. Specifically, the T-index T_{ij} between measures at electrode sites i and j and at time t is defined as

$$T_{ij}(t) = \sqrt{m}\frac{|\hat{D}_{ij}(t)}{\hat{\sigma}_{ij}(t)} \tag{6.1}$$

where $||$ is the absolute value, and $\hat{D}_{ij}(t)$ and $\hat{\sigma}_{ij}(t)$ denote the sample mean and standard deviation respectively of all the m differences between the $STLmax$ values (one $STLmax$ value is produced per 10.24 sec EEG segment) at electrodes i and j, within a moving window $w(t) = [t, t - m * 10.24sec]$ over the available EEG recording (see Fig. 6.1 d).

We have defined disentrainment (dynamical desynchronization) between electrode sites i and j when $T_{ij}(t)$ is significantly different from zero at a significance level α. The disentrainment condition between the electrode sites i and j, as detected by a paired t-test, is $T_{ij}(t) > t_{\alpha/2,m-1}$, where $t_{\alpha/2,m-1}$ is the $100(1-\alpha/2$ critical value of the t-distribution with m-1 degrees of freedom. If $T_{ij}(t) < t_{\alpha/2,m-1}$ (which means that we do not have satisfactory statistical evidence at the α level that the differences of values of a measure between electrode sites i and j within

the time window w(t) are not zero), we consider that sites *i* and *j* are entrained with respect to STL_{max} at time t. Using α = 0.01 and m = 60, that is, using a window $w(t)$ of 10 minutes in duration, the threshold T_{th} =2.662. It should be noted that similar *STLmax* values does not mean that the sites interact. However, progressive convergence over time of *STLmax* points to a diminishing probability that the sites are unrelated [127, 25]. In accordance to the T-index between brain sites at time *t* we define its equivalent for a single site with respect to the evolution of its dynamics between two consecutive time windows. The single channel T-index $T_i(t)$ is given by

$$T_i(t) = \sqrt{m}\frac{|\hat{L}_i(t) - \hat{L}_i(t+h+m)}{\hat{\sigma}_i^p(t)} \tag{6.2}$$

where $\hat{L}_i(t)$ is the sample mean of the *STLmax* values in the moving window $w(t)$ of length *m*, $\hat{\sigma}_i^p(t)$ the pooled standard deviation (average of standard deviations) of the *STLmax* values in the windows $w(t)$ and $w(t+h+m)$, and *h* a buffer separating these two windows which we took equal to the maximum duration of a patients recorded seizures.

6.2.4 Dynamical Resetting

We have shown that the observed spatial entrainment of dynamics at critical brain sites in the pre-ictal period is changed to disentrainment in the postictal period of epileptic seizures [7-9]. We have named this phenomenon dynamical resetting. Those studies on intracranial EEG from epileptic patients also demonstrated that dynamical resetting is quite specific to epileptic seizures; that is, dynamical resetting occurs with a significantly higher probability following epileptic seizures compared to randomly selected time points in interictal periods (statistical significance level $\alpha = 0.05$). Epileptic seizures reset the excessive pathological entrainment occurring minutes prior to their onset and appear to play a homeostatic role

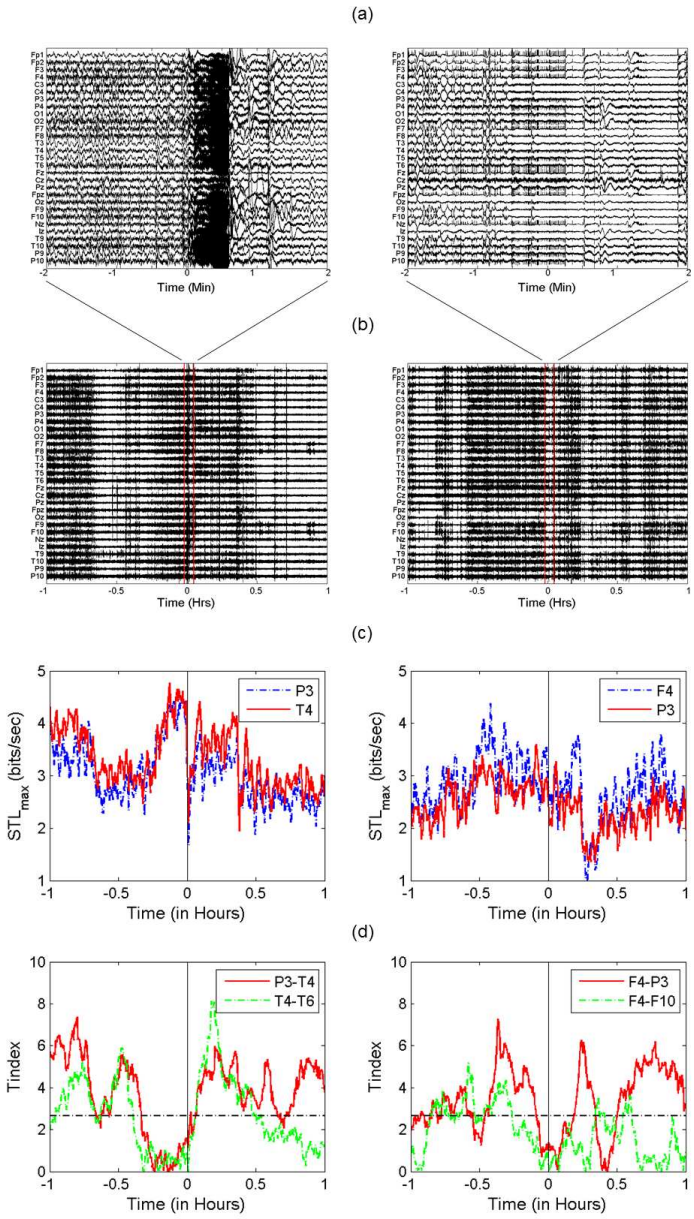

Figure 6.1: Resetting of brain dynamics at seizures / events. Left panels: Epileptic seizure #3 from patient E5. Right panels: Event #1 from patient P5. (a) Scalp EEG recordings 1 minute perictally (event at t=0). (b) Smoothed salp EEG recordings 1 hour perictally (event at t=0). (c) Smoothed STL_{max} profiles from a pair of electrodes over the same time interval as in (b). (d) T-index profiles from the pair of electrodes in (c) and an additional preictally entrained pair. The horizontal dotted line is the T_{th} for entrainment.

of restoring the balance between synchronization and desynchronization of brain dynamics [9].

One way to quantify dynamical resetting at seizures is via the number of preictally entrained pairs of sites that reset in the immediate postictal period. The pairs of sites (i, j), whose $T_{ij}(t)$ values is below T_{th} for $w(t)$ immediately prior to seizure onset are selected as entrained pairs for that seizure. (Note: the results we report herein do not change significantly, and the final conclusions remain the same, if we select as entrained pairs the ones that remain entrained for every t within the whole interval of 10 minutes before a seizure onset.) By dividing this number of pairs of sites by the total number of available pairs of recording sites, we define the entrainment power $EP(t)$ at time t as

$$EP(t) = \frac{2}{N_e(N_e-1)} \sum_{i=1}^{N_e-1} \sum_{i=i+1}^{N_e} \Theta(T_{ij}(t) < T_{th}) \tag{6.3}$$

Out of those pairs of sites, a subset of pairs will get disentrained after the seizure ($T_{ij}(t) > T_{th}$ at some time t in the immediate after the seizures end time interval). Moreover, only a portion of this subset of disentrained pairs of sites (i, j) will also have their corresponding individual $STLmax$ values significantly change with respect to the values they had during the preictal entrainment ($T_i > T_{th}$ and $T_j > T_{th}$). Fig. 6.1 illustrates the application of these resetting conditions at a typical seizure in an ES patient and an event in a PNES patient.

Considering the above conditions for resetting, and by dividing this number of pairs of sites by the total number of available pairs of recording sites, we can define the resetting power $RP(t)$ at time t mathematically as

$$\begin{aligned} RP(t) = \frac{2}{N_e(N_e-1)} \sum_{i=1}^{N_e-1} \sum_{i=i+1}^{N_e} & \Theta(T_{ij}(t) < T_{th}) \Theta(T_i(t) > T_{th}, T_j(t) > T_{th}) \\ & \Theta(\exists t' \in [t, t+h+m] : T_{ij}(t') > T_{th}) \end{aligned} \tag{6.4}$$

where N_e is the total number of available electrode sites, and Θ is the Heaviside function such that $\Theta(A) = 1$ if A is true and $\Theta(A) = 0$ if A is false.

We apply the same methodology to check for resetting of dynamics at non-seizure points too. Actually, we applied this methodology for every single available time point t on the STL_{max} profiles per recording site, that is, for every 10.24 sec on the available EEG from every electrode and patient. For consistency in statistics, we have kept the same values for m and h for the analysis at non-seizure points too, that is, m=60 points (10 minutes) and h=maximum duration of seizures per patient. As a result, we end up with a value of our measures of entrainment (EP) and resetting (RP) for every 10.24 sec per EEG recording.

For a specific time point t_0, in a recording of length N_{rec}, the entrainment power is $EP(t_0)$ and the resetting power is $RP(t_0)$. We can then define the EP score and the RP score as

$$SEP(t_0) = \frac{1}{N_{rec}} \sum_{t=1}^{N_{rec}} \Theta(EP(t) > EP(t_0)) \tag{6.5}$$

$$SRP(t_0) = \frac{1}{N_{rec}} \sum_{t=1}^{N_{rec}} \Theta(RP(t) > RP(t_0)) \tag{6.6}$$

These scores quantify how unlikely it is to observe larger entrainment and resetting power at a time t anywhere in the entire EEG recording than those at time t_0. *SEP* and *SRP* are simple counting metrics on the sets of EP and RP values respectively, therefore, these scores are independent measures of the overall entrainment and resetting power over an EEG recording. In this sense, the *SEP* and *SRP* values in different recordings (patients) can be directly comparable. For both *SEP* and *SRP* scores, small values indicate a rare event of high entrainment or resetting respectively.

From Eq. 6.6, the SEP and SRP values at seizure points can be perceived as the p-values of testing if the respective entrainment (EP) and resetting (RP) at a seizure

are significant different than in the interictal period. Therefore, by using Fishers method for combining p-values [128] we can obtain the statistical significance of overall entrainment and resetting at seizures per patient. Given k, with k equal to a patients number of seizures, p-values p_i, the quantity

$$X^2 = -2\sum_i log(p_i) \tag{6.7}$$

follows a χ^2-distribution with $2k$ degrees of freedom. Substituting for p_i the SEP and SRP values at seizure points t and comparing the obtained X^2 with the appropriate χ^2-distribution we can estimate the combined p-value for each patients seizures. A small combined p-value indicates significant entrainment (EP) or resetting (RP) at seizures for each patient.

6.2.5 Data Analyzed

Long-term (days) scalp EEG recordings from six patients diagnosed with psychogenic non-epileptic seizures and five patients with epileptic seizures were analyzed (see Table 6.1). EEG signals were recorded from twenty-nine channels overlaying 6 brain regions using a standard EEG montage (extended international 10-20 system) including auricular references. The analog data were low-pass filtered at 70 Hz and then digitized at 200 Hz (sampling frequency) and stored on a digital hard drive in Nihon-Kohden data format. No other (digital) filters were applied to the EEG data before the subsequent dynamical analysis. This analysis was conducted continuously (without subjective or objective rejection of any EEG data segment from the dynamical analysis for any reason, even when artifacts are present and irrespectively of the vigilance state of the patient) and sequentially for non-overlapping 10.24 sec running windows over the entire scalp EEG available over days per patient.

Table 6.1: Patient and EEG Data Characteristics

Patient	Age	Number of Events	Average Event Duration (sec)	EEG Recording Duration (hrs)	Clinical Assement of Events	Focus
E1	35	5	84	52	Parital Complex Seizures	Right Temporal
E2	69	2	38	69.5	Intractable Parital Complex Seizures	Left Frontotemporal
E3	54	2	90	142.5	Epilepsy without right frontal polymicrogyria	Right Frontocentral
E4	45	5	94	64	Temporal Lobe Partial Epilepsy	Left Temporal
E1	18	5	52	48	Intractable Epilepsy	Not Localized
P1	23	4	100	106.5	Non-Epileptic spells	N/A
P2	39	3	280	52	Non-Epileptic spells	N/A
P3	49	2	480	70.5	Non-Epileptic spells	N/A
P4	22	3	1200	24	Non-Epileptic spells	N/A
P5	64	2	380	28.5	Non-Epileptic spells	N/A
P6	39	5	25	72	Non-Epileptic spells	N/A

6.2.6 Dynamical Resetting following ES and PNES

We estimated the EP and RP measures over the entire available EEG recording from each patient, and subsequently the SEP and SRP scores for each seizure / event. As an example, we demonstrate the distributions of EP and RP for one patient with epilepsy (E1) and one with PNES (P5) in Fig. 6.2. The entrainment power (EP) observed at seizures (indicated by black vertical lines) in either patient is not statistically different from the one observed interictally. This is not the case for the resetting power (RP). The RP values for the epileptic patients seizures fall into the higher end of the resetting distribution, while for the PNES patient they do not. That was a typical trend across patients from the two groups that is statistically quantified by the SEP and SRP measures.

In Table 6.2, we present the SEP and SRP values for all events (epileptic seizures and PNES) per patient. The SRP values for patient E1 are very low (0.022 to 0.065) indicating seizures with high resetting power. Patient P5 in contrast has high SRP values (0.389 and 0.536) indicating that the resetting observed at his PNES events is not different with respect to other points in the interictal period. All epileptic seizures, except the ones of patient E3, exhibited significantly low SRP values. Even though the finding for patient E3 was an outlier in our analysis of dynamical resetting at epileptic seizures, this patients medical history was consistent with short but frequent episodes of seizure clusters / status epilepticus, an indication of a serious pathology of brains dynamics where individual epileptic seizures (like the two ones we herein analyzed from this patient) cannot reset the dynamics [87]. All PNES patients exhibited non-significant resetting at their events (significantly large SRP values).

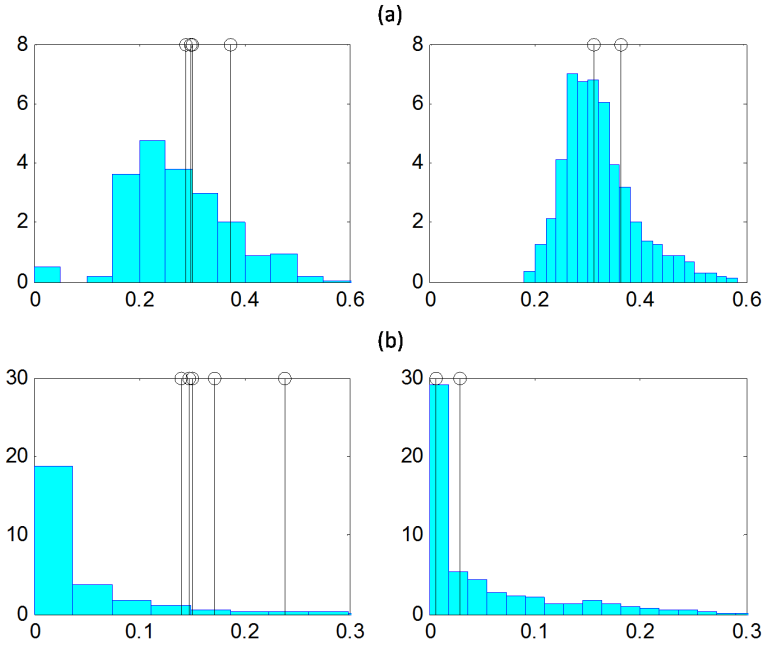

Figure 6.2: Distribution for the measures of (a) entrainment power (EP) and (b) resetting power (RP) estimated every 10.24 sec over the entire EEG recordings from patient E1 (Left panels) and patient P5 (Right panels). The black vertical lines indicate the position of the EP and RP values at seizure / events per patient (5 seizures for E1, 2 events for P5). For both patients, the power of entrainment (EP) values at events fall relative close to the center of the corresponding distribution rendering them statistically non-significant, while the power of resetting (RP) values at seizures for patient E1 are located near the tail of the distribution rendering them statistically significant.

Furthermore, PNES patients exhibited less entrainment and resetting at events than the ones by ES patients. In Fig. 6.3 we show the boxplots for SEP and SRP values at events, taken from Table 2, for the two groups of patients, along with the p-value of the performed Students t-test for equality of means between the two groups. Since these p-values are less than 0.001, the two groups of epileptic seizures and PNES are statistically different with respect to either entrainment or resetting. For the group of PNES patients, the mean values of SEP and SRP at events is near

Table 6.2: SEP and SRP values for ES and PNES events

Patient with ES (Seizure No.)	SEP -ES-	SRP -ES-	Patient with PNES (Seizure No.)	SEP -PNES-	SRP -PNES-
E1(1)	0.370	0.044	P1(1)	0.810	0.585
E1(2)	0.342	0.058	P1(2)	0.736	0.193
E1(3)	0.361	0.065	P1(3)	0.909	0.185
E1(4)	0.334	0.056	P1(4)	0.414	0.490
E1(5)	0.137	0.022	P2(1)	0.890	0.200
E2(1)	0.700	0.132	P2(2)	0.147	0.224
E2(2)	0.661	0.596	P2(3)	0.206	0.525
E3(1)	0.043	0.069	P3(1)	0.749	0.207
E3(2)	0.358	0.054	P3(2)	0.913	0.128
E4(1)	0.048	0.118	P4(1)	0.981	0.303
E4(2)	0.395	0.106	P4(2)	0.521	0.454
E4(3)	0.109	0.081	P4(3)	0.499	0.407
E4(4)	0.113	0.096	P5(1)	0.477	0.389
E4(5)	0.174	0.126	P5(2)	0.209	0.536
E5(1)	0.046	0.058	P6(1)	0.182	0.665
E5(2)	0.179	0.223	P6(2)	0.484	0.174
E5(3)	0.139	0.008	P6(3)	0.440	0.786
E5(4)	0.117	0.280	P6(4)	0.693	0.195
E5(5)	0.008	0.006	P6(5)	0.949	0.786

0.5 indicating a random entrainment and resetting at events, while for the group of epileptic patients the means are quite lower, indicating high entrainment and resetting at seizures.

Finally, in Table 6.3, the combined p-value for each patients events is shown. According to the combined p-values, entrainment is significant ($p<0.05$) for two, while resetting is significant for four out of the 5 epileptic patients. For patients with PNES, both resetting and entrainment are not significant. It is noteworthy that while p-values (i.e., SEPs or SRPs) of some individual events may not be low enough to be statistically significant, combined through Fishers test to form the combined p-value per patient may reach statistical significance levels.

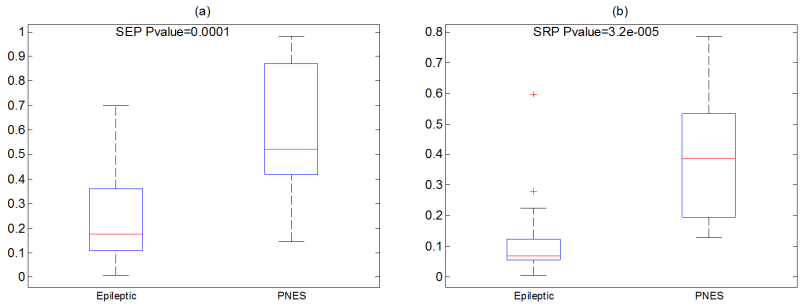

Figure 6.3: Boxplots (box-and-whisker diagrams) from 19 events in each of the two groups of ES and PNES patients based on the values of the score of (a) entrainment power (SEP), (b) resetting power (SRP) measures from Table 2. Each box represents the interquartile range of the mean of each measure across events, the bar within the box represents the median of the measures, and the bottom and top whiskers represent the 1.5 times below and above the lower and upper quartiles respectively. The corresponding p-value for the t-tests of equality of means between the two groups are very low ($p<0.001$) for either measure, with resetting having an edge over entrainment, indicating significant difference between the two groups of patients in terms of entrainment and resetting with respect to their respective interictal values. These results appear to be promising for the use of SEP and SRP measures in differential diagnosis between ES and PNES.

Table 6.3: Statistical significance of entrainment and resetting per patient via Fishers combined p-test

Patient	Entrainment (combined p-value)	Resetting (combined p-value)
E1	0.305	0.001
E2	0.832	0.281
E3	0.083	0.025
E4	0.028	0.012
E5	0.002	0.001
P1	0.942	0.328
P2	0.340	0.322
P3	0.952	0.112
P4	0.923	0.481
P5	0.343	0.570
P6	0.675	0.563

6.3 SPIKES

In this section we investigate dynamical resetting at seizures using spike synchronization profiles we estimated and discussed in Chapter 3. We showed in Chapter 3, the presence of synchronized spiking across pairs of sites in the preictal periods and desynchronization in the postictal ones. Figs. 3.13 and 3.14 indicate that dynamical resetting occurs more prominently at seizure time points compared to interictal time points. We develop here a measure to quantify these dynamical changes at seizures based upon changes in the number of synchronized pairs peri-ictally.

6.3.1 Measure of resetting based on spike synchronization

One way to quantify dynamical resetting at seizures is via the number of preictally synchronized pairs of sites that may then desynchronize in the immediate postictal period. At time point t, for the each pair of sites (i, j), we define as $Q_{ij}^{pre}(t)$ the vector that has as components the spike synchronization values within the preictal window $w_{pre}(t) = \{t - 60 * 10.24, \ldots, t\}$ and $Q_{ij}^{post}(t)$ as the vector of spike synchronization values in the postictal window $w_{pre}(t) = \{t + d_{sz}, \ldots, t + d_{sz} + 60 * 10.24\}$, where $d_{sz} = 5mins$ is the average duration of a seizure. We then perform Mann-Whitney's U test to compare the distribution of $Q_{ij}^{pre}(t)$ and $Q_{ij}^{post}(t)$. Since Mann-Whitneys U test can only suggests that the distributions are different (strictly that the medians of the two distributions are different), we perform a Z-test on the distribution to test whether the mean of one distribution is larger than the other. We now define the resetting power ($RP_Q(t)$) at time t as

$$RP_Q(t) = \frac{2}{N_e(N_e-1))} \sum_{i=1}^{N_e-1} \sum_{j=i+1}^{N_e} \Theta_M(Q_{ij}^{pre}(t) \neq Q_{ij}^{post}(t)) \Theta(Z_{ij}(t) > Z_{thr}) \quad (6.8)$$

where Θ_M denotes the Mann-Whitney U test outcome and is equal to 1 when the distributions are dissimilar. $\Theta(n)$ is the Heaviside step function and is equal to 1

when n is true and is equal to 0 when n is false. Z_{thr} is the statistical threshold on the Z-score and is set to 4 (corresponding to a significance level of $\alpha =< 0.001$) and N_e is the number of available electrode sites. It should be noted here that the distributions may not normal in nature, however we use z-score as a way to determine which distribution has a larger mean without paying attention to the significance level α. Along similar lines we check for the opposite hypothesis; i.e. there is more postictal synchronization compared to preictal synchronization. We define the inverse resetting power (IRP_Q) at time t as

$$IRP_Q(t) = \frac{2}{N_e(N_e-1))} \sum_{i=1}^{N_e-1} \sum_{j=i+1}^{N_e} \Theta_M(Q_{ij}^{pre}(t) \neq Q_{ij}^{post}(t))\Theta(Z_{ij}(t) < -Z_{thr}) \quad (6.9)$$

We now estimate the $RP_S(t)$, i.e. the resetting power using the STL_{max} profiles, as defined in the previous section. Comparison between RP_S and RP_Q measures of resetting at seizures is provided in Fig. 6.4. It is interesting to observe that both RP_S and RP_Q follow similar trends across seizures in both patients analyzed, indicating robustness of resetting at seizures. The probability distribution of the new measure of resetting power (RP_Q) is shown in Fig. 6.5 for three of our patients.

To statistically validate the significance of resetting at seizures compared to interictal, we define the resetting score (SRP_Q) at time t_0 as

$$SRP_Q(t_0) = \frac{1}{N_{rec}} \sum_{t=1}^{N_{rec}} \Theta(RP_Q(t) \geq RP_Q(t_0)) \quad (6.10)$$

where N_{rec} is the recording length of the EEG. Along similar lines, we also estimate the inverse resetting score ($SIRP_Q$) at time t_0 as

$$SIRP_Q(t_0) = \frac{1}{N_{rec}} \sum_{t=1}^{N_{rec}} \Theta(IRP_Q(t) \geq IRP_Q(t_0)) \quad (6.11)$$

The resetting score quantifies how unlikely it is to observe large resetting power at a time t anywhere in the entire EEG recording compared to those at time t_0.

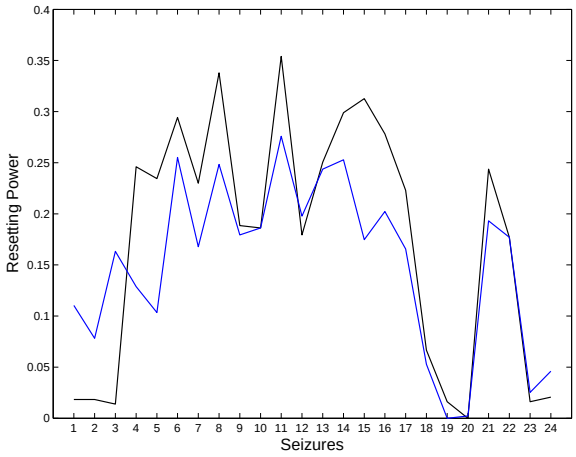

(a)

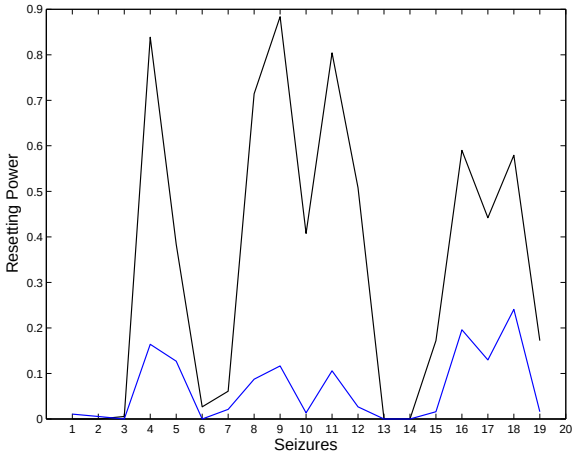

(b)

Figure 6.4: Comparison between RP_S and RP_Q resetting measures at seizures for: (a) Patient 1, (b) Patient 2. The blue curve denotes the resetting power(RP_S) at seizures estimated using the STL_{max} profiles. The black curve denotes the resetting power(RP_Q) at seizures estimated using the spike synchronization profiles.

Since SRP_Q is an independent measure of overall resetting power, we can compare the values of SRP_Q across patients. Each SRP_Q can be perceived as the p value of the test that "resetting at time t_0 is significantly different than anytime in the interictal period". Therefore, by using Fischer's method for combining p values [128], we can obtain the statistical significance of the overall resetting power at seizures per patient. Given k a patient's number of seizures and p_i the p values at each one of them , the quantity

$$X^2 = -2\sum_i ln(p_i) \tag{6.12}$$

follows a χ^2 distribution with $2k$ degrees of freedom. Substituting p_i with the SRP_Q values at seizure points t_{sz}, and using the thus obtained X^2 with appropriate χ^2 distribution, we can estimate the *combined P value* for each patient. A small combined p value suggests significant resetting at seizures for that patient. We also estimate the *combined P value* using the $SIRP_Q$ score. The combined p values using SRP_Q and $SIRP_Q$ for the five patients analyzed is shown in Table 6.4. As these p values are less than 0.001, we can state that statistically significant resetting occurs at epileptic seizures compared to random point in the interictal. However the p values for the inverse case is not significant in four out of five patients, which means that preictal synchronization and postictal desynchronization is more prominent that preictal desynchronization and postictal synchronization.

To test whether the observed resetting depends on the spike rates the brain sites exhibit in the preictal and postictal periods, we re-estimated SRP_Q using sites that had no change in spike rate in the preictal versus the postictal period (See Sec. 5.1). Towards this goal, we took the following steps: 1) Remove channels which have no significant spike rate, for example, we required a minimum of 10 spikes in the preictal or postictal segment. 2) Select the 10 sites with the minimum spike

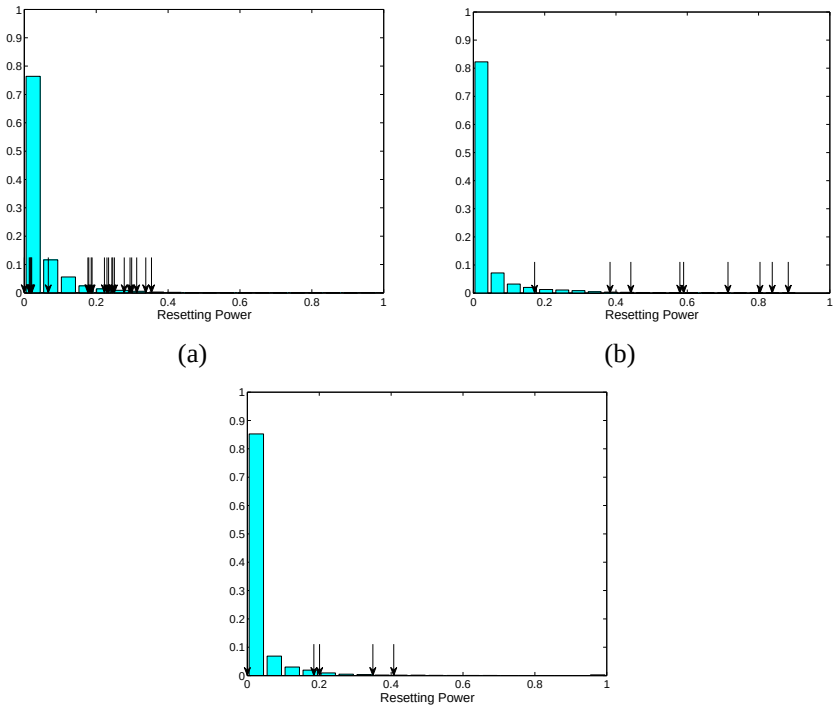

(a) (b)

(c)

Figure 6.5: Probability distribution of resetting power RP_Q estimated every 10.24 seconds over entire EEG recordings from (a) Patient 1, (b) Patient 2, (c) Patient 3. The arrows denote the resetting power at seizures points and are mostly into the tail of the distribution with high values of resetting power.

Table 6.4: Statistical significance of resetting per patient (Fischer's combined p test)

Patient ID	Number of Clinical Seizures	Combined p value (SRP_Q)	Combined p value ($SIRP_Q$)	Combined p value (STL_{max})
1	23	< 0.001	< 0.001	< 0.001
2	9	< 0.001	0.28	< 0.001
3	6	< 0.001	0.61	< 0.001
4	10	< 0.001	0.98	< 0.001
5	6	< 0.001	0.76	< 0.001

Table 6.5: Statistical significance of resetting using sites with no spike rate changes at seizures per patient (Fischer's combined p test)

Patient ID	Number of Clinical Seizures	Combined p value (SRP_Q)
1	23	< 0.001
2	9	< 0.001
3	6	0.03
4	10	< 0.001
5	6	0.049

rate changes peri-ictally per seizure. The re-estimated SRP_Q scores are provided in Table 6.5. From this table we can observe that SRP_Q scores for all patients are also statistically significant ($\alpha = 0.05$). Thus preictal synchronization and postictal desynchronization of spikes does not depend on changes in spike rates but on changes in spike synchronization between brain sites.

6.4 CONCLUSIONS

In this chapter, we investigated resetting of brain dynamics using measures for epileptic spike synchronization and chaos (STL_{max}).

Analysis of long-term scalp EEG recorded from patients with ES and PNES was performed on the basis of resetting of brain dynamics. This study showed that analysis of brain dynamics constitutes a valuable route for differentiation between epileptic seizures and non-epileptic seizures of psychogenic origin. The initial basis for the produced results was the previously observed pathological gradual convergence of the rates of generation of information between critical brain sites in the order of tens of minutes before an epileptic seizure (dynamical entrainment), and their quick divergence (dynamical disentraiment) after seizures end, thus implying a functional role of epileptic seizures for the recovery from the developed pathol-

ogy of brains dynamics. Combining both observations, we have called dynamical resetting the phenomenon of the preictal entrainment and postictal disentrainment.

We herein developed new measures of entrainment (entrainment power EP) and resetting (resetting power RP) of brain dynamics, at any time point in the challenging, but clinically practical, condition of EEG recorded from patients with scalp electrodes. We then developed statistical measures of this entrainment (SEP) and resetting (SRP) at ES or PNES events per patient with respect to his/her interictal EP and RP values. On the basis of the SEP and SRP values, we have shown at a high level of statistical significance that: a) PNES patients exhibit less level of dynamical entrainment and resetting at events than ES patients at seizures (see Figure 6.3; $p < 0.001$), and b) Events in PNES patients do not reset brains dynamics (see Table 6.3); combined p-values per patient > 0.1), while they typically do (4 out of 5 patients) in ES (combined p-values < 0.05). These results, combined with prior ones from intracranial EEG in ES by Iasemidis et al. [55, 54], show quantitatively that epileptic seizures typically reset the brains dynamics. They also show that PNES events typically do not.

The results on ES and PNES from this study suggest that the proposed methodology of measuring the resetting of brain dynamics could be useful for differentiation between PNES and epileptic seizures. Future studies with a larger number of PNES and ES patients, as well as PNES patients with concomitant epilepsy, are contemplated to further investigate the sensitivity and specificity of our results and the possibility for the development of a robust diagnostic tool for PNES. In addition to shedding light on the mechanisms of generation of ES and PNES, such analytical tools could drastically reduce years of diagnostic delays, improve very early the quality of life of patients with PNES, and reduce the associated health care costs.

In Chapter 3, we had shown through application of measures of spike synchrony on epileptic spikes from five patients that the epileptic brain transits to a state of high synchrony prior to a seizure and is followed by dynamical desynchronization in the postictal. We quantified this observed change in preictal/postictal synchronization by a measure of resetting (Resetting Power; RP_Q) based on the fraction of pairs that synchronize preictally and desynchronize postictally. RP_Q profiles were estimated at every time point for the entire duration of depth EEG recordings of five patients with temporal lobe epilepsy. We further developed a statistical measure of resetting (SRP_Q) at seizures with respect to interictal RP_Q values. On the basis of SRP_Q values, we have shown with high level of statistical significance ($p < 0.001$) resetting of epileptic spike synchronization occur more commonly at seizures than interictally. Comparison with our previous measures of resetting based on STL_{max} and T-index profile, we observed a similar trend in this newly introduced power of resetting. To determine any effect of spike rate on the resetting metric, we tested for resetting, on channels that exhibit no change in their preictal/postictal spike rate. We also then observed significant resetting ($\alpha = 0.05$) on all the patients. Hence we conclude that resetting at seizures occur independently of the values of spike rate at brain sites.

Chapter 7
CONCLUSIONS

The main objective of this PhD dissertation was to investigate the role of spike activity in ictogenesis. Through the study of interictal spike synchronization, we were able to localize the epileptogenic focus. Through the study of prei-ictal spike synchronization were were able to show resetting of spike synchronization at seizures in patients with focal intractable epilepsy. Long term intracranial electroencephalographic (EEG) recordings from five patients were used for this study. Dynamical changes at ninety six seizures clinical and subclinical across five patients were analyzed using advanced measures of spike synchronization and nonlinear dynamics.

In Chapter 2, a novel and online spike detection algorithm based on morphological filtering technique was developed and tested. Spike detection was performed on EEG data from five patients with focal epilepsy and long term trends in spike rate profiles were investigated. In particular, we observed increased activation of epileptic spikes for EEG signals recorded from the orbito-frontal cortex in the preictal period followed by supression in the postictal, both across seizures and patients. The spike rate profiles of the epileptogenic focus failed to show consistency across seizures and patients with seizures occuring at periods of low as well as high rate of spike activity.

In Chapter 3, we developed a novel measure of synchronization between spike trains called as Epileptic Spike Synchronization (ESS). ESS was evaluated on unidirectionally and bi-directionally coupled spiking neuron models and its ability to measure spike synchronization was tested at various degrees of coupling. Application of ESS to spike trains detected from different brain sites was then performed

and long-term trends in spatiotemporal spike synchronization was observed. Study showed that across seizures and patients that there is an increase in synchronization between pairs of sites preictally followed by desynchronization postictally.

In Chapter 4, we investigated the connectivity of the epileptogenic focus with the rest of the brain in terms of graph theory and the spike synchronization measures we developed in Chapter 3. A measure to quantify the degree of centrality (Eigenvector Centrality) of a node in a network was developed and was tested on network models of coupled neurons. The centricity measure was then applied to the matrix of synchronization profiles of pairs of electrode over tume for the entire duration of EEG recording. Focus localization was achieved using the estimated centricity values over time from the interictal EEG data. This analysis revealed that the focus acts as the most central node of the epileptic network and forms strong and significant connection with other regions of the brain in terms of synchronization of their spike occurence. Based on this observation, we developed a focus localization algorithm that accurately identified the epileptogenic focus in all patients prior to the onset of the first clinical seizure (interictal period).

In Chapter 5, we classified seizures based on their preictal and postictal spike rate. We compared the severity of seizures with the preictal/postictal spike rate they exhobit across brain sites and showed that a severe seizure is preceded by increased spike frequency across a higher number of brain sites and is followed by suppression of spike rate. A classification accuracy of 88% was observed using a K-means classifier with two states to separate clinical seizures from subclinical seizures.

In Chapter 6, we quantified the previously observed reversal of dynamics at seizures, in terms of preictal spike synchronization and postictal spike desynchronization, using a measure of resetting. Further statistical analysis revealed that re-

setting of spike synchronization occurred more prominently at seizures than in the interictal periods. Along similar lines, we developed a measure of resetting in terms of synchronization of chaos (STL_{max}). CApplication of this measure to the EEG from with epileptic seizures and patients with psychogenic nonepileptic seizures revealed that differential diagnosis is possible between the two groups of patients, with epileptic seizures resetting the brain dynamics by psychogenic nonepileptic seizures not.

Overall, we laid down a mathematical framework within which interictal spikes were investigated in terms of their spatio-temporal dynamics. The hypothesis that were postulated and tested in this research can further the understanding of epileptogenesis and ictogenesis, the development of better seizure prediction algorithms as well as the control of seizures through electrical or other physiological intervention. Investigation of the significance of different types of epileptic spikes and validation of the results inmore subjects and types of seizures within the framework we developed appear to be feasible and worth pursuing endeavours in the near future.

REFERENCES

[1] M. de Curtis and G. Avanzini, "Interictal spikes in focal epileptogenesis," *Progress in Neurobiology*, vol. 63, no. 5, pp. 541 – 567, 2001.

[2] M. De Curtis, C. Radici, and M. Forti, "Cellular mechanisms underlying spontaneous interictal spikes in an acute model of focal cortical epileptogenesis," *Neuroscience*, vol. 88, no. 1, pp. 107–117, 1999.

[3] J. P. Lieb, S. C. Woods, A. Siccardi, P. H. Crandall, D. O. Walter, and B. Leake, "Quantitative analysis of depth spiking in relation to seizure foci in patients with temporal lobe epilepsy," *Electroencephalography and Clinical Neurophysiology*, vol. 44, no. 5, pp. 641 – 663, 1978.

[4] I. Sherwin, "Interictal-ictal transition in the feline penicillin epileptogenic focus," *Electroencephalography and Clinical Neurophysiology*, vol. 45, no. 4, pp. 525 – 534, 1978.

[5] H. H. Lange, J. P. Lieb, J. E. Jr., and P. H. Crandall, "Temporo-spatial patterns of pre-ictal spike activity in human temporal lobe epilepsy," *Electroencephalography and Clinical Neurophysiology*, vol. 56, no. 6, pp. 543 – 555, 1983.

[6] J. Engel, Jr., and R. F. Ackermann, "Interictal eeg spikes correlate with decreased, rather than increased, epileptogenicity in amygdaloid kindled rats," *Brain Research*, vol. 190, no. 2, pp. 543 – 548, 1980.

[7] R. J. Racine, "Modification of seizure activity by electrical stimulation: Ii. motor seizure," *Electroencephalography and Clinical Neurophysiology*, vol. 32, no. 3, pp. 281 – 294, 1972.

[8] J. Gotman, "Relationships between triggered seizures, spontaneous seizures, and interictal spiking in the kindling model of epilepsy," *Experimental Neurology*, vol. 84, no. 2, pp. 259 – 273, 1984.

[9] J. Gotman and M. Marciani, "Electroencephalographic spiking activity, drug levels, and seizure occurence in epileptic patients," *Annals of neurology*, vol. 17, no. 6, 1985.

[10] J. Gotman, "Relationships between interictal spiking and seizures - Human and Experimental Evidence," *Canadian Journal Of Neurological Sciences*, vol. 18, pp. 573–576, Nov 1991.

[11] A. Katz, D. Marks, G. McCarthy, and S. Spencer, "Does interictal spiking change prior to seizures?," *Electroencephalography and clinical neurophysiology*, vol. 79, no. 2, p. 153, 1991.

[12] J. S. Duncan, "Antiepileptic drugs and the electroencephalogram," *Epilepsia*, vol. 28, no. 3, pp. 259–266, 1987.

[13] J. Bourien, J. Bellanger, F. Bartolomei, P. Chauvel, and F. Wendling, "Mining reproducible activation patterns in epileptic intracerebral eeg signals: application to interictal activity," *Biomedical Engineering, IEEE Transactions on*, vol. 51, no. 2, pp. 304–315, 2004.

[14] A. Ossadtchi, J. Mosher, W. Sutherling, R. Greenblatt, and R. Leahy, "Hidden markov modelling of spike propagation from interictal meg data," *Physics in Medicine and Biology*, vol. 50, p. 3447, 2005.

[15] M. S. Jensen and Y. Yaari, "The relationship between interictal and ictal paroxysms in an in vitro model of focal hippocampal epilepsy," *Annals of Neurology*, vol. 24, no. 5, pp. 591–598, 1988.

[16] L. C. Katz and C. J. Shatz, "Synaptic activity and the construction of cortical circuits," *Science*, vol. 274, no. 5290, pp. 1133–1138, 1996.

[17] Y. Ben-Ari, E. Cherubini, R. Corradetti, and J. L. Gaiarsa, "Giant synaptic potentials in immature rat CA3 hippocampal neurones.," *J Physiol*, vol. 416, no. 1, pp. 303–325, 1989.

[18] L. I. Zhang and M.-m. Poo, "Electrical activity and development of neural circuits.," *Nature Neuroscience*, vol. 4, no. 11, pp. p1207 –, 2001.

[19] K. J. Staley and F. E. Dudek, "Interictal spikes and epileptogenesis.," *Epilepsy Currents*, vol. 6, no. 6, pp. p199 – 202, 20061101.

[20] K. Staley, J. L. Hellier, and F. E. Dudek, "Do Interictal Spikes Drive Epileptogenesis?," *Neuroscientist*, vol. 11, no. 4, pp. 272–276, 2005.

[21] J.-P. Wuarin and F. E. Dudek, "Excitatory Synaptic Input to Granule Cells Increases With Time After Kainate Treatment," *J Neurophysiol*, vol. 85, no. 3, pp. 1067–1077, 2001.

[22] G. Buzski, "Two-stage model of memory trace formation: A role for noisy brain states," *Neuroscience*, vol. 31, no. 3, pp. 551 – 570, 1989.

[23] L. Iasemidis and J. Sackellares, "The evolution with time of the spatial distribution of the largest Lyapunov exponent on the human epileptic cortex," *Measuring chaos in the human brain. Singapore: World Scientific*, pp. 49–82, 1991.

[24] L. Iasemidis, "On the dynamics of the human brain in temporal lobe epilepsy," 1991.

[25] L. Iasemidis, J. Principe, and J. Sackellares, "Measurement and quantification of spatio-temporal dynamics of human epileptic seizures," *Nonlinear biomedical signal processing*, vol. 2, pp. 294–318, 2000.

[26] J. Gotman and P. Gloor, "Automatic recognition and quantification of interictal epileptic activity in the human scalp EEG.," *Electroencephalogr Clin Neurophysiol*, vol. 41, no. 5, pp. 513–29, 1976.

[27] P. Guedes de Oliveira, C. Queiroz, and F. Lopes da Silva, "Spike detection based on a pattern recognition approach using a microcomputer.," *Electroencephalography and clinical neurophysiology*, vol. 56, no. 1, p. 97, 1983.

[28] B. Davey, W. Fright, G. Carroll, and R. Jones, "Expert system approach to detection of epileptiform activity in the eeg," *Medical and Biological Engineering and Computing*, vol. 27, no. 4, pp. 365–370, 1989.

[29] R. Sankar and J. Natour, "Automatic computer analysis of transients in EEG," *Computers in biology and medicine*, vol. 22, no. 6, pp. 407–422, 1992.

[30] H. Adeli, Z. Zhou, and N. Dadmehr, "Analysis of EEG records in an epileptic patient using wavelet transform," *Journal of Neuroscience Methods*, vol. 123, no. 1, pp. 69–87, 2003.

[31] H. Park, Y. Lee, D. Lee, and S. Kim, "Detection of epileptiform activity using wavelet and neural network," in *Engineering in Medicine and Biology Society. Proceedings of the 19th Annual International Conference of the IEEE*, vol. 3, 1997.

[32] L. Senhadji, J. Dillenseger, F. Wendling, C. Rocha, and A. Kinie, "Wavelet analysis of EEG for three-dimensional mapping of epileptic events," *Annals of biomedical engineering*, vol. 23, no. 5, pp. 543–552, 1995.

[33] S. Mallat and Z. Zhang, "Matching pursuits with time-frequency dictionaries," *IEEE Transactions on Signal Processing*, vol. 41, no. 12, pp. 3397–3415, 1993.

[34] P. Durka and K. Blinowska, "Analysis of EEG transients by means of matching pursuit," *Annals of biomedical engineering*, vol. 23, no. 5, pp. 608–611, 1995.

[35] G. Hellmann, "Multifold features determine linear equation for automatic spike detection applying neural nin interictal ecog," *Clinical neurophysiology*, vol. 110, no. 5, pp. 887–894, 1999.

[36] C. Ko and H. Chung, "Automatic spike detection via an artificial neural network using raw eeg data: effects of data preparation and implications in the limitations of online recognition," *Clinical neurophysiology*, vol. 111, no. 3, pp. 477–481, 2000.

[37] O. Ozdamar, I. Yaylali, P. Jayaker, and C. Lopez, "Multilevel neural network system for eeg spike detection," in *Computer-Based Medical Systems, 1991. Proceedings of the Fourth Annual IEEE Symposium*, pp. 272–279, IEEE, 1991.

[38] S. Wilson, C. Turner, R. Emerson, and M. Scheuer, "Spike detection II: automatic, perception-based detection and clustering," *Clinical Neurophysiology*, vol. 110, no. 3, pp. 404–411, 1999.

[39] W. Webber, B. Litt, K. Wilson, and R. Lesser, "Practical detection of epileptiform discharges (EDs) in the EEG using an artificial neural network: a comparison of raw and parameterized EEG data.," *Electroencephalogr Clin Neurophysiol*, vol. 91, no. 3, pp. 194–204, 1994.

[40] S. Nishida, M. Nakamura, A. Ikeda, and H. Shibasaki, "Signal separation of background eeg and spike by using morphological filter," *Medical engineering & physics*, vol. 21, no. 9, pp. 601–608, 1999.

[41] L. Pon, M. Sun, and R. Sclabassi, "The bi-directional spike detection in eeg using mathematical morphology and wavelet transform," in *Signal Processing, 2002 6th International Conference on*, vol. 2, pp. 1512–1515, IEEE, 2002.

[42] G. Xu, J. Wang, Q. Zhang, S. Zhang, and J. Zhu, "A spike detection method in eeg based on improved morphological filter," *Computers in Biology and Medicine*, vol. 37, no. 11, pp. 1647–1652, 2007.

[43] P. Maragos and R. Schafer, "Morphological filters–part i: Their set-theoretic analysis and relations to linear shift-invariant filters," *Acoustics, Speech and Signal Processing, IEEE Transactions on*, vol. 35, no. 8, pp. 1153–1169, 1987.

[44] P. Maragos and R. Schafer, "Morphological filters–part ii: Their relations to median, order-statistic, and stack filters," *Acoustics, Speech and Signal Processing, IEEE Transactions on*, vol. 35, no. 8, pp. 1170–1184, 1987.

[45] J. Serra and L. Vincent, "An overview of morphological filtering," *Circuits, Systems, and Signal Processing*, vol. 11, no. 1, pp. 47–108, 1992.

[46] J. Serra, "Morphological filtering: an overview," *Signal Processing*, vol. 38, no. 1, pp. 3–11, 1994.

[47] P. Durka, "Spikes and artifacts." Website. `http://eeg.pl/Members/durka/spikes-detection-mp`.

[48] H. Catenoix, M. Magnin, M. Guenot, J. Isnard, F. Mauguiere, and P. Ryvlin, "Hippocampal-orbitofrontal connectivity in human: an electrical stimulation study," *Clinical neurophysiology*, vol. 116, no. 8, pp. 1779–1784, 2005.

[49] J. Lieb, K. Hoque, C. Skomer, and X. Song, "Inter-hemispheric propagation of human mesial temporal lobe seizures: a coherence/phase analysis," *Electroencephalography and clinical neurophysiology*, vol. 67, no. 2, pp. 101–119, 1987.

[50] J. Lieb, R. Dasheiff, J. Engel, *et al.*, "Role of the frontal lobes in the propagation of mesial temporal lobe seizures," *Epilepsia*, vol. 32, no. 6, pp. 822–837, 1991.

[51] J. Lieb, J. Joseph, J. Engel Jr, J. Walker, and P. Crandall, "Sleep state and seizure foci related to depth spike activity in patients with temporal lobe epilepsy," *Electroencephalography and clinical neurophysiology*, vol. 49, no. 5-6, pp. 538–557, 1980.

[52] B. Malow, R. Kushwaha, X. Lin, K. Morton, and M. Aldrich, "Relationship of interictal epileptiform discharges to sleep depth in partial epilepsy," *Electroencephalography and clinical neurophysiology*, vol. 102, no. 1, pp. 20–26, 1997.

[53] B. Malow, X. Lin, R. Kushwaha, and M. Aldrich, "Interictal spiking increases with sleep depth in temporal lobe epilepsy," *Epilepsia*, vol. 39, no. 12, pp. 1309–1316, 1998.

[54] S. Sabesan, N. Chakravarthy, K. Tsakalis, P. Pardalos, and L. Iasemidis, "Measuring resetting of brain dynamics at epileptic seizures: application of global optimization and spatial synchronization techniques," *Journal of Combinatorial Optimization*, vol. 17, no. 1, pp. 74–97, 2009.

[55] L. Iasemidis, D. Shiau, J. Sackellares, P. Pardalos, and A. Prasad, "Dynamical resetting of the human brain at epileptic seizures: application of nonlinear dynamics and global optimization techniques," *IEEE Transactions on Biomedical Engineering*, vol. 51, no. 3, pp. 493–506, 2004.

[56] J. Victor and K. Purpura, "Metric-space analysis of spike trains: theory, algorithms and application," *Network: computation in neural systems*, vol. 8, no. 2, pp. 127–164, 1997.

[57] J. Victor, "Spike train metrics," *Current opinion in neurobiology*, vol. 15, no. 5, pp. 585–592, 2005.

[58] S. Schreiber, J. Fellous, D. Whitmer, P. Tiesinga, and T. Sejnowski, "A new correlation-based measure of spike timing reliability," *Neurocomputing*, vol. 52, pp. 925–931, 2003.

[59] R. Quiroga, T. Kreuz, and P. Grassberger, "Event synchronization: A simple and fast method to measure synchronicity and time delay patterns," *Physical Review E*, vol. 66, no. 4, p. 041904, 2002.

[60] T. Kreuz, J. Haas, A. Morelli, H. Abarbanel, and A. Politi, "Measuring spike train synchrony," *Journal of neuroscience methods*, vol. 165, no. 1, pp. 151–161, 2007.

[61] T. Kreuz, D. Chicharro, R. Andrzejak, J. Haas, and H. Abarbanel, "Measuring multiple spike train synchrony," *Journal of neuroscience methods*, vol. 183, no. 2, pp. 287–299, 2009.

[62] T. Kreuz, D. Chicharro, M. Greschner, and R. Andrzejak, "Time-resolved and time-scale adaptive measures of spike train synchrony," *Journal of neuroscience methods*, 2010.

[63] J. Hindmarsh and R. Rose, "A model of neuronal bursting using three coupled first order differential equations," *Proceedings of the Royal society of London. Series B. Biological sciences*, vol. 221, no. 1222, p. 87, 1984.

[64] A. Hodgkin and A. Huxley, "A quantitative description of membrane current and its application to conduction and excitation in nerve," *The Journal of physiology*, vol. 117, no. 4, p. 500, 1952.

[65] M. Teich, C. Heneghan, S. Lowen, T. Ozaki, and E. Kaplan, "Fractal character of the neural spike train in the visual system of the cat," *JOSA A*, vol. 14, no. 3, pp. 529–546, 1997.

[66] M. Le Van Quyen, C. Adam, J. Martinerie, M. Baulac, S. Clemenceau, and F. Varela, "Spatio-temporal characterizations of non-linear changes in intracranial activities prior to human temporal lobe seizures," *European Journal of Neuroscience*, vol. 12, no. 6, pp. 2124–2134, 2000.

[67] K. Lehnertz and C. Elger, "Can epileptic seizures be predicted? evidence from nonlinear time series analysis of brain electrical activity," *Physical Review Letters*, vol. 80, no. 22, pp. 5019–5022, 1998.

[68] L. Iasemidis, P. Pardalos, D. Shiau, W. Chaovalitwongse, K. Narayanan, S. Kumar, P. Carney, and J. Sackellares, "Prediction of human epileptic seizures based on optimization and phase changes of brain electrical activity," *Optimization Methods and Software*, vol. 18, no. 1, pp. 81–104, 2003.

[69] R. Hodrick and E. Prescott, "Postwar us business cycles: an empirical investigation," *Journal of Money, Credit, and Banking*, pp. 1–16, 1997.

[70] L. Iasemidis and J. Sackellares, "Chaos theory and epilepsy," *The Neuroscientist*, vol. 2, no. 2, pp. 118–125, 1996.

[71] L. Iasemidis, J. Chris Sackellares, H. Zaveri, and W. Williams, "Phase space topography and the Lyapunov exponent of electrocorticograms in partial seizures," *Brain Topography*, vol. 2, no. 3, pp. 187–201, 1990.

[72] B. Krishnan, A. Faith, and I. e. Vlachos, "Resetting of brain dynamics: epileptic versus psychogenic nonepileptic seizures," *Epilepsy Behav*, 2011.

[73] S. Demont-Guignard, P. Benquet, U. Gerber, and F. Wendling, "Analysis of intracerebral eeg recordings of epileptic spikes: insights from a neural network model," *Biomedical Engineering, IEEE Transactions on*, vol. 56, no. 12, pp. 2782–2795, 2009.

[74] K. Tsakalis, N. Chakravarthy, and L. Iasemidis, "Control of epileptic seizures: Models of chaotic oscillator networks," in *Decision and Control, 2005 and 2005 European Control Conference. CDC-ECC'05. 44th IEEE Conference on*, pp. 2975–2981, IEEE, 2005.

[75] K. Tsakalis and L. Iasemidis, "Control aspects of a theoretical model for epileptic seizures," *International Journal of Bifurcation and Chaos*, vol. 16, no. 7, pp. 2013–2027, 2006.

[76] K. Tsakalis, N. Chakravarthy, S. Sabesan, L. Iasemidis, and P. Pardalos, "A feedback control systems view of epileptic seizures," *Cybernetics and Systems Analysis*, vol. 42, no. 4, pp. 483–495, 2006.

[77] N. Chakravarthy, S. Sabesan, L. Iasemidis, and K. Tsakalis, "Controlling synchronization in a neuron-level population model," *International journal of neural systems*, vol. 17, no. 2, p. 123, 2007.

[78] N. Chakravarthy, K. Tsakalis, S. Sabesan, and L. Iasemidis, "Homeostasis of brain dynamics in epilepsy: A feedback control systems perspective of seizures," *Annals of biomedical engineering*, vol. 37, no. 3, pp. 565–585, 2009.

[79] S. Sabesan, L. Good, K. Tsakalis, A. Spanias, D. Treiman, and L. Iasemidis, "Information flow and application to epileptogenic focus localization from intracranial eeg," *Neural Systems and Rehabilitation Engineering, IEEE Transactions on*, vol. 17, no. 3, pp. 244–253, 2009.

[80] J. Arnhold, P. Grassberger, K. Lehnertz, and C. Elger, "A robust method for detecting interdependences: application to intracranially recorded eeg," *Physica D: Nonlinear Phenomena*, vol. 134, no. 4, pp. 419–430, 1999.

[81] K. Lehnertz, R. Andrzejak, J. Arnhold, T. Kreuz, F. Mormann, C. Rieke, G. Widman, and C. Elger, "Its possible use for interictal focus localization, seizure anticipation, and prevention: Nonlinear eeg analysis in epilepsy," *Journal of Clinical Neurophysiology*, vol. 18, no. 3, p. 209, 2001.

[82] J. Ebersole and S. Pacia, "Localization of temporal lobe foci by ictal eeg patterns," *Epilepsia*, vol. 37, no. 4, pp. 386–399, 1996.

[83] J. Ebersole, "Defining epileptogenic foci: past, present, future," *Journal of clinical neurophysiology*, vol. 14, no. 6, p. 470, 1997.

[84] P. Bonacich, "Factoring and weighting approaches to status scores and clique identification," *Journal of Mathematical Sociology*, vol. 2, no. 1, pp. 113–120, 1972.

[85] P. Bonacich, "Power and centrality: A family of measures," *American journal of sociology*, pp. 1170–1182, 1987.

[86] F. Grubbs, "Procedures for detecting outlying observations in samples," *Technometrics*, pp. 1–21, 1969.

[87] L. Iasemidis, S. Sabesan, L. Good, N. Chakravarthy, D. Treiman, J. Sirven, and K. Tsakalis, "A new look into epilepsy as a dynamical disorder: Seizure prediction, resetting and control," *Encyclopedia of Basic Epilepsy Research*, vol. 3, pp. 1295–1302, 2009.

[88] J. Gotman and M. Marciani, "Electroencephalographic spiking activity, drug levels, and seizure occurence in epileptic patients," *Annals of neurology*, vol. 17, no. 6, 1985.

[89] W. Rand, "Objective criteria for the evaluation of clustering methods," *Journal of the American Statistical association*, pp. 846–850, 1971.

[90] L. Hubert and P. Arabie, "Comparing partitions," *Journal of classification*, vol. 2, no. 1, pp. 193–218, 1985.

[91] L. Iasemidis, "Seizure prediction and its applications," *Neurosurgery Clinics of North America*, vol. 22, no. 4, p. 489, 2011.

[92] A. Medvedev, "Temporal binding at gamma frequencies in the brain: paving the way to epilepsy?," *Australasian Physical & Engineering Science in Medicine*, vol. 24, no. 1, pp. 37–48, 2001.

[93] A. Medvedev, "Epileptiform spikes desynchronize and diminish fast (gamma) activity of the brain:: An," *Brain research bulletin*, vol. 58, no. 1, pp. 115–128, 2002.

[94] D. Masco, N. Sahibzada, R. Switzer, and K. Gale, "Electroshock seizures protect against apoptotic hippocampal cell death induced by adrenalectomy," *Neuroscience*, vol. 91, no. 4, pp. 1315–1319, 1999.

[95] M. Fink, "Electroshock revisited electroconvulsive therapy, once vilified, is slowly receiving greater interest and use in the treatment of mental illness," *American Scientist*, vol. 88, no. 2, pp. 162–167, 2000.

[96] N. Bodde, J. Brooks, G. Baker, P. Boon, J. Hendriksen, O. Mulder, and A. Aldenkamp, "Psychogenic non-epileptic seizuresdefinition, etiology, treatment and prognostic issues: a critical review," *Seizure*, vol. 18, no. 8, pp. 543–553, 2009.

[97] C. Galimberti, M. Ratti, R. Murelli, E. Marchioni, R. Manni, and A. Tartara, "Patients with psychogenic nonepileptic seizures, alone or epilepsy-associated, share a psychological profile distinct from that of epilepsy patients," *Journal of neurology*, vol. 250, no. 3, pp. 338–346, 2003.

[98] M. Reuber, "Psychogenic nonepileptic seizures: answers and questions," *Epilepsy & Behavior*, vol. 12, no. 4, pp. 622–635, 2008.

[99] M. Reuber, S. Howlett, A. Khan, and R. Grünewald, "Non-epileptic seizures and other functional neurological symptoms: predisposing, precipitating, and perpetuating factors," *Psychosomatics*, vol. 48, no. 3, pp. 230–238, 2007.

[100] A. Fiszman, S. Alves-Leon, R. Nunes, I. Figueira, *et al.*, "Traumatic events and posttraumatic stress disorder in patients with psychogenic nonepileptic seizures: a critical review," *Epilepsy & Behavior*, vol. 5, no. 6, pp. 818–825, 2004.

[101] W. Fleisher, D. Staley, P. Krawetz, N. Pillay, J. Arnett, and J. Maher, "Comparative study of trauma-related phenomena in subjects with pseudoseizures and subjects with epilepsy," *American Journal of Psychiatry*, vol. 159, no. 4, pp. 660–663, 2002.

[102] J. Kuyk, F. Leijten, H. Meinardi, P. Spinhoven, and R. Dyck, "The diagnosis of psychogenic non-epileptic seizures: a review," *Seizure*, vol. 6, no. 4, pp. 243–253, 1997.

[103] U. Seneviratne, D. Reutens, and W. DSouza, "Stereotypy of psychogenic nonepileptic seizures: Insights from video-eeg monitoring," *Epilepsia*, vol. 51, no. 7, pp. 1159–1168, 2010.

[104] D. Cragar, D. Berry, T. Fakhoury, J. Cibula, and F. Schmitt, "A review of diagnostic techniques in the differential diagnosis of epileptic and nonepileptic seizures," *Neuropsychology Review*, vol. 12, no. 1, pp. 31–64, 2002.

[105] M. Reuber, G. Fernandez, J. Bauer, C. Helmstaedter, and C. Elger, "Diagnostic delay in psychogenic nonepileptic seizures," *Neurology*, vol. 58, no. 3, pp. 493–495, 2002.

[106] D. Cragar, D. Berry, F. Schmitt, and T. Fakhoury, "Cluster analysis of normal personality traits in patients with psychogenic nonepileptic seizures," *Epilepsy & Behavior*, vol. 6, no. 4, pp. 593–600, 2005.

[107] T. Betts and S. Boden, "Diagnosis, management and prognosis of a group of 128 patients with non-epileptic attack disorder. part i," *Seizure*, vol. 1, no. 1, pp. 19–26, 1992.

[108] J. Kuyk, P. Spinhoven, and R. Dyck, "Hypnotic recall: a positive criterion in the differential diagnosis between epileptic and pseudoepileptic seizures," *Epilepsia*, vol. 40, no. 4, pp. 485–491, 1999.

[109] J. Parra, J. Iriarte, and A. Kanner, "Are we overusing the diagnosis of psychogenic non-epileptic events?," *Seizure*, vol. 8, no. 4, pp. 223–227, 1999.

[110] S. Benbadis and W. Allen Hauser, "An estimate of the prevalence of psychogenic non-epileptic seizures," *Seizure*, vol. 9, no. 4, pp. 280–281, 2000.

[111] W. Hauser and L. Kurland, "The epidemiology of epilepsy in rochester, minnesota, 1935 through 1967," *Epilepsia*, vol. 16, no. 1, pp. 1–66, 1975.

[112] K. Alper, O. Devinsky, K. Perrine, B. Vazquez, and D. Luciano, "Nonepileptic seizures and childhood sexual and physical abuse," *Neurology*, vol. 43, no. 10, pp. 1950–1950, 1993.

[113] M. Witgert, J. Wheless, and J. Breier, "Frequency of panic symptoms in psychogenic nonepileptic seizures," *Epilepsy & Behavior*, vol. 6, no. 2, pp. 174–178, 2005.

[114] J. Iriarte, J. Parra, E. Urrestarazu, and J. Kuyk, "Controversies in the diagnosis and management of psychogenic pseudoseizures," *Epilepsy & Behavior*, vol. 4, no. 3, pp. 354–359, 2003.

[115] S. Benbadis, V. Agrawal, and W. Tatum IV, "How many patients with psychogenic nonepileptic seizures also have epilepsy?," *Neurology*, vol. 57, no. 5, pp. 915–917, 2001.

[116] A. Abubakr, A. Kablinger, and G. Caldito, "Psychogenic seizures: clinical features and psychological analysis," *Epilepsy & Behavior*, vol. 4, no. 3, pp. 241–245, 2003.

[117] P. de Timary, P. Fouchet, M. Sylin, J. Indriets, T. de Barsy, A. Lefebvre, and K. van Rijckevorsel, "Non-epileptic seizures: delayed diagnosis in patients presenting with electroencephalographic (eeg) or clinical signs of epileptic seizures," *Seizure*, vol. 11, no. 3, pp. 193–197, 2002.

[118] W. Nowack *et al.*, "Epilepsy: a costly misdiagnosis.," *Clinical EEG (electroencephalography)*, vol. 28, no. 4, p. 225, 1997.

[119] R. Martin, F. Gilliam, M. Kilgore, E. Faught, and R. Kuzniecky, "Improved health care resource utilization following video-eeg-confirmed diagnosis of nonepileptic psychogenic seizures," *Seizure*, vol. 7, no. 5, pp. 385–390, 1998.

[120] S. Benbadis, "Psychogenic non-epileptic seizures," *The treatment of epilepsy: principles and practice. Lippincott, Williams, & Wilkins, Philadelphia*, pp. 623–630, 2005.

[121] S. Carton, P. Thompson, and J. Duncan, "Non-epileptic seizures: patients' understanding and reaction to the diagnosis and impact on outcome," *Seizure*, vol. 12, no. 5, pp. 287–294, 2003.

[122] L. Selwa, J. Geyer, N. Nikakhtar, M. Brown, L. Schuh, and I. Drury, "Nonepileptic seizure outcome varies by type of spell and duration of illness," *Epilepsia*, vol. 41, no. 10, pp. 1330–1334, 2000.

[123] J. Eckmann, S. Kamphorst, D. Ruelle, and S. Ciliberto, "Liapunov exponents from time series," *Physical Review A*, vol. 34, no. 6, pp. 4971–4979, 1986.

[124] A. Wolf, J. Swift, H. Swinney, and J. Vastano, "Determining Lyapunov exponents from a time series," *Physica. D*, vol. 16, no. 3, pp. 285–317, 1985.

[125] A. Faith, B. Krishnan, A. Roth, E. Kondylis, K. Williams, J. Sirven, and L. Iasemidis, "Lack of resetting of brain dynamics following psychogenic non-epileptic seizures," in *Imaging and Signal Processing in Healthcare and Technology*, ACTA Press, 2011.

[126] B. Krishnan, A. Faith, I. Vlachos, A. Roth, K. Williams, K. Noe, J. Drazkowski, L. Tapsell, J. Sirven, and L. Iasemidis, "Resetting of brain dynamics: epileptic versus psychogenic nonepileptic seizures," *Epilepsy & Behavior*, vol. 22, pp. S74–S81, 2011.

[127] L. Iasemidis, A. Prasad, J. Sackellares, P. Pardalos, and D. Shiau, "On the prediction of seizures, hysteresis and resetting of the epileptic brain: insights from models of coupled chaotic oscillators," *Order and Chaos*, vol. 8, pp. 283–305, 2003.

[128] S. Fisher, *Statistical methods for research workers*. No. 5, Genesis Publishing Pvt Ltd, 1932.